SwRI-2253/3

STUDY OF HIGH TEMPERATURE FAILURE MECHANISMS IN CERAMICS

By

Richard A. Page
James Lankford
Kwai S. Chan

AFOSR FINAL REPORT

This research was sponsored by the Air Force Office of Scientific Research,
Electronic and Materials Sciences Directorate
Under Contract F49620-88-C-0081

Approved for release; distribution unlimited.

January 1992

SOUTHWEST RESEARCH INSTITUTE
SAN ANTONIO HOUSTON
DETROIT WASHINGTON, DC

REPORT DOCUMENTATION PAGE

Form Approved
OMB No. 0704-0188

1. AGENCY USE ONLY (Leave blank)	2. REPORT DATE	3. REPORT TYPE AND DATES COVERED
	January 1992	Final Report (Dec. '89 - Sept. '91)

4. TITLE AND SUBTITLE

High Temperature Failure Mechanisms in Ceramics

5. FUNDING NUMBERS

Contract F49620-88-C-0081

6. AUTHOR(S)

R. A. Page, J. Lankford, and K. S. Chan

7. PERFORMING ORGANIZATION NAME(S) AND ADDRESS(ES)

Southwest Research Institute
6220 Culebra Road
San Antonio, Texas 78228-0510

8. PERFORMING ORGANIZATION REPORT NUMBER

SwRI-2253/3

9. SPONSORING / MONITORING AGENCY NAME(S) AND ADDRESS(ES)

Lt. Col. Larry Burggraf
Air Force Office of Scientific Research
Bolling Air Force Base
Washington, D.CC. 20332

10. SPONSORING / MONITORING AGENCY REPORT NUMBER

11. SUPPLEMENTARY NOTES

12a. DISTRIBUTION / AVAILABILITY STATEMENT

Approved for public release;
distribution unlimited.

12b. DISTRIBUTION CODE

13. ABSTRACT (Maximum 200 words)

This final report documents the results of a basic research program aimed at (1) studying the high temperature failure mechanisms in ceramics, (2) establishing relationships between cavitation mechanisms and creep crack growth characteristics, and (3) developing a damage mechanism-based life prediction model. The growth rate, near-tip creep responses, and damage processes of creep cracks in a pyroceram glass-ceramic were studied under tensile loading at elevated temperatures. The results of these studies indicated that creep crack growth in the pyroceram glass-ceramic occurred both in continuous and discontinuous manners, with the damage processes manifested as the nucleation, growth, and coalescence of inhomogeneously distributed cavities and microcracks. Sintering of cavities led to the existence of a growth threshold below which the creep crack would open, blunt, but not propagate. Measurements of the total accumulated creep strain near the crack-tip revealed that creep crack extension followed a critical strain criterion. Relationships between cavitation mechanisms and creep crack growth characteristics of the glass-ceramic are discussed.

14. SUBJECT TERMS

Ceramics, glass-ceramics, creep crack growth, cavitation mechanisms, creep crack growth threshold

15. NUMBER OF PAGES

16. PRICE CODE

17. SECURITY CLASSIFICATION OF REPORT	18. SECURITY CLASSIFICATION OF THIS PAGE	19. SECURITY CLASSIFICATION OF ABSTRACT	20. LIMITATION OF ABSTRACT
Unclassified	Unclassified	Unclassified	Unlimited

SOUTHWEST RESEARCH INSTITUTE
Post Office Drawer 28510, 6220 Culebra Road
San Antonio, Texas 78228-0510

STUDY OF HIGH TEMPERATURE FAILURE MECHANISMS IN CERAMICS

By
Richard A. Page
James Lankford
Kwai S. Chan

AFOSR FINAL REPORT

This research was sponsored by the Air Force Office of Scientific Research,
Electronic and Materials Sciences Directorate
Under Contract F49620-88-C-0081
Approved for release; distribution unlimited.

January 1992

Approved:

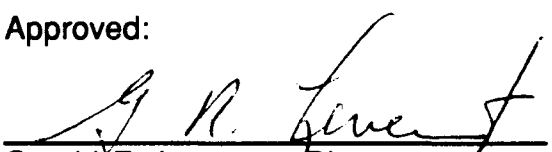

Gerald R. Leverant, Director
Department of Materials and Mechanics

Table of Contents

I. INTRODUCTION

A. Scope

Because of the attractive properties of ceramics at elevated temperatures, there is great interest in developing a new generation of aerospace propulsion systems capitalizing on advanced ceramics technology. These new propulsion systems would potentially offer higher operating temperatures and lower weights, thus providing dramatic increases over current engine designs in both efficiency and performance. While present engines utilize hot-stage components fabricated from nickel or cobalt-base superalloys, it is anticipated that evolving ceramic turbines will be based on silicon nitride and silicon carbide. In service, the ceramic components will experience tensile and/or cyclic loadings. Very little is known, however, about the behavior of these ceramics under tensile creep or cyclic creep conditions. An understanding of the basic failure mechanisms and an ability to predict lifetimes will be necessary before ceramics can be successfully utilized in engine applications.

B. Objectives and Approaches

The primary objectives of this basic research program were to characterize the creep damage accumulation processes in high temperature structural ceramics and to develop a predictive creep lifetime model based on the damage mechanism information. The approaches for achieving these goals were as follows:

1. Characterize creep crack growth and experimentally measure, using stereoimaging strain analysis, the crack-tip displacement field, strain distribution, and creep strain rates as functions of stress intensity, temperature, and microstructure.

2. Identify the damage processes associated with creep crack growth and characterize the damage development process.

3. Incorporate the crack-tip micromechanical information and damage evolution information in a fundamental creep crack growth model for ceramics.

II. SUMMARY OF THE RESEARCH EFFORT

Research efforts for this program included studies of high temperature failure mechanisms, crack growth behavior, and crack-tip micromechanics of creep cracks in ceramics. The research efforts were focused on establishing quantitative relationships between cavitation mechanisms, crack-tip micromechanics, and creep crack growth kinetics. For these studies, a magnesium-aluminosilicate glass-ceramic (Corning 9606 pyroceram) was employed as a model material representative of liquid-phase sintered ceramics. The microstructure of the glass-ceramic was typical of those commonly found in many liquid-phase sintered ceramics, and it consisted of ≈ 0.5 μm diameter cordierite grains surrounded by an amorphous grain boundary phase which softens at ≈ 600°C. Once the amorphous phase starts to soften, deformation of the glass-ceramic occurs by a combination of grain boundary sliding and cavitation.

The creep crack growth characteristics of the glass ceramic were characterized as a function of temperature by testing inside a scanning electron microscope (SEM) equipped with a high-temperature loading stage. During the creep crack growth experiments, the near-tip region of the creep crack was photographed as a function of time of creep. Still photographs of the near-tip region from different times of creep were analyzed using the machine-vision-based stereoimaging technique, which was developed at SwRI, to obtain the near-tip displacement and the creep strain fields. Replication techniques were also used to characterize quantitatively the damage processes that accompanied creep crack growth. Relationships between the damage mechanisms and the crack growth processes were iden..fied, including the origin of the growth threshold and the criterion for creep crack growth in the $K > K_{th}$ regime. In particular, the threshold for creep crack growth in the glass-ceramic was shown to arise from sintering of creep cavities at stress intensity, K, levels below the threshold, K_{th}. At $K > K_{th}$, creep crack growth was found to extend according to a critical creep strain criterion, which might in fact be an indication of a critical damage criterion for creep crack growth.

In addition to creep crack growth experiments involving pre-cracked specimens, creep experiments of smooth specimens were performed under both compression and tension. Efforts to develop a life prediction model based on the information on damage mechanisms during creep crack growth were initiated. Extension of the creep crack growth experiments to zirconia had been attempted as an effort to examine the generality of the creep damage processes in the pyroceram glass-ceramic. Creep testing of the zirconia was performed in the SEM loading stage at 800°C, but significant creep was not observed due to the relatively low test temperature. Discussion of the more important results obtained in this proram are briefly presented in the next five sections. A more detailed discussion can be found in the papers included in the appendix.

A. Characterization of the Creep Crack Growth Process

In-situ observations of creep crack growth experiments performed inside the SEM stage revealed that creep crack growth in the pyroceram glass-ceramic occurred either in a continuous or discontinuous manner [1]. During continuous growth, the main crack tip extended without any visible microcracking directly ahead of the crack tip. In contrast, discontinuous crack growth occurred with the formation of one or more microcrack(s) ahead of the crack tip. Further crack extension required the linkage of the microcrack(s) with the main crack; this process could take as much as 30 minutes or more. In some instances, the linkage of the microcrack and main crack was not complete, leaving ligaments which bridged the crack surfaces.

The creep crack growth rates were measured as a function of the stress intensity factor, K, at 700, 750, and 775°C. These results showed that the crack growth rates can be correlated in terms of the K parameter. At both 750 and 775°C, the crack growth curve showed a threshold, K_{th}, below which no detectable crack growth occurred. The threshold was determined by unloading the propagating creep crack in small load increments until it was arrested. The K level was then increased until the crack resumed propagation. A duplicate specimen was used to verify the growth threshold by testing at $K \approx K_{th}$ under increasing K levels without prior unloading. The same K_{th} values were obtained in both cases, indicating the observed growth threshold is a material property of a large crack and not a load-history effect due to unloading.

B. The Origin of the Creep Crack Growth Threshold

The observation of a threshold for creep crack growth in the glass-ceramic is consistent with previous findings on alumina and silicon carbide, which indicated the existence of a growth threshold for creep cracks that originated from pre-existing flaws (i.e., large cracks) in the ceramics. A growth threshold, however, was not observed in creep cracks that were initiated by creep damage. For life prediction, a growth threshold can significantly affect the predicted creep rupture life. Identifying the origin of the growth threshold for creep cracks in ceramics is therefore important. This was accomplished by performing the critical experiments which are discussed below.

The observed K_{th} value for the pyroceram glass-ceramic was ≈ 0.6 MPa$\sqrt{m}$ at 775°C. In order to investigate its origin, a fatigue-precracked specimen of the glass-ceramic was crept inside the SEM loading stage at 775°C under a stress intensity factor of 0.59 MPa$\sqrt{m}$. The near-tip region of the creep crack was photographed at 30 minute intervals. Photographs of the same region taken under identical K levels, but of different times of creep were analyzed for crack opening displacements and crack-tip strain distributions using the machine-vision-based stereoimaging technique. The surfaces of the creep crack were found to open, with the crack opening displacements increasing with increasing times of creep. Furthermore, the creep crack was found to propagate at $\approx 1 \times 10^{-6}$ m/hr. After 390 minutes of creep, the specimen was removed from the loading stage, and one of its surfaces was ion-milled for four hours. The surface of the specimen was replicated; the replicas were examined in a transmission electron microscope to evaluate the level of creep damage in the cracked specimen. The specimen was found to be heavily cavitated, but contained no well-defined microcracks. After damage characterization, the specimen was returned to the SEM loading stage for additional creep testing at 775°C for 8 hours at K = 0.59 MPa $\sqrt{m}$. The creep crack was observed to open, blunt, and extend during this period. The K level was then lowered to 0.5 MPa $\sqrt{m}$ and crept for 10 hours during which period the crack was observed to open, blunt, but not propagate. The result indicated the K level was below the growth threshold. The specimen was removed from the SEM stage, ion-milled, and replicated. Subsequent observation indicated that all the previously observed near-tip cavities had disappeared. This observation indicated that the growth threshold of the glass-ceramic originated from sintering of creep cavities and removal of creep damage from the cracked specimen including the crack-tip region. This result is in agreement with a previous model [2] which predicted that sintering of cavities at the crack tip would lead to an abrupt drop in the creep crack growth rate and the formation of a threshold below which creep crack growth would not occur.

In addition, the creep crack was also found to exhibit different near-tip strain distribution and crack surface opening behavior at K levels at and below the growth threshold, K_{th}. Comparison revealed that regions of higher creep strain generally correspond to regions of high creep cavity density. Thus, the difference in the near-tip strain distribution observed at $K = K_{th}$ for a propagating crack and at K levels below K_{th} for a nonpropagating crack was due to the difference in the near-tip damage accumulation process. At $K = K_{th}$, cavities were nucleated near the crack tip, leading to creep crack growth. In contrast, cavities were not nucleated, but sintered at the crack tip at K levels less than K_{th}.

The rates of crack surface opening for the creep crack at K = 0.5 MPa $\sqrt{m}$ were compared with those for K = 0.59 MPa $\sqrt{m}$. The comparison revealed that the creep crack exhibited crack opening displacement rates at K = 0.5 MPa $\sqrt{m}$, but their magnitudes were lower than those observed at K = 0.59 MPa $\sqrt{m}$. The finite rate of crack opening displacement indicated that the crack tip

continued to blunt at K levels below the growth threshold, even though no cavities or crack extension were generated. These observations suggested that at least two different deformation mechanisms were operative at K levels at and above the growth threshold. One of these mechanisms, which is probably grain boundary sliding, led to cavitation, while the other, which is probably creep (diffusion or solution-reprecipitation), resulted in crack-tip blunting, but no cavitation. Based on these results, it is clear that the growth threshold originates from a healing process which removes creep damage by the sintering of cavities. Physically, the growth threshold represents the stress intensity level at which cavity nucleation occurs near the crack tip and below which sintering of these cavities commences.

C. Criterion For Creep Crack Growth

At $K > K_{th}$, creep crack growth occurred by the accumulation of creep strain and cavitation damage near the crack tip. In order to develop a better understanding of this process, both the near-tip creep strain and cavitation damage were quantitatively characterized. The near-tip cumulative creep strain measurement was obtained by the machine-vision-based stereoimaging technique. The experimental procedures for these measurements involved taking high-resolution micrographs of the crack tip region in a scanning electron microscope. The micrographs were taken both before and after creep crack growth into the region of interest. This pair of photographs was then analyzed to obtain the cumulative creep strain using the stereoimaging technique. These results indicated that creep crack growth in the model ceramic obeyed a critical cumulative strain criterion. The critical cumulative creep strain was measured for various K levels and times of creep. The results indicate that the critical value of the cumulative creep strain for creep crack growth is approximately 2%, and it is independent of K level and time of creep.

D. Characterization of Creep Damage

The damage processes which occurred during creep crack growth in the pyroceram glass-ceramic were identified by direct observations of the crack extension sequence *in-situ* via the SEM and by examining replicas of the surfaces of the specimens via scanning and transmission electron microscopies. As indicated earlier, *in-situ* observation revealed that creep crack growth occurred by either a continuous or discontinuous process. Consistent with this observation, the replicating technique revealed the presence of two different cavitation defects in the glass-ceramic. These two types of creep-induced damage include (1) pockets of heavily cavitated regions of creep cavities, and (2) microcracks that are comprised of a row of cavities aligned in a linear fashion. In both cases, the creep cavities located within the pockets or the microcracks were generally of approximately equal size, spacing, and shape. Based on the similarity in cavity size, shape, and spacing, it appears that the creep cavitation process could have occurred through two possible mechanisms. The first possible mechanism was that all the creep cavities were nucleated at the same time, and they exhibited equivalent growth rates until coalescence. The second possible mechanism, which is considered more plausible, is a cavitation process which involves the nucleation of cavities that could not grow beyond a critical size. Under this circumstance, cavitation is dominated by continuous nucleation of cavities until the cavities are sufficiently close for coalescence to take place. The nucleation of cavities is in turn controlled by stochastic grain boundary sliding and the availability of potential nucleation sites [3], both are governed by the microstructure of the grain boundaries. Such a process of nucleation dominated cavitation with

cavities which would not grow beyond a critical size has been observed in Lucalox and AD99 alumina [4,5], the latter is a liquid-phase, sintered ceramic which contains an amorphous phase along grain boundaries, as in the pyroceram glass-ceramic.

Both the microcracks and heavily cavitated regions were inhomogeneously distributed throughout the microstructure. It was quite common for one region to be heavily cavitated, while the contiguous regions were cavity-free, In order to better understand the damage process, qualitative measurement techniques were used to characterize the distribution of microcracks and the heavily cavitated regions. The microcrack density was measured as a function of distance ahead of the crack tip. Additionally, the area fraction of heavily cavitated regions was measured. The results indicated that both the microcrack density and the area fraction of heavily cavitated regions increased with decreasing distance from the crack tip. Based on these results, it can be suggested that the critical cumulative strain criterion might in fact be an indication that creep crack growth in the ceramic is dictated by attaining a critical level of creep damage.

E. Life Prediction Modeling

The development of a life prediction model based on the cavitation damage mechanisms is in the initial stage. Experimental observation revealed that creep cavitation damage was related to the creep rate. The proposed model, therefore, is formulated by considering the creep rates as functions of time, K levels, distance ahead of the crack tip, and the damage process. Observations indicated that creep damage accumulates within a "process zone" located ahead of the tip of the creep crack. The "process zone" is embedded within the Ridel-Rice (RR) field [7], which is, in turn, surrounded by the K-field and the field due to the remote stress, σ_∞. Creep damage within the "process zone" increases with increasing time of creep, and the creep crack extends when the creep strain or the amount of creep damage within the process zone reaches a critical value. Healing of creep damage by sintering of creep cavities will be incorporated into the model describing the damage evolution in the process zone. The sintering term is expected to result in a growth threshold for creep cracks originated from large pre-existing flaws.

F. References

1. K. S. Chan and R. A. Page, "Creep Crack Growth by Damage Accumulation in a Glass-Ceramic," *J. of the Am. Cer. Soc.*, 1990 (submitted).

2. M. D. Thoules and A. G. Evans, *Scripta Met.*, Vol. 18, 1984, pp. 1175-1180.

3. K. S. Chan and R. A. Page, "Transient Cavity Growth in Ceramics Under Compression," *J. Mat. Science*, 1990 (submitted).

4. R. A. Page, J. Lankford, and S. Spooner, *Acta Met.*, Vol. 32, 1984, p. 1275.

5. R. A. Page, J. Lankford, K. S. Chan, K. Hardman-Rhyne, and S. Spooner, *J. Am. Ceram. Soc.*, Vol. 70, 1987, p. 137.

6. R. A. Page, K. S. Chan, D. L. Davidson, and J. Lankford, "The micromechanics of Creep Crack Growth," *J. Am. Cer. Soc.*, Vol. 73, No. 10, 1990, pp. 2977-2986.

7. H. Riedel and J. R. Rice, *J. Mech. Phys. Solids*, Vol. 29, 1981, pp. 35-49.

III. ACCOMPLISHMENTS

The significant accomplishments achieved in this program during the last year are as follows:

1. The mechanisms of creep crack growth were identified for a model ceramic. Correlations between creep crack growth rates and the stress intensity factor were established.

2. Sintering of cavities was identified as the mechanism leading to the growth threshold below which a creep crack does not propagate.

3. A critical creep strain criterion for creep crack growth in a glass-ceramic was identified.

4. The creep damage processes associated with creep crack growth in the model ceramic were identified. Relationships between cavitation mechanisms and crack growth kinetics were partially established.

IV. PUBLICATIONS (AFOSR SPONSORSHIP)

1. "Automated High-Resolution Displacement Measurements for Deformation and Fracture Research," by D. L. Davidson, K. S. Chan, and R. A. Page, in Micromechanics: Experimental Techniques, ASME, edited by W. N. Sharpe, Jr., AMD-Vol. 102, pp. 73-87, 1989.

2. "Micromechanics of Creep Crack Growth in a Glass-Ceramic," by R. A. Page, K. S. Chan, D. L. Davidson, and J. Lankford, *Journal of the American Ceramic Society*, Vol. 73, p. 2977, 1990.

3. "Near-tip Behavior of Deflected Creep Cracks," by K. S. Chan, R. A. Page, and D. L. Davidson, *International Journal of Fracture*, Vol. 50, p. 281, 1991.

4. "Creep Crack Growth by Damage Accumulation in a Glass-Ceramic," by K. S. Chan and R. A. Page, *Journal of the American Ceramic Society*, Vol. 74, p. 1605, 1991.

5. "Origin of the Creep Crack Growth Threshold in a Glass-Ceramic," by K. S. Chan and R. A. Page, *Journal of the American Ceramic Society*, 1990 (in press).

6. "Creep Damage Development in Structural Ceramics," by K. S. Chan and R. A. Page, *Journal of the American Ceramic Society*, (submitted as an invited feature article).

V. INTERACTIONS

"Creep Crack Growth in a Glass-Ceramic Material," by R. A. Page and J. Lankford, 91st Annual Meeting of the American Ceramic Society, Indianapolis, IN, April 1989.

"Creep Crack Growth by Damage Accumulation in a Glass-Ceramic," by K. S. Chan and R. A. Page, 93rd Annual Meeting of the American Ceramic Society, Cincinnati, OH, April 1991.

"Creep Crack Growth Threshold Behavior," by R. A. Page and K. S. Chan, 94th Annual Meeting of the American Ceramic Society, Minneapolis, MN, April 1992.

VI. PROGRAM PERSONNEL

Name	Title	
Dr. Richard A. Page	Staff Scientist and Section Manager	Co-Principal
Dr. James Lankford	Institute Scientist	Investigators
Dr. Kwai S. Chan	Principal Engineer	
Dr. David L. Davidson	Institute Scientist	
Mr. Harold G. Saldana	Supervisor	
Mr. John B. Campbell	Staff Technician	
Mr. James S. Spencer	Staff Technician	

Appendix

journal

Reprinted from the Journal of the American Ceramic Society, Vol. 73, No. 10, October 1990

J. Am. Ceram. Soc., 73 [10] 2977–86 (1990)

Micromechanics of Creep-Crack Growth in a Glass-Ceramic

Richard A. Page,* Kwai S. Chan,* David L. Davidson, and James Lankford*

Southwest Research Institute, San Antonio, Texas 78228–0510

The near-tip strain and opening behavior of creep cracks in a glass-ceramic were studied at temperatures for which grain-boundary sliding is the dominant deformation mechanism. Using the stereoimaging displacement measurement technique, near-tip creep strain and crack-opening displacement (COD) increments were obtained as functions of distance from the crack tip and time of creep. Both the time and radial dependence of the strain and COD were observed to be consistent with the Riedel and Rice (RR) field when the time of creep and crack extension were small. Increasing creep time and crack extension led to the formation of a localized shear zone located directly ahead of the crack tip. Further crack extension tended to follow this shear zone within which creep damage accumulated. Neither the rate of COD nor the strain-rate distribution within this shear zone could be described by the RR field or the Hui and Riedel (HR) field for growing cracks. Steady-state, stable crack growth exhibiting both Mode I and II components was observed in the glass-ceramic despite a creep exponent of ≈2. Varying the test temperature and applied stress intensity influenced both the development of the crack-tip shear zone and the crack growth process. These observations are discussed on the basis of the interrelationships between the near-tip field, creep damage accumulation, and grain-boundary sliding. [Key words: crack growth, glass-ceramics, creep, models, strain.]

I. Introduction

CREEP failure of structural ceramics can occur either by the accumulation of damage, generally in the form of grain-boundary cavities throughout the bulk of the material, or by the subcritical growth of a dominant flaw. The processes associated with bulk damage accumulation in creeping ceramics have been investigated in numerous studies and will, therefore, not be addressed in this paper. Rather, attention will be focused on the subject of creep-crack growth.

Subcritical crack growth has been observed in a number of ceramics during elevated temperature loading.[1–6] Generally, such subcritical, or creep, crack growth is intergranular and is thought to occur by the nucleation, growth, and coalescence of cavities ahead of the crack tip. Since cavitation is either limited to or most pronounced within the region near the tip of the crack, the rate of cavitation and, subsequently, the rate of crack propagation are both expected to be related to the stress and strain fields associated with the crack tip. Prediction of the fields associated with a growing creep crack can be a formidable problem, however, because of the complex interrelationships between the field conditions, the cavitation rates, and the crack propagation rates.

In spite of the inherent complexities, attempts at modeling creep-crack growth by grain-boundary cavitation due to either diffusional or plastic processes have been made by a number of investigators.[7–23] In these models, continuum crack-tip stress fields were used as the driving force for grain-boundary cavitation and crack growth. More than three different fracture mechanic parameters were utilized to describe the continuum crack-tip stress fields and for relating creep-crack growth rates. They include (1) the stress intensity factor, K, for characterizing the stress field of an elastic crack for treating small-scale creep;[7–16] (2) the time-dependent contour-integral parameter, $C(t)$, for treating transient creep-crack growth;[17,18] and (3) the time-independent contour-integral parameter, C^*, for treating steady-state creep-crack growth.[19–23] A small creep process zone was generally assumed and grain-boundary cavitation was considered not to alter significantly the continuum crack-tip stress fields. The early creep-crack growth models were generally formulated on the basis of K-controlled[7–16] and subsequently C^*-controlled[19–23] processes by neglecting time-dependent variations of the crack-tip stresses due to competing effects of creep relaxation, cavitation, and crack growth. More recent models have considered time-dependent stress variations in creep-crack growth by using the $C(t)$ integral as the crack-growth driving-force parameter.[17,18] For small-scale creep conditions, the near-tip transient stress, σ_{ij}, and strain rate, $\dot{\varepsilon}_{ij}$, fields ahead of a stationary crack after a short time following the application of the applied load are described by the Riedel and Rice (RR) field[24] as

$$\sigma_{ij} = \left(\frac{C(t)}{BI_n r}\right)^{1/(n+1)} \tilde{\sigma}_{ij}(\theta;n) \tag{1}$$

$$\dot{\varepsilon}_{ij} = B\left(\frac{C(t)}{BI_n r}\right)^{n/(n+1)} \tilde{\varepsilon}_{ij}(\theta;n) \tag{2}$$

where $\tilde{\sigma}_{ij}(\theta)$ and $\tilde{\varepsilon}_{ij}(\theta)$ are normalization functions, and B and n are material constants in the constitutive equation for creep strain rate, $\dot{\varepsilon}$, represented by

$$\dot{\varepsilon} = \dot{\sigma}/E + B\sigma^n \tag{3}$$

for uniaxial loading. The rate of crack-tip opening, $\dot{\delta}$, is then given by

$$\dot{\delta}_i = 2B\left(\frac{C(t)}{BI_n}\right)^{n/(n+1)} r^{1/(n+1)} \tilde{u}_i(\theta;n) \tag{4}$$

with

$$C(t) = (1 - \nu^2)K^2/[(n + 1)Et] \tag{5}$$

for short-time creep, and $C(t) = C^*$ for steady-state creep. In Eqs. (4) and (5), E is Young's modulus, ν is Poisson's ratio, and $\tilde{u}_i(\theta;n)$ is a normalization function.

The near-tip stress and strain fields calculated for a growing creep crack differ substantially from those calculated for a stationary crack. Previously, Hui and Riedel[25] showed that the near-tip behavior of a creep crack in materials with $n < 3$ is dominated by the elastic singularity; as a consequence, creep-crack growth in these materials cannot attain the steady-state condition. On the other hand, the Hui and Riedel near-tip stress and strain fields for a steady-state growing

R. Raj—contributing editor

Manuscript No. 197952. Received November 21, 1989; approved June 12, 1990.

Supported by the Air Force Office of Scientific Research through Contract No. F49620-88-C-0081.

*Member, American Ceramic Society

creep crack in materials with $n > 3$ are[25,26]

$$\sigma_{ij} = \alpha_n \left(\frac{\dot{a}}{EBr}\right)^{1/(n-1)} \tilde{\sigma}_{ij}(\theta) \tag{6}$$

$$\varepsilon_{ij} = \frac{\alpha_n}{E}\left(\frac{\dot{a}}{EBr}\right)^{1/(n-1)} \tilde{\varepsilon}_{ij}(\theta) \tag{7}$$

where α_n is a numerical constant depending on n and $\dot{a}$ is the crack velocity.

A peculiar feature of the Hui and Riedel (HR) field is that the amplitudes of the stress, strain, and crack-tip opening displacement are uniquely determined by the crack velocity. Therefore, the crack-tip stress intensity is related to the crack length, specimen geometry, and loading conditions only through a fracture criterion. A critical fracture strain criterion was suggested;[27] it leads to the critical crack-tip fracture strain being proportional to $\dot{a}^{1/(n-1)}$. In this case, crack growth is inherently unstable since an increase in velocity leads to an increase in crack-tip strain.

Although considerable progress has been made through the above modeling efforts, the relevancy of the $C(t)$, C^*, and the recently proposed C_t[28,29] parameters for correlating creep-crack growth are still in question, even in the metallic systems for which they were originally developed. Since crack propagation should preferably be tied to the near-tip fields, determination of the proper near-tip fields is considered essential to improved understanding and predictive capabilities in creep-crack growth. This paper describes an experimental study aimed at measuring the displacement and strain fields associated with a creep crack growing in a glass-ceramic. The results of the study are described and then used to determine the validity of present models.

II. Experimental Procedure

(1) Material

A magnesium aluminosilicate glass-ceramic† was used throughout this study. The microstructure of this material consisted of fine (~0.5-μm diameter) cordierite crystallites surrounded by a thin continuous amorphous grain-boundary phase.[30] This material is thus believed to be representative of the many liquid-phase-sintered ceramics. Previous characterization of this glass-ceramic has indicated that the grain-boundary phase begins to soften at around 600°C.[31,32] These experiments also demonstrated that, once the amorphous phase starts to soften, deformation occurs by a combination of grain-boundary sliding and cavitation. The creep exponent, n, of the cordierite glass-ceramic was ≈2,[30] which was somewhat higher than the n value of unity observed in a lithium aluminosilicate (LAS) glass-ceramic,‡[33,34] but was consistent with an n value of 1.5 to 2.2 reported for other LAS glass-ceramics.[35]

(2) Crack-Growth Procedures

Single-edge-notched (SEN) specimens were machined from the glass-ceramic. The dimensions of the test specimens are indicated in Fig. 1. Following machining, both faces of the specimens were polished to a 0.05-μm finish and then chemically etched to reveal surface features. Sharp cracks were introduced into the specimens by compression–compression fatigue precracking,[36] which was performed at room temperature using a stress intensity range of 12 MPa·m$^{1/2}$ and an R ratio of 0.1.

Following fatigue precracking, the SEN specimens were coated with gold to provide a conductive surface and tested in a scanning electron microscope equipped with a high-temperature hydraulic loading stage. The specimens were

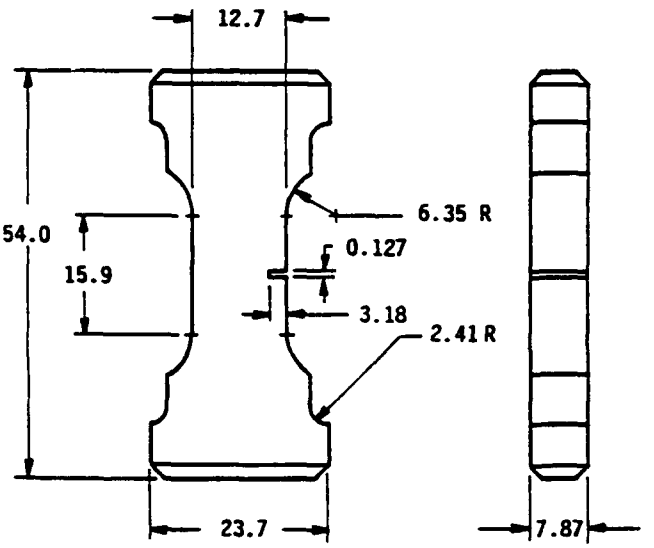

Fig. 1. Schematic of the specimen geometry used for the creep-crack growth experiments. All dimensions are listed in millimeters.

heated to the desired operating temperature while being held under a nominal tensile preload of approximately 0.1 MPa·m$^{1/2}$. Once the specimen temperature had stabilized, the tensile load on the specimen was increased to provide the desired applied Mode I stress-intensity factor. The Mode I stress-intensity factor, K, for the SEN specimens was calculated from[37]

$$K = \sigma(\pi a F)^{1/2} \tag{8}$$

$$F = 1.25/[1 - 0.7(a/w)^{1.5}]^{0.5}$$

where σ is the applied stress, a is the crack length, and w is the specimen width. Subsequent creep-crack propagation was performed under various K levels.

(3) Displacement and Strain Measurement

Photographs of the crack-tip region were taken at 15-min intervals during the creep-crack growth experiments. These photographs, at magnifications ranging from 400× to 2000×, were used to determine crack velocities, crack openings, and the displacements and strains around the crack-tip region. The in-plane displacements associated with a given increment of crack growth were determined by analyzing photographs of the crack-tip region taken immediately before and after the growth increment using a machine vision-based stereoimaging technique.[38] This procedure allowed determination of the strain tensor, ε_{xx}, ε_{yy}, and ε_{xy}.[39] The principal strains and maximum shear strains were then computed using the Mohr circle construction. Crack-opening displacements (CODs) were calculated from the relative displacements of points located on either side of the crack. It should be noted that all of the displacements, crack openings, and strain fields presented in this paper are associated with a relatively small time increment (≈15 min). Total accumulated openings and strains have yet to be determined. All the crack-tip strain and COD measurements were obtained from a single specimen.

III. Results

(1) Crack Growth at 700°C

A nominal Mode I creep crack was grown from the fatigue precrack by heating the glass-ceramic to 700°C and then loading the crack to an applied stress intensity of 0.8 MPa·m$^{1/2}$. Under these temperature and stress-intensity conditions, a creep crack initiated from the fatigue precrack and grew in a more or less stable manner. Propagation of the crack was

†Corning No. 9606, Corning Glass Works, Corning, NY.
‡Corning No. 9608, Corning Glass Works.

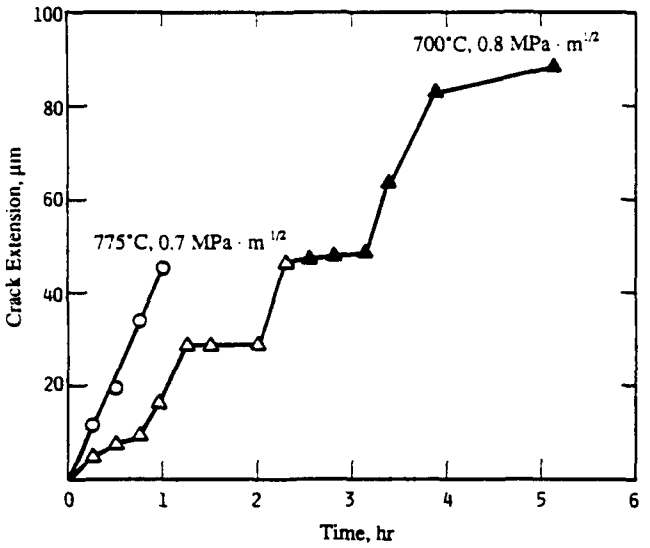

Fig. 2. Crack extension versus time plot illustrating the creep-crack growth behavior observed at 700°C and 0.8 MPa · $m^{1/2}$ and at 775°C and 0.7 MPa · $m^{1/2}$.

characterized over a 5-h period. A plot of the crack extension that occurred during this time period is provided in Fig. 2. Although alternating periods of rapid extension and slow extension are apparent, the average growth rate observed during the period was 0.3 μm/min.

Propagation of the creep crack occurred in a nonplanar manner, as shown in Fig. 3, resulting in a mixed Mode I and II character. The angle of crack deflection, ϕ, ranged from 0° to 50°. For this mixed-mode type of crack it was convenient to determine the effective rate of crack-opening displacement, $\dot{\delta}_{eff}$, defined as

$$\dot{\delta}_{eff} = [(\dot{\delta}_1)^2 + (\dot{\delta}_2)^2]^{1/2}$$

where $\dot{\delta}_1$ and $\dot{\delta}_2$ are the Mode II and I crack-opening displacement rates, respectively. Note that the subscripts 1 and 2 refer to the 1-axis (x-axis) and 2-axis (y-axis), respectively. The crack-opening displacement rates, $\dot{\delta}_{eff}$, for four different periods during the initial growth of the crack are plotted versus distance behind the crack tip in Fig. 4. Three major observations can be made from these $\dot{\delta}_{eff}$ results. First, at relatively short times $\dot{\delta}_{eff}$ increased with increasing distance from the tip. Second, once the crack had been propagating for approximately 110 min, a relatively stable condition developed in which $\dot{\delta}_{eff}$ was independent of distance over the 4- to 40-μm distance behind the crack tip for which $\dot{\delta}_{eff}$ measurements were obtained. Third, $\dot{\delta}_{eff}$ decreased with time during the transient period between initiation of stable creep-crack growth and the development of the r-independent regime. This behavior is better illustrated by the $\dot{\delta}_{eff}$ versus time plot in Fig. 5, which indicates that the rate of crack opening measured at a constant distance behind the crack tip slowly decreased during the first 100 min of creep-crack growth, after which time a relatively stable opening rate was maintained.

In addition to the COD measurements, displacement fields near the tip of the creep cracks were also determined. A typical displacement field indicating the initial position and both the magnitude and the direction of displacement of each of a rectangular array of reference points is shown in Fig. 6. A plot of the strains associated with creep-crack growth is shown in Fig. 7 in terms of the Mohr circles of strains. In all instances, relatively narrow regions of high strain were observed emanating from the tip of the propagating creep crack. The development of creep damage in these high-strain regions has been inferred from the observation that subsequent crack propagation invariably occurred through the regions of high strain.

Creep cracks that had been propagating for less than 110 min exhibited the $r^{-n/(n+1)}$ dependence that is predicted by the (RR) field[24] for stationary creep cracks, where r is the radial distance from the crack tip and n is the power-law creep exponent. A plot of incremental effective strain, $\Delta\varepsilon_{eff}$,

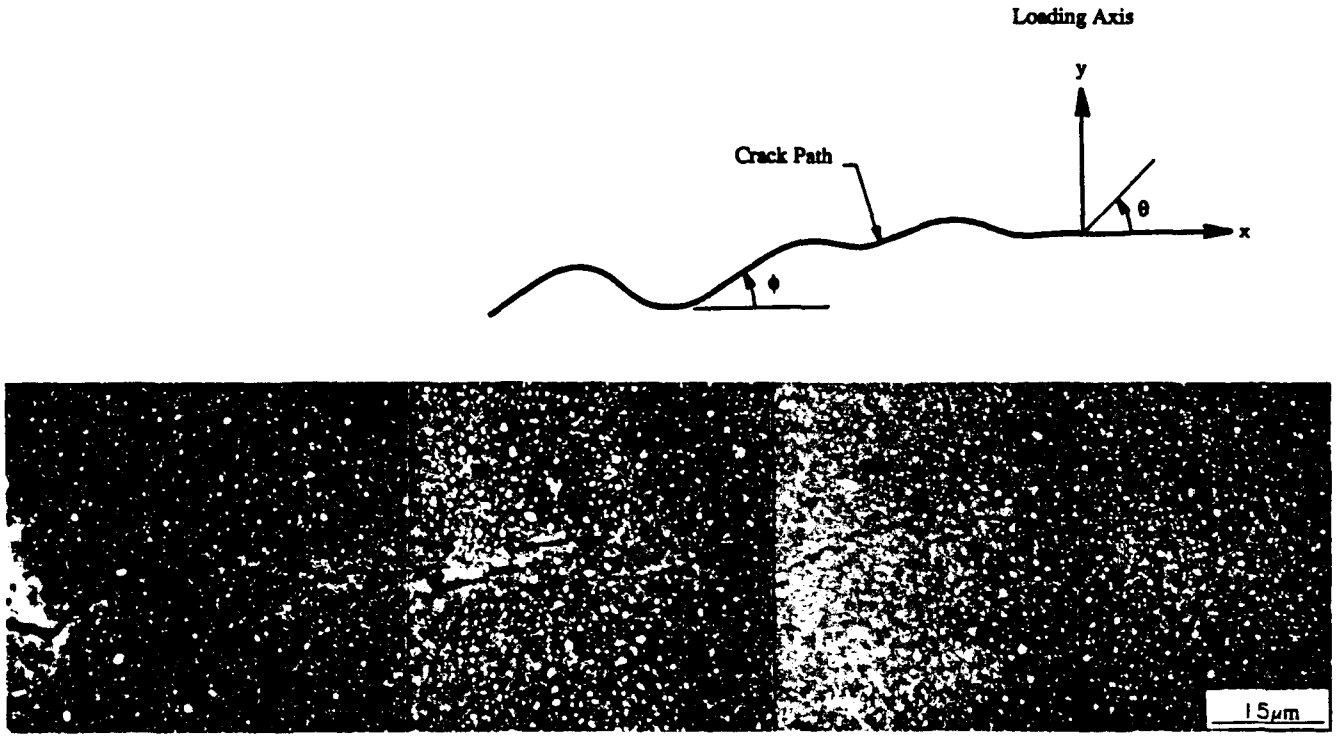

Fig. 3. SEM micrograph illustrating the morphology of the creep crack. Loading direction is vertical, while the macroscopic crack-growth direction is from left to right. Angle of crack deflection is denoted by ϕ.

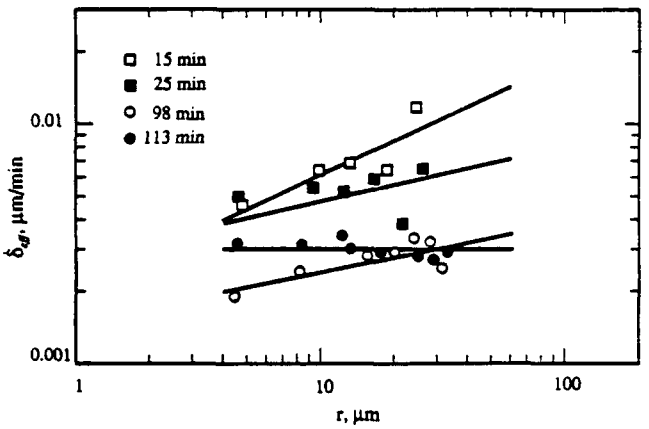

Fig. 4. Plot of effective crack-opening displacement rate, $\dot{\delta}_{eff}$, versus distance behind the crack tip, r, for various times after the initiation of creep-crack growth.

defined as

$$\Delta\varepsilon_{eff} = \left(\frac{2}{3}\Delta\varepsilon_{ij}\,\Delta\varepsilon_{ij}\right)^{1/2}$$

for a crack that had been propagating for 25 min is provided in Fig. 8 which shows a power-law fit to all data points for three different values of the angle, θ, measured from the tip of the creep crack, where θ is defined in Fig. 3. At times longer than 100 min, the radial dependence disappeared along the crack plane, $\theta = 0$, for distances of up to 40 μm ahead of the crack tip, as shown in Fig. 9. The narrow band of almost constant strain magnitude can be seen clearly in the plot of equal maximum shear–strain contours of Fig. 10. The loss of r dependence in the near-tip strain field occurred at the same time as the loss of r dependence in the rate of crack-opening displacement. It should also be noted that, even though the creep crack was propagating in a nominal Mode I condition, large shear components were present in the high-strain region directly ahead of the crack tip. A plot showing the shear–strain components associated with crack growth is shown in Fig. 11.

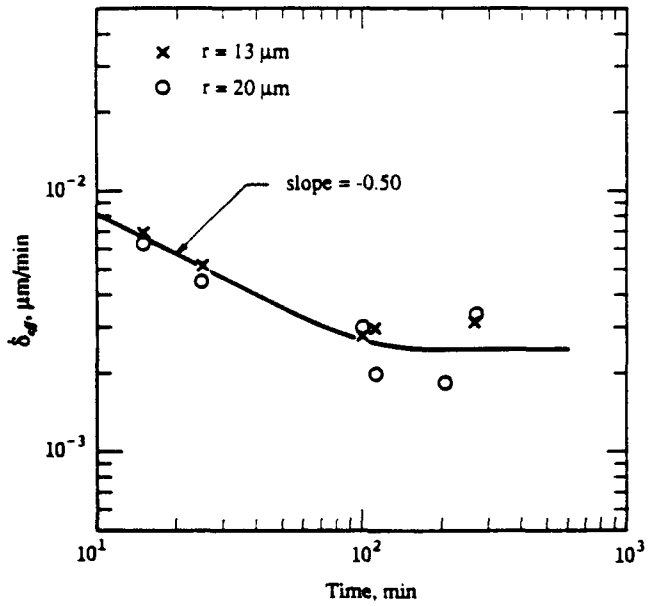

Fig. 5. Plot of effective crack-opening displacement rate, $\dot{\delta}_{eff}$, versus time illustrating the evolution of the opening rate as measured from the start of creep-crack growth.

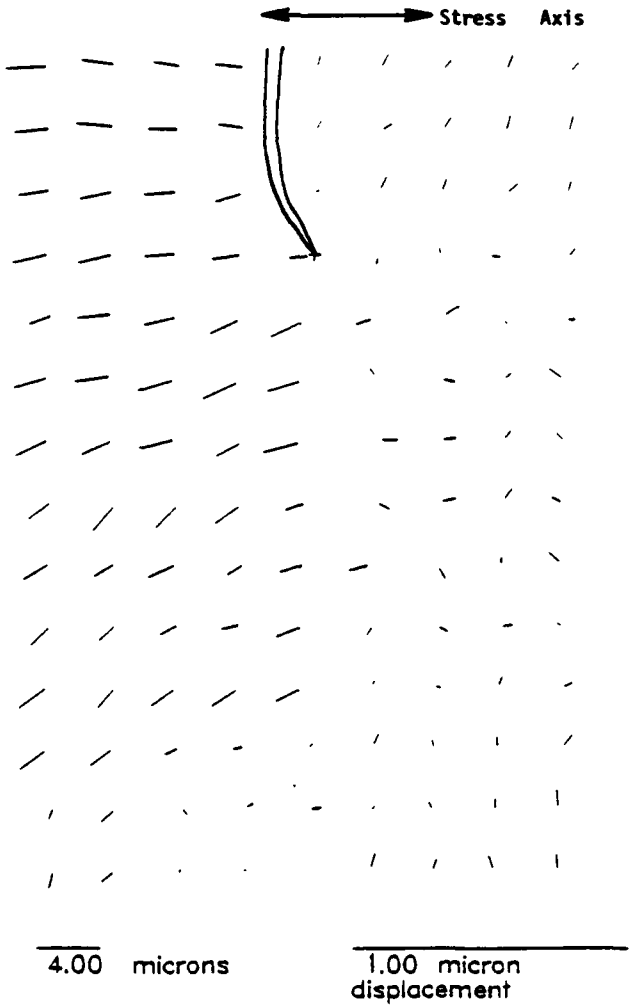

Fig. 6. Displacements observed around the tip of a creep crack propagating in the glass-ceramic after 98 min of creep at 700°C and 0.8 MPa · $m^{1/2}$. Both the magnitudes and the directions of the displacements are indicated.

(2) Crack Growth at 775°C

After propagating the crack for 5 h at 700°C and 0.8 MPa · $m^{1/2}$, the stress intensity was reduced to 0.7 MPa · $m^{1/2}$ and the temperature was increased to 775°C. These conditions were maintained for 1 h. The crack extension that occurred during this period is shown in Fig. 2. Fairly stable propagation was observed with an average crack growth rate of 0.75 μm/min. A typical plot of the maximum shear–strain contours obtained during growth at 775°C and 0.7 MPa · $m^{1/2}$ is shown in Fig. 12. The presence of narrow high-strain regions exhibiting relatively constant strain amplitude for large distances ahead of the crack were observed, just as at 700°C and 0.8 MPa · $m^{1/2}$ for times greater than 110 min. Effective crack-opening displacement rates independent of distance behind the crack at all but the very near-tip region were also observed, as they had been at 700°C.

Following the 60-min growth period at 0.7 MPa · $m^{1/2}$, the stress intensity was lowered to 0.6 MPa · $m^{1/2}$ and held for 80 min. The crack, which had been propagating at 0.75 μm/min at 0.7 MPa · $m^{1/2}$, arrested[9] almost immediately at 0.6 MPa · $m^{1/2}$, indicating that the stress intensity had been reduced below the threshold for crack growth. Although no

[9]Resolution considerations indicate that the absence of discernible crack propagation over an 80-min period is equivalent to a growth rate of less than 0.01 μm/min.

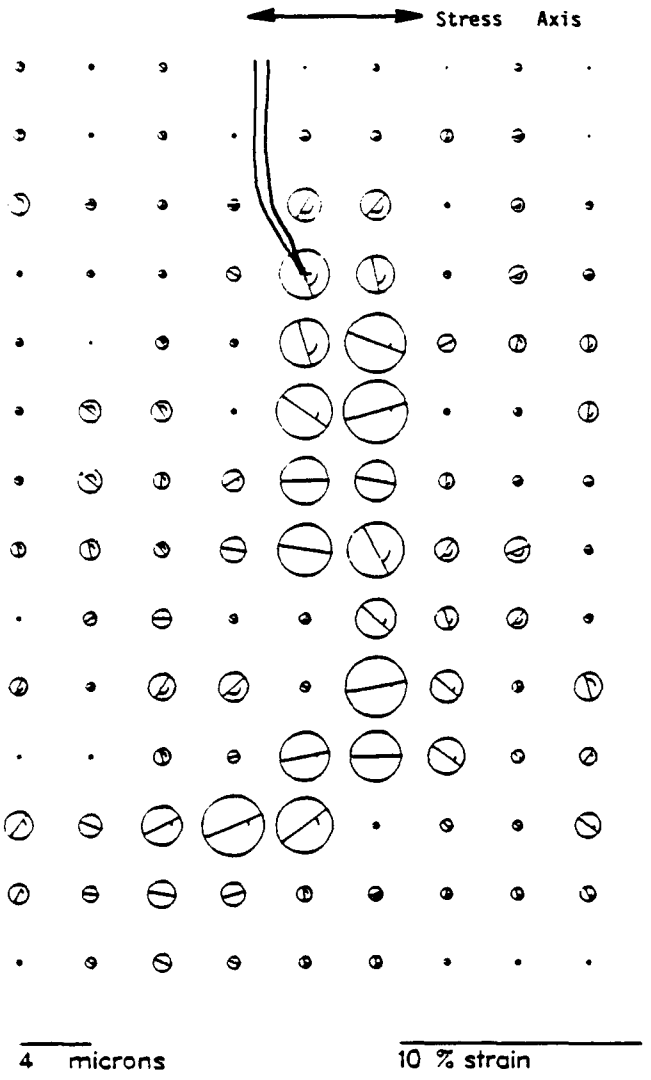

Fig. 7. Strains obtained from the displacements in Fig. 6. Strains are represented by Mohr circles indicating both the magnitude and the direction of the maximum shear strains.

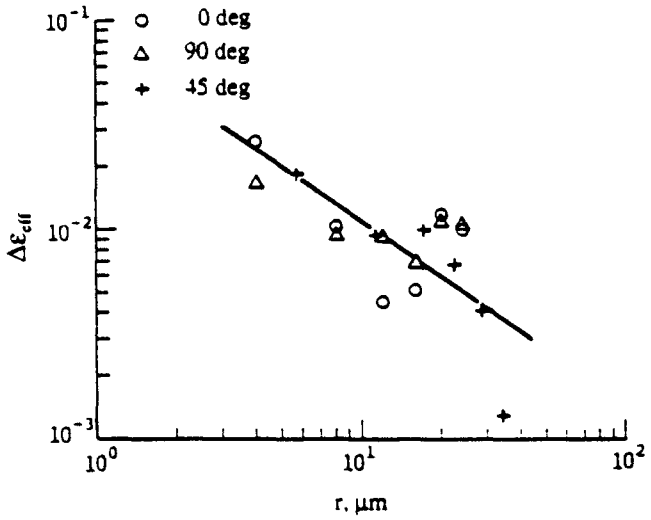

Fig. 8. Radial dependence of the incremental effective strain, $\Delta\varepsilon_{eff}$, at $\theta = 0°$, 45°, and 90° for a creep crack that had been propagating for 25 min.

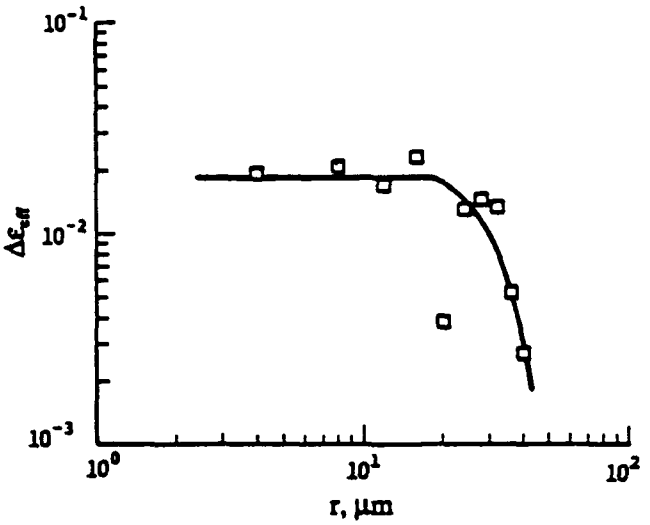

Fig. 9. Radial dependence of the incremental effective strain, $\Delta\varepsilon_{eff}$, at $\theta = 0°$ for a creep crack that had been propagating for 113 min.

forward movement of the crack tip was observed, considerable opening of the crack flanks did occur. A plot of the measured effective crack-opening rate for the arrested crack is presented in Fig. 13, along with similar measurements for a propagating crack. It is obvious from these data that $\dot{\delta}_{eff}$ for the arrested crack was still 50% of that for the crack propagating at 0.75 μm/min.

As one would expect, the continued opening observed for the arrested crack was associated with the accumulation of strain in the near-tip region. However, unlike the well-organized regions of high-strain accumulation that were present in front of growing cracks, the creep-strain accumulation around the arrested crack was distributed throughout a number of isolated areas. A comparison of the strain field associated with a propagating creep crack with that of an arrested creep crack is shown in Fig. 14.

Following the 80-min arrest period at 0.6 MPa·m$^{1/2}$, the stress intensity was increased to 0.7 MPa·m$^{1/2}$. The increase in stress intensity resulted in renewal of crack growth. Measurement of the crack velocity over a 60-min period resulted in a measured growth rate of 0.75 μm/min, thus, duplicating the original growth period at 0.7 MPa·m$^{1/2}$.

IV. Discussion

(1) Comparison of Theory and Experiment

The effective crack-opening displacement rate, $\dot{\delta}_{eff}$, and the effective creep rate, $\dot{\varepsilon}_{eff}$, associated with the RR field[24] can be expressed as

$$\dot{\delta}_{eff} \propto K^{2s} t^{-s} r^{m} \tag{9}$$

$$\dot{\varepsilon}_{eff} \propto K^{2s} t^{-s} r^{-s}$$

where

$$s = n/(n+1) \tag{10}$$

and

$$m = 1/(n+1) \tag{11}$$

The exponents m and s have been determined from the slopes of crack-opening displacement rate versus distance, r, and time of creep, t, shown in Figs. 4 and 5, respectively; their values are summarized in Table I. The experimental values of

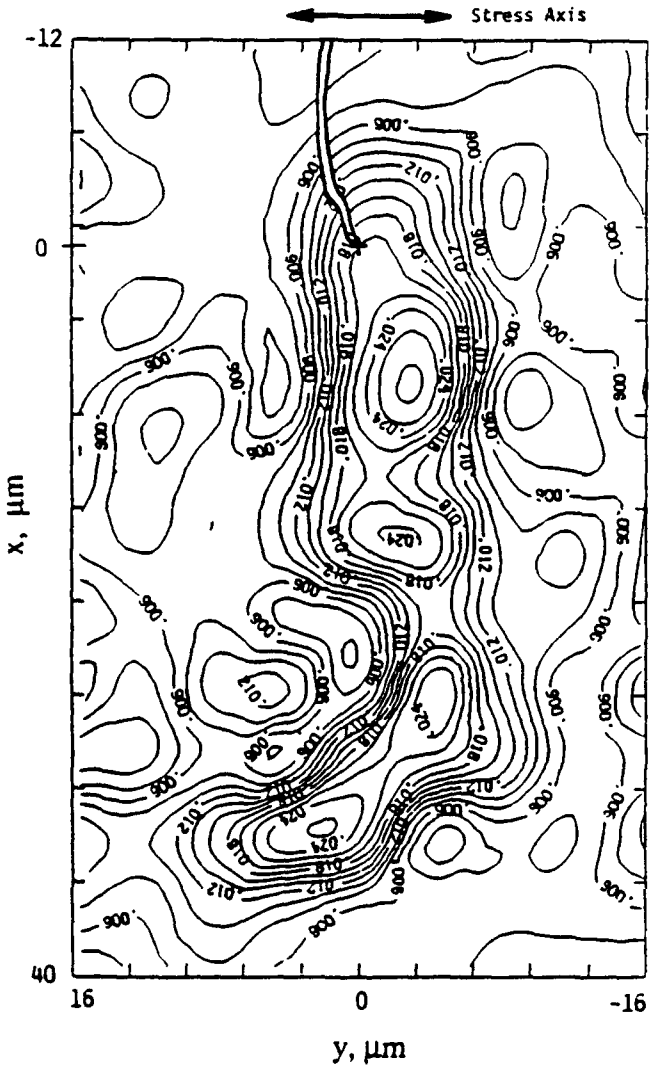

Fig. 10. Contours of equal maximum shear strain associated with creep-crack growth at 700°C and 0.8 MPa·m$^{1/2}$ after 98 min of creep.

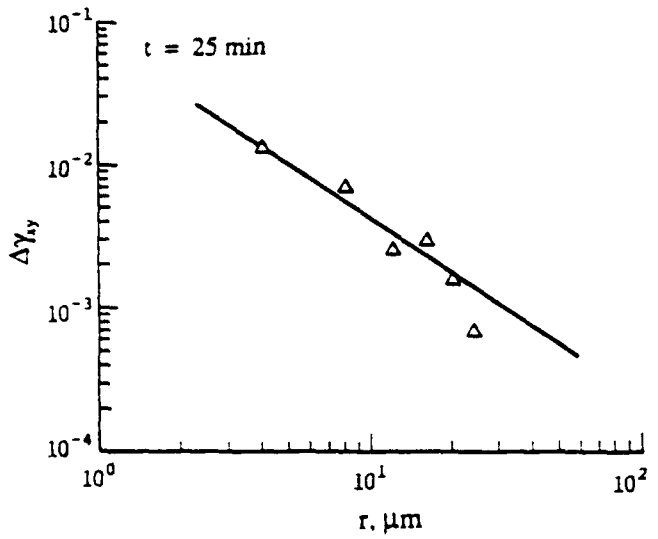

Fig. 11. Radial dependence of the incremental shear strain, $\Delta\gamma_{xy}$, observed directly in front of, $\theta = 0°$, a propagating creep crack after 25 min of creep.

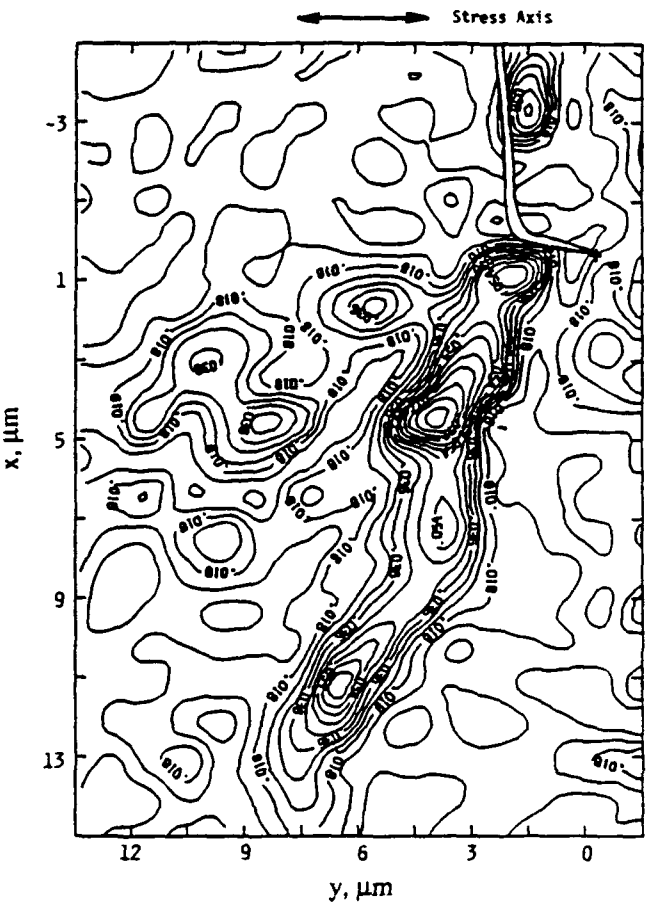

Fig. 12. Contours of equal maximum shear strain associated with creep-crack growth at 775°C and 0.7 MPa·m$^{1/2}$ after 1 h of creep.

m and s measured at short creep time (≈15 min) are 0.47 and 0.50, respectively. In comparison, a value of $s = 0.65$ is obtained from the plot of $\Delta\varepsilon_{eff}$ vs r in Fig. 8. Considering the large scatter in the experimental data, these values of m and s are consistent with the theoretical values of $m = 0.33$ and $s = 0.67$ computed based on Eqs. (10) and (11) using $n = 2$ (Ref. 30) for the creep exponent of the glass-ceramic. In addition to the RR theory, the observed value of s of 0.50 to 0.65 can possibly be explained in terms of the elastic field. However, the elastic field cannot explain the experimental observation of decreasing values of $\dot{\delta}_{eff}$ with increasing time of creep shown in Figs. 4 and 5. Since this type of time-dependent crack-opening behavior is a unique characteristic of the RR field, it can be concluded, based on the crack-opening displacement rate and the strain-rate data, that the creep crack in the glass-ceramic maintained many of the aspects of the RR field for a stationary crack during its initial stages of propagation.

As the creep time was increased, a process zone developed ahead of the crack tip and the RR-type field expanded to lie at a greater distance from the crack tip. This is illustrated by the plots of effective strain rate versus distance from the crack tip in Fig. 15 for $t = 268$ min and $\theta = 0°$. At relatively large distances from the crack tip ($r > 20$ μm), the effective strain rate which was obtained by dividing $\Delta\varepsilon_{eff}$ by Δt exhibited the RR-type behavior. The measured slopes within this region ranged from 0.45 to 0.77 as creep time varied from 25 to 268 min as tabulated in Table II. Within the process zone and at small values of r ($r < 20$ μm), the dependence of $\dot{\varepsilon}_{eff}$ on r deviated from that predicted by the RR field, however. In particular, the value of s decreased from 0.65 to 0 for $\theta = 0°$, as shown in Fig. 15. Similar decreases in the value of s from 0.5 to 0 with increasing time of creep are shown in the plots of

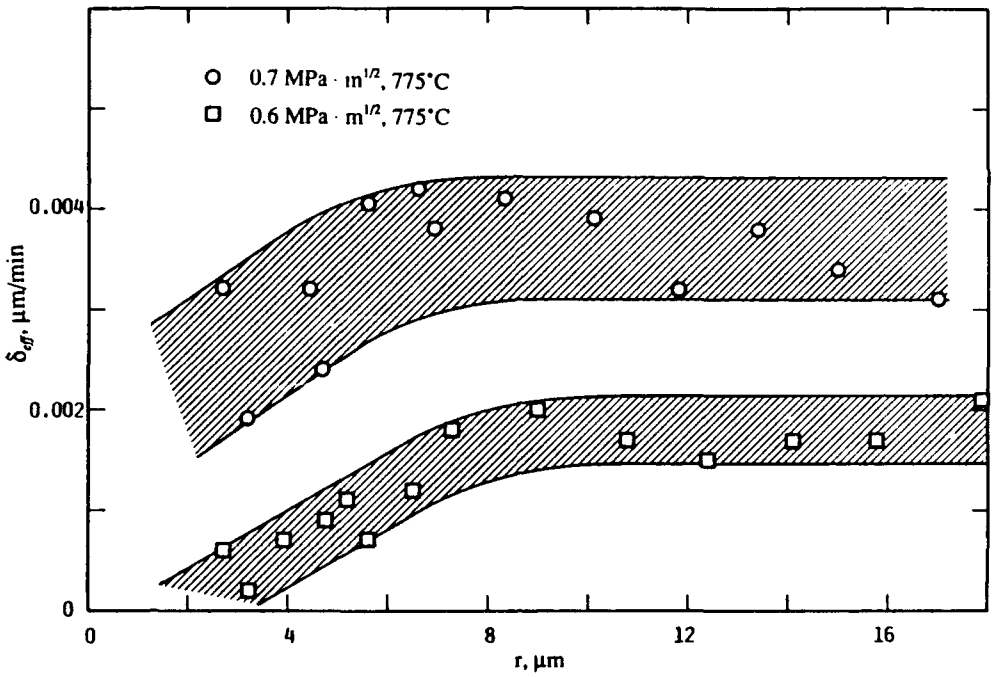

Fig. 13. Comparison of the effective crack-opening displacement rates for a growing crack (0.7 MPa · $m^{1/2}$, above K_{th}) and an arrested crack (0.6 MPa · $m^{1/2}$, below K_{th}) after 60 and 80 min of creep, respectively.

$\dot{\delta}_{eff}$ vs r in Fig. 4 and also from Table I. In addition to being relatively independent of r, the values of $\dot{\delta}_{eff}$ and $\dot{\varepsilon}_{eff}$ within the process zone decreased with increasing creep time and eventually both became constant values when $t \geq 100$ min (see Fig. 5). These results indicate that steady-state creep-crack growth prevailed at times exceeding ≈100 min.

The observation of steady-state crack growth in a creeping solid with a power-law creep exponent of ≈2 contradicts the Hui and Riedel theory,[25] which predicts that steady-state creep-crack growth in materials with $n < 3$ is not possible because the creep crack is dominated by the elastic singularity. Neither domination by the elastic singularity nor the absence of steady-state crack growth is supported by the current results. The discrepancies between theory and experiment are not surprising. The Hui and Riedel model does not adequately treat the effects of either stochastic grain-boundary sliding or creep cavitation, both of which are prominent in the process zone associated with a growing creep crack in the glass-ceramic.[40] It is also possible that the intermittent growth behavior affected the near-tip region, with the crack behaving as a stationary crack in some time increments and as a growing crack in others. The possible effects of the intermittent growth behavior have not yet been determined.

(2) Role of Microstructure in the Creep-Crack Growth Process

The creep crack in the glass-ceramic exhibited moderate deflections even though the crack was nominally straight and of the Mode I type. Figure 3 illustrates that the angle, ϕ, of crack deflection could be as large as 20° to 50°. Thus, it is not surprising that both Mode I and II crack-opening displacements were observed, as shown in Fig. 16. Additionally, relatively large shear-strain-rate components were observed within the process zone ahead of the crack tip, indicating the presence of Mode II loading locally near the crack tip. One possible explanation for the Mode II component is the local deflection and mixed-mode of the cracking mode associated with the saw-tooth crack. Using the procedures described in Refs. 40–42, the amount of Mode II opening that would be associated with the observed degree of crack deflection is found to be significantly lower than the observed Mode II components, as shown in Fig. 16. Thus, crack deflection does not appear to be solely responsible for the large Mode II openings nor the large shear strains. Another possible explanation is that crack-tip deformation in the glass-ceramic is dominated by sliding of grain boundaries that contain a viscous glassy phase, which is an inherently stochastic shear process, and the experimental crack-tip shear strain and opening displacement rates are reflections of this process. Grain-boundary sliding, in turn, can lead to buildup of local tensile stresses which can cause the nucleation, growth, and coalescence of cavities within the grain-boundary glassy phase.[43,44] Since there is no shear stress immediately ahead of the tip of a Mode I crack, sliding and cavitation would have to occur at inclined grain boundaries, leading to the saw-tooth-like crack path shown in Fig. 3. Further work is needed to determine the validity of this hypothesis. Note, however, that unaccountably high levels of shear strain and Mode II opening were not observed in similar measurements of a creep crack in a material that deformed predominantly by dislocation creep.[42]

(3) Implications

The nucleation and growth of creep cavities in ceramics can be facilitated by either normal or shear stresses. The observations of a saw-tooth crack path and relatively large shear components in the crack-tip-opening displacement and strain rates in the glass-ceramic indicate that shear stresses, and by implication grain-boundary sliding, are important in creep cavitation of this material. Almost all of the creep-crack growth models in the literature consider creep-cavity growth to be driven by normal stresses; with few exceptions,[43,45] the contributions of shear stress and grain-boundary sliding are generally ignored. The applicability of these crack-growth models to the glass-ceramic of this study (and possibly other ceramics) is therefore suspect; modification of these models is required to include the contributions of shear stress and grain-boundary sliding to cavitation and crack propagation.

The RR field was originally derived for straight cracks subject to individually applied Mode I, II, or III loading. Despite the saw-tooth-like crack path, the RR field appears to be applicable for the glass-ceramic in the short-time creep regime. Crack deflection changed the near-tip strain-rate distribution and the modes of crack-tip opening of the creep crack, but the amplitude of the near-tip field was still characterized by

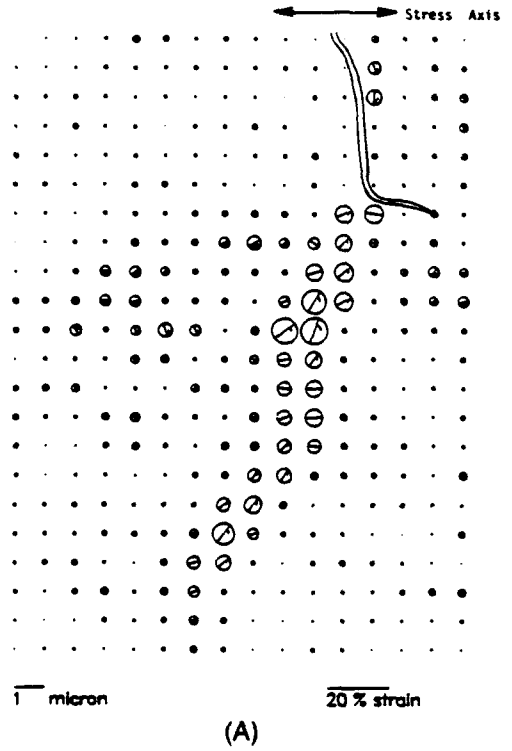

Fig. 14. Strain distributions in the near-tip region of (A) a crack growing above threshold at 775°C and 0.7 MPa · $m^{1/2}$ and (B) a stationary crack below threshold at 775°C and 0.6 MPa · $m^{1/2}$.

Table I: Comparison of the Measured and the Predicted Values of the Radial and Time Exponents of the Crack-Opening Displacement Rate*

Time (min)	Measured values		Predicted values	
	s†	m‡	s	m
15	0.50	0.47	0.67	0.33
25	0.50	0.23	0.67	0.33
113	0	0.22	0§	0.33
128	0	0	0§	0.33
268	0	0	0§	0.33

*$\dot{\delta}_{yy} = K^{2n} t^{-1} r^{-m}$. †$s = n/(n+1)$. ‡$m = 1/(n+1)$. §Steady state.

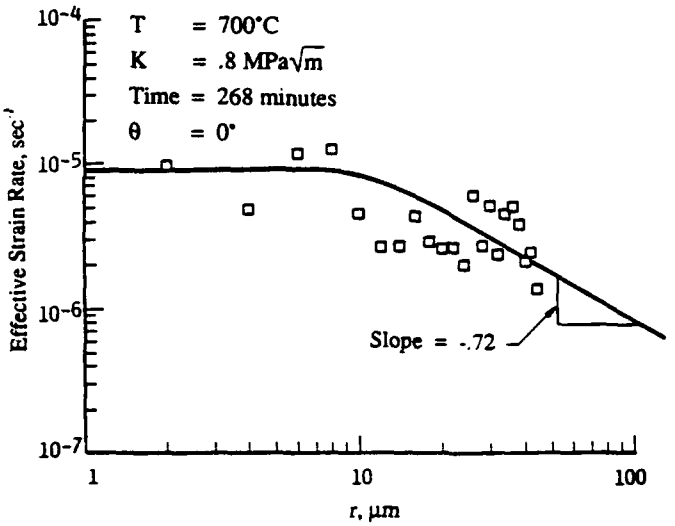

Fig. 15. Plot of effective strain rate versus distance, r, ahead of the crack tip showing that the effective strain rate is independent of r in the process zone ($r \leq 10$ μm) but exhibits the Riedel and Rice dependence at $r > 10$ μm.

the $C(t)$ integral. This suggests that the RR fields for mixed-mode creep cracks should have the same form as those suggested for mixed-mode elastic–plastic straight cracks or for branched cracks in an elastic–plastic field,[40,41] as discussed in Ref. 42.

Although it is clear that $C(t)$ controlled the near-tip field at short times, it does not appear that $C(t)$ controlled the crack growth rate in the glass ceramic. During the short-time regime in which $C(t)$ controlled the near-tip fields, $C(t)$ decreased with time, but the average crack growth rate remained relatively constant. A possible explanation is that the near-tip field and the damage zone were constrained by the remote K field such that the crack growth rate actually correlated with K, which remained constant during testing, in much the same manner as the slower creep processes in the surrounding matrix are often found to constrain cavitation in polycrystalline materials.[46]

Finally, comparison of the observed behaviors slightly above and slightly below the apparent stress-intensity threshold for creep-crack growth identifies a number of interesting aspects of the threshold. The presence of significant levels of crack-opening displacement and the continued accumulation of near-tip strain in fully arrested cracks certainly supports the widely held, although not highly enlightening, assumption that cracks loaded below the threshold stress intensity experience significant blunting. Perhaps more important is the observation that cracks loaded slightly below

Table II: Summary of the Measured Values of Radial Dependence of Effective Strain Rate*

Time of creep (min)	θ (deg)	Measured s†
25	0	0.73
	45	0.70
	90	0.65
113	0	0.53
	45	0.65
	90	0.69
173	0	0.62
	45	0.45
	90	0.50
268	0	0.72
	45	0.77
	90	0.56

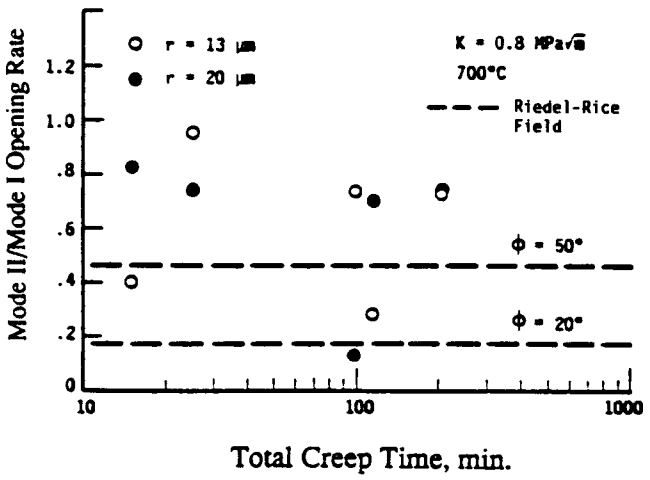

Fig. 16. Comparison of measured and calculated ratios of Mode II to Mode I crack-opening displacement rates as a function of creep time for the pyroceram glass-ceramic.

threshold tended to accumulate strain in small localized regions spaced throughout the near-tip region, while cracks loaded slightly above threshold accumulated strain in highly organized channels directly ahead of the tip. Although these observations, in and of themselves, do not identify the critical process or processes that lead to a crack-growth threshold, they do suggest that the manner in which a creep crack accumulates strain and damage may be an important factor in the definition of a threshold.

V. Conclusions

The following conclusions regarding creep-crack growth in the pyroceram glass-ceramic can be drawn from the results of this work.

(1) Crack deflection and stable crack growth exhibiting both Mode I and II components were observed in the glass-ceramic despite a creep exponent of ≈ 2.

(2) Both the time and radial dependence of the near-tip strain and crack-opening displacement were observed to fit the predictions of the Riedel and Rice field when the time of creep and the amount of crack extension were small.

(3) At longer times and larger crack extensions, a localized shear zone formed directly ahead of the crack tip. Subsequent crack extension tended to follow this shear zone and neither the rate of crack-opening displacement nor the strain-rate distribution within the shear zone could be described by the Riedel and Rice field for stationary cracks or the Hui and Riedel field for growing cracks.

(4) Although $C(t)$ controlled the near-tip fields at short times, it does not appear that $C(t)$ controlled the crack growth rate. The parameter controlling the growth rate has not yet been identified.

(5) Unusually high Mode II openings and shear strains were associated with the growing creep cracks. Since none of the available theoretical treatments can account for such high shear components, it has been hypothesized that they are the result of the unique creep deformation mechanisms exhibited by this and other ceramic materials.

(6) Crack blunting was observed at stress intensities below the threshold for crack growth. Development of an extended, localized shear zone ahead of the crack tip, such as observed during crack growth, was not observed during the blunting process.

Acknowledgment: The encouragement by the Program Manager of the Air Force Office of Scientific Research, Dr. L. J. Schioler, is acknowledged

References

[1]A. G. Evans and F. F. Lange, "Crack Propagation and Fracture in Silicon Carbide," *J. Mater. Sci.*, **10** [10] 1659–64 (1975).

[2]F. F. Lange, "High-Temperature Strength Behavior of Hot-Pressed Si_3N_4: Evidence for Subcritical Crack Growth," *J. Am. Ceram. Soc.*, **57** [2] 84–87 (1974).

[3]M. G. Mendiratta and J. J. Petrovic, "Slow Crack Growth from Controlled Surface Flaws in Hot-Pressed Si_3N_4," *J. Am. Ceram. Soc.*, **61** [5–6] 226–30 (1978).

[4]K. D. McHenry and R. E. Tressler, "Fracture Toughness and High-Temperature Slow Crack Growth in SiC," *J. Am. Ceram. Soc.*, **63** [3–4] 152–56 (1980).

[5]E. J. Minford and R. E. Tressler, "Determination of Threshold Stress Intensity for Crack Growth at High Temperature in Silicon Carbide Ceramics," *J. Am. Ceram. Soc.*, **66** [5] 338–40 (1983)

[6]H. G. Schmid, T. Haug, A. Bornhauser, V. Gerold, and R. F. Pabst, "Crack Growth in Al_2O_3 with 3 wt% Glassy Phase"; pp. 631–41 in Deformation of Ceramics II. Edited by R. E. Tressler and R. C. Bradt. Plenum, New York, 1984.

[7]J. T. Barnby, "Crack-Tip Stresses under Creep Conditions," *Eng. Fract. Mech.*, **6** [4] 627–30 (1974).

[8]J. T. Barnby, "Crack Propagation During Steady-State Creep," *Eng. Fract. Mech.*, **7** [2] 299–304 (1975).

[9]K. C. To, "Phenomenological Theory of Subcritical Creep Crack Growth under Constant Loading in an Inert Environment," *Int. J. Fract.*, **11** [4] 641–48 (1975).

[10]S. Purnshothaman and J. K. Tien, "A Theory of Creep Crack Growth," *Scr. Metall.*, **10** [8] 663–66 (1976).

[11]R. Raj and S. Baik, "Creep Crack Propagation by Cavitation Near Crack Tips," *Met. Sci.*, **14** [8,9] 385–94 (1980).

[12]R. J. Dimelfi and W. D. Nix, "The Stress Dependence of the Crack Growth Rate During Creep," *Int. J. Fract.*, **13** [3] 341–48 (1977).

[13]W. D. Nix, D. K. Matlock, and R. J. Dimelfi, "A Model for Creep Fracture Based on the Plastic Growth of Cavities at the Tips of Grain-Boundary Wedge Cracks," *Acta Metall.*, **25** [5] 495–503 (1977).

[14]H. Riedel, "A Dugdale Model for Crack Opening and Crack Growth under Creep Condition," *Mater. Sci. Eng.*, **30**, 187–96 (1977).

[15]V. Vitek, "A Theory of Diffusion-Controlled Intergranular Creep Crack Growth," *Acta Metall.*, **26** [9] 1345–56 (1978).

[16]D. S. Wilkinson and V. Vitek, "The Propagation of Cracks by Cavitation: A General Theory," *Acta Metall.*, **30** [9] 1723–32 (1982)

[17]F. H. Wu, J. L. Bassani, and V. Vitek, "Transient Crack Growth under Creep Conditions Due to Grain-Boundary Cavitation," *J. Mech. Phys. Solids*, **34** [5] 455–75 (1986).

[18]F. Z. Li, A. Needleman, and C. F. Shih, "Creep-Crack Growth by Grain-Boundary Cavitation: Crack-Tip Fields and Crack Growth Rates under Transient Conditions," *J. Fract.*, **38** [4] 241–73 (1988).

[19]H. Riedel, "The Extension of a Macroscopic Crack at Elevated Temperature by the Growth and Coalescence of Microvoids"; pp. 504–19 in Creep in Structures. Edited by A. R. S. Ponter and D. R. Hayhurst. Springer Verlag, Berlin, FRG, 1981.

[20]C. Y. Hui and V. Banthia, "The Extension of Cracks at High Temperature by Growth and Coalescence of Voids," *Int. J. Fract.*, **25** [1] 53–67 (1984).

[21]R. M. McMeeking and F. A. Leckie, "An Incremental Crack Growth Model for High-Temperature Rupture in Metals"; pp. 699–704 in Advances in Fracture Research (Fracture 81), Vol. 2. Edited by D. Francois, Pergamon Press, New York, 1981.

[22]K. S. Chan, "The Constitutive Representation of High-Temperature Creep Damage," *Int. J. Plast.*, **4** [4] 355–70 (1988).

[23]H. Yin, M. Gao, and R. P. Wei, "Deformation and Subcritical Crack Growth under Static Loading," *Mater. Sci. Eng. A*, **119**, 51–58 (1989).

[24]H. Riedel and J. R. Rice, "Tensile Cracks in Creeping Solids," *J. Mech. Phys. Solids*, **29**, 35–49 (1981).

[25]C. Y. Hui and H. Riedel, "The Asymptotic Stress and Strain Field Near the Tip of a Growing Crack under Creep Conditions," *Int. J. Fract.*, **17** [4] 409–25 (1981).

[26]C. Y. Hui, "Steady-State Crack Growth in Elastic Power Law Creeping Materials"; pp. 573–93 in Elastic-Plastic Fracture, Vol. 1, ASTM STP 803. American Society for Testing and Materials, Philadelphia, PA, 1983.

[27]H. Riedel and W. Wagner, "The Growth of Macroscopic Cracks in Creeping Materials"; pp. 683–90 in Advances in Fracture Research. Proceedings of the Fifth International Conference on Fracture, Vol. 2. Edited by D. F. Cannes. Pergamon, New York, 1981.

[28]A. Saxena, "Creep Crack Growth under Non-Steady-State Conditions"; pp. 185–201 in ASTM STP 905. Edited by J. H. Underwood, R. Chait, C. W. Smith, D. P. Wilhem, W. A. Andrews, and J. C. Newman. American Society for Testing and Materials, Philadelphia, PA, 1986.

[29]C. P. Leung, D. L. McDowell, and A. Saxena, "Consideration of Primary Creep at a Stationary Crack Tip: Implication of the C_t Parameter," *Int. J. Fract.*, **36** [4] 275–89 (1988)

[30]T. I. Barry, L. A. Lay, and R. Morrell, "High-Temperature Mechanical Properties of Cordierite Refractory Glass Ceramics," *Proc. Br. Ceram. Soc.*, **24**, 67–84 (1975).

[31]J. Lankford, "Strength of Monolithic and Fiber-Reinforced Glass Ceramics at High Rates of Loading and Elevated Temperature," *Ceram. Eng. Sci. Proc.*, **9** [7–8] 843–52 (1988).

[32]J. Lankford, "Dynamic Compressive Fracture in Fiber-Reinforced Ceramic Matrix Composites," *Mater. Sci. Eng.*, **A107**, 261–68 (1989).

[33]R. Raj and C. K. Chyung, "Solution-Precipitation Creep in Glass Ceramics," *Acta Metall.*, **29** [1] 159–66 (1981)

[34]R. F. Cooper, D. L. Kohlstedt, and K. Chyung, "Solution-Precipitation

Enhanced Creep in Solid Liquid Aggregates Which Display a Non-Zero Dihedral Angle," *Acta Metall.*, **37** [7] 1759–71 (1989).

[35]E. M. Heuse and G. Partridge, "Creep Testing of Glass-Ceramics," *J. Mater. Sci.*, **9** [8] 1255–61 (1974).

[36]L. Ewart and S. Suresh, "Dynamic Fatigue Crack Growth in Polycrystalline Alumina under Cyclic Compression," *J. Mater. Sci. Lett.*, **5** [8] 774–78 (1986).

[37]T. G. F. Gray, "Convenient Closed Form Stress Intensity Factors for Common Crack Configurations," *Int. J. Fract.*, **13** [1] 65–75 (1977).

[38]E. A. Franke, D. J. Wenzel, and D. L. Davidson, "Measurement of Micro-Displacements by Machine Vision Photogrammetry (DISMAP)"; to be published in *Rev. Sci. Instrum.*

[39]D. R. Williams, D. L. Davidson, and J. Lankford, "Fatigue-Crack-Tip Plastic Strains by the Stereoimaging Technique," *Exp. Mech.*, **20** [4] 134–39 (1980).

[40]C. F. Shih, "Small-Scale Yielding Analysis of Mixed Mode Plane-Strain Crack Problems"; pp. 187–210 in Fracture Analysis, ASTM STP 560. American Society for Testing and Materials, Philadelphia, PA, 1974.

[41]S. Suresh and C. F. Shih, "Plastic Near-Tip Fields for Branched Cracks," *Int. J. Fract.*, **30** [4] 237–59 (1986).

[42]K. S. Chan, R. A. Page, and D. L. Davidson, "Near-Tip Behavior of Deflected Creep Cracks"; unpublished work.

[43]R. L. Tsai and R. Raj, "Creep Fracture in Ceramics Containing Small Amounts of a Liquid Phase," *Acta Metall.*, **30** [6] 1043–58 (1982).

[44]R. A. Page and K. S. Chan, "Stochastic Aspects of Creep Cavitation in Ceramics," *Metall. Trans. A.*, **18A** [11] 1843–54 (1987).

[45]V. Tvergaard, "Effect of Grain Boundary on Creep Constrained Diffusive Cavitation," *J. Mech. Phys. Solids*, **33** [5] 447–69 (1985).

[46]R. Raj and A. K. Ghosh, "Stress Rupture," *Metall. Trans. A*, **12A** [7] 1291–302 (1981). □

International Journal of Fracture **50**: 281–292, 1991.

Near-tip behavior of deflected creep cracks

K.S. CHAN, R.A. PAGE and D.L. DAVIDSON
Southwest Research Institute, San Antonio, Texas 78228-0510, USA

Received 30 October 1989; accepted 12 November 1990

Abstract. Near-tip displacement fields of a creep crack which exhibited moderate deflection from its initially mode I condition have been measured using the stereoimaging technique. From the measured displacement fields, near-tip strains and crack opening displacements (*CODs*) are obtained and compared with existing asymptotic solutions for stationary, deflected cracks. The comparison reveals that the near-tip strain field and *CODs* of a stationary deflected creep crack in stainless steel (creep exponent of 8) are of the Riedel–Rice type. The degree of mode mixity is also adequately predicted for the deflected crack. The results for stainless steel are compared with previous results for a glass-ceramic (creep exponent of 1.5), to assess the range of applicability of the RR field. Discrepancies between theory and experiment are discussed in terms of the dominant creep mechanism, which is dislocation creep for the stainless steel and grain boundary sliding for the glass-ceramic.

1. Introduction

It is well established that for power-law creeping materials, the stresses and strain rates asymptotically near the tip of a stationary crack are dominated by the creep term [1]. For small scale creep conditions, the near-tip strain rate, $\dot{\varepsilon}_{ij}$, ahead of a mode I stationary crack, shortly following the application of the external load, is described by the Riedel and Rice (RR) field [1], which is analogous to the Hutchinson [2], Rice, and Rosengren [3] (HRR) field for elastic-plastic materials. The RR fields for creep cracks can be obtained from the HRR fields for elastic-plastic cracks by replacing

1. the plastic strain term with the creep rate,
2. the crack-tip opening displacement with its rate, and
3. the J-integral with another contour-integral, $C(t)$, which is the analog of the J-integral for short time creep [1, 4].

For small scale creep, the creep zone is constrained by the surrounding elastic field and $C(t)$ is proportional to $(K^2/Et)^{n/(n+1)}$ [1], where K is the stress intensity factor, E is Young's modulus, t is the time of creep, and n is the creep exponent.

The dominance of the RR field for creep cracks has been recently observed experimentally in pyroceram, which is a glass-ceramic with a creep exponent of 1.5 and deforms at elevated temperature primarily by sliding along grain boundaries containing a viscous, glassy phase. In this study by Page et al. [5] the near tip creep rates were found to exhibit the RR-type field when the time of creep and the amount of crack extension were small. The time and radial dependence of the crack opening displacement rate were observed to be those of the RR field, as well. A surprise finding by Page et al. [5] was the observation of the development of a localized shear zone directly ahead of the creep crack. The strain distribution within this shear zone could not be described or explained on the basis of the RR field. Crack extension in the glass-ceramic tended to follow the shear zone within which creep damage appeared to accumulate. Since the predominant deformation mode in pyroceram at elevated temperature is

the sliding of grain boundaries containing a viscous glassy phase, it is possible that the shear zone could be the consequence of the grain boundary sliding. One means of resolving this issue is to compare the crack-tip behavior of the glass-ceramic with that of a creep crack in a material which does not contain glassy grain boundaries and deforms predominantly by dislocation creep.

The objective of this paper is to present experimental results of the near-tip creep rates and crack surface opening behavior of creep cracks in a 304 stainless steel tested at 600°C. At this temperature, the creep mechanism in smooth (uncracked) 304 stainless steel specimens is predominantly dislocation creep and grain boundary sliding is a significant contributor to the creep rate only at stresses less than 13 MPa [6]. Experimental results for the stainless steel will be compared first with asymptotic solutions for stationary cracks. They will then be compared with similar results from a glass-ceramic to determine whether or not the near-tip strain fields of creep cracks are influenced by the operative deformation mechanism. Since creep cracks in the 304 stainless steel are deflected cracks, the experimental crack-tip measurements will also be used to show that the RR fields are pertinent for mixed-mode stationary creep cracks.

2. Asymptotic near-tip fields for mixed mode stationary creep cracks

The crack-tip fields for mixed mode or deflected creep cracks have not been presented in the literature. It appears, however, that the analogy between creep and plasticity that has been used to obtain the fields for mode I creep cracks should also apply for mixed mode cracks. Consider a crack lying along the x-axis with the crack normal parallel to the y-axis, the crack-tip fields for this mixed mode I and II creep crack under small scale creep conditions could be obtained from those for similarly mixed mode elastic-plastic cracks under small-scale yielding [7–9] as follows:

$$\sigma_{ij} = \sigma_0 \left[\frac{C(t)}{\alpha \sigma_0 \dot{\varepsilon}_0 I_n r} \right]^{1/(n+1)} \tilde{\sigma}_{ij}(\theta; M^P, n), \tag{1}$$

$$\dot{\varepsilon}_{ij} = \alpha \dot{\varepsilon}_0 \left[\frac{C(t)}{\alpha \sigma_0 \dot{\varepsilon}_0 I_n r} \right]^{n/(n+1)} \tilde{\varepsilon}_{ij}(\theta; M^P, n), \tag{2}$$

$$\dot{u}_i = \alpha \dot{\varepsilon}_0 r \left[\frac{C(t)}{\alpha \sigma_0 \dot{\varepsilon}_0 I_n r} \right]^{n/(n+1)} \tilde{u}_i(\theta; M^P, n), \tag{3}$$

where the distance, r, and the angle, θ, are polar coordinates centered at the crack tip; E is Young's modulus; M^P is the plastic mixity factor; I_n is a dimensionless normalization parameter whose value depends on the stress state, creep exponent (n), and the plastic mixity factor, M^P; σ_0, $\dot{\varepsilon}_0$ and n are material constants in the constitutive equation for creep strain rate, $\dot{\varepsilon}$, represented by

$$\dot{\varepsilon} = \alpha \dot{\varepsilon}_0 \left(\frac{\sigma}{\sigma_0} \right)^n \tag{4}$$

for uniaxial loading. The rate of crack surface opening, $\dot{\delta}_i$, is then given by

$$\dot{\delta}_i = \alpha\dot{\varepsilon}_0 r\left[\frac{C(t)}{\alpha\sigma_0\dot{\varepsilon}_0 I_n r}\right]^{n/(n+1)}[\tilde{u}_i(-\pi; M^P, n) - \tilde{u}_i(\pi; M^P, n)], \tag{5}$$

with the amplitude of the crack-tip singularity, $C(t)$, given by [1]

$$C(t) = \frac{(1-\nu^2)K^2}{(n+1)Et}, \tag{6}$$

after a short time, t, of creep, with ν being the Poisson ratio. The normalization functions represented by $\tilde{\sigma}_{ij}$, $\tilde{\varepsilon}_{ij}$, and $\tilde{u}$ are functions of θ, M^P, and n; the values of these normalization functions have been given by Shih and co-workers [9] for the plane strain condition. Similar tables for the plane stress condition do not appear to be available. The value of M^P is related to the elastic mixity factor, M^e, which depends on the nominal mode I and II stress intensity factors.

For mixed mode I and II creep cracks, it is often more convenient to treat the creep rates in terms of an effective (or equivalent) creep rate, $\dot{\varepsilon}_{\text{eff}}$, which is related to the creep rate components by

$$\dot{\varepsilon}_{\text{eff}} = (\tfrac{2}{3}\dot{\varepsilon}_{ij}\dot{\varepsilon}_{ij})^{1/2}, \tag{7}$$

$$\dot{\varepsilon}_{\text{eff}} = \alpha\dot{\varepsilon}_0\left[\frac{C(t)}{\alpha\sigma_0\dot{\varepsilon}_0 I_n r}\right]^{n/(n+1)}\tilde{\varepsilon}_{\text{eff}}(\theta; M^P, n), \tag{8}$$

with

$$\tilde{\varepsilon}_{\text{eff}} = (\tfrac{2}{3}\tilde{\varepsilon}_{ij}\tilde{\varepsilon}_{ij})^{1/2}, \tag{9}$$

which indicates that the HRR singularity remains pertinent for mixed mode creep cracks. Similarly, an effective crack surface opening displacement rate, $\dot{\delta}_{\text{eff}}$, may be defined as

$$\dot{\delta}_{\text{eff}} = [(\dot{\delta}_1)^2 + (\dot{\delta}_2)^2]^{1/2}, \tag{10}$$

to give

$$\dot{\delta}_{\text{eff}} = \alpha\dot{\varepsilon}_0 r\left[\frac{C(t)}{\alpha\sigma_0\dot{\varepsilon}_0 r}\right]^{n/(n+1)}\tilde{u}_{\text{eff}}, \tag{11}$$

with

$$\tilde{u}_{\text{eff}} = [(\Delta\tilde{u}_1)^2 + (\Delta\tilde{u}_2)^2]^{1/2} \tag{12}$$

and

$$\Delta\tilde{u}_i = \tilde{u}_i(-\pi) - \tilde{u}_i(\pi),$$

where $\dot{\delta}_1$ and $\dot{\delta}_2$ are the mode II and mode I crack surface opening rates, respectively.

3. Experimental procedures

Single edge notched, pin-loaded specimens of 304 stainless steel were used. The 3 mm thick, fatigue precracked specimens were fatigued at $\Delta K = 15\,\text{MPa}\sqrt{m}$ and at 600°C in a vacuum of 1.33×10^{-3} Pa. The minimum to maximum load ratio was 0.1. After substantial fatigue crack propagation, the cracked specimens were held at the maximum load at a K level of $16.5\,\text{MPa}\sqrt{m}$ for 10 minutes. At this K level, the region ahead of the tip of the fatigue crack underwent creep deformation with crack extension. The creep zone was a greater portion of the specimen thickness than that recommended by ASTM for plane strain testing; thus, crack tip deformation of the stationary creep crack was thought to occur under the plane stress condition. Still photographs of the crack tip region under load were taken as a function of time using a long focal length optical microscope which allowed viewing of the specimen within the vacuum furnace. Using photographs of the crack tip region taken at two different times of creep, the displacements of individual points near the crack tip were measured by the stereoimaging technique. Details of the stereoimaging technique have been described previously [10, 11]. From the measured displacements, the displacement gradients and the creep strains were computed. The opening displacements of the crack surfaces were also measured as a function of distance behind the crack tip. Preliminary results of this work were presented earlier in [11].

Creep constants for 304 stainless steel were obtained from the literature [12]. Figure 1 shows the steady-state creep rate data from Simmons and Cross [12, 13], which were fitted to (4). From these data, the creep exponent, n, was determined to have a value of 8, while the value of σ_0 was determined to be 1190 MPa based on $\alpha = 1$ and $\dot{\varepsilon}_0 = 1\,\text{sec}^{-1}$.

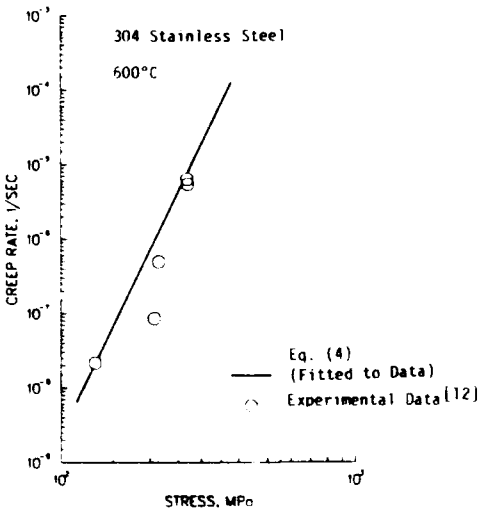

Fig. 1. Steady-state creep rate of 304 stainless steel as a function of stress

4. Results

Figure 2 shows the measured displacements near the tip of a creep crack in 304 stainless steel at 600 C. The displacement field for the crack after 2 minutes of creep is shown in Fig. 2(a), while that after 10 minutes of creep is shown in Fig. 2(b). Note that the creep crack was not an ideal mode I crack, but was a deflected crack aligned at an angle of ≈ 30 from the loading axis. The nonlinear nature of the crack, however, made it difficult to obtain an accurate value of the crack angle. The length of the kinks along the crack was approximately 100 μm and the creep zone was about 300 μm. The strains ahead of the crack tip after 2 minutes of creep are shown in Fig. 3 as a function of distance, r, ahead of the crack tip for $\theta = 0$, 45 , and 90 . Similarly, the crack tip strains for the crack after 10 minutes of creep are shown in Fig. 4. Both Figs. 3 and 4 show that the creep strains ahead of the crack tip exhibit the $r^{-n/(n+1)}$ distribution for stationary creep cracks. The strains at the tip ($r = 0$) of the creep crack were found to be finite, but they were excluded from Figs. 3 and 4 because of the difficulty of representing $r = 0$ in a log-log plot. The slopes of the creep strain versus distance curves in Figs. 3 and 4 range from -0.79 to -0.92 with an average value of -0.84. The creep exponent for 304 stainless steel at 600 C is 8 ($n = 8$); this leads to a calculated slope of -0.89 (slope $= -n/[n+1]$).

Creep rates were computed from the incremental creep strains by dividing by the time increments. Figures 5 and 6 show the effective strain rates as functions of distance, r, ahead of the crack tip for creep times of 2 and 10 minutes, respectively. The RR strain fields shown in Figs. 5 and 6 as solid lines were obtained from (6) and (8) by assuming the plane strain condition. The values of the pertinent normalization functions in (8) and (11) were obtained from

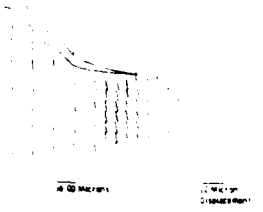

(a) Displacement diagram, 0-2 min.

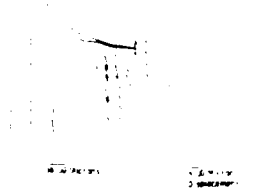

(b) Displacement diagram, 8-10 min.

Fig. 2. Near-tip displacements for a deflected crack in 304 stainless steel tested at 600 C for two different times of creep (a) 0–2 minute, and (b) 8–10 minute. The nominal stress intensity factor level was 16.5 MPa$\sqrt{m}$.

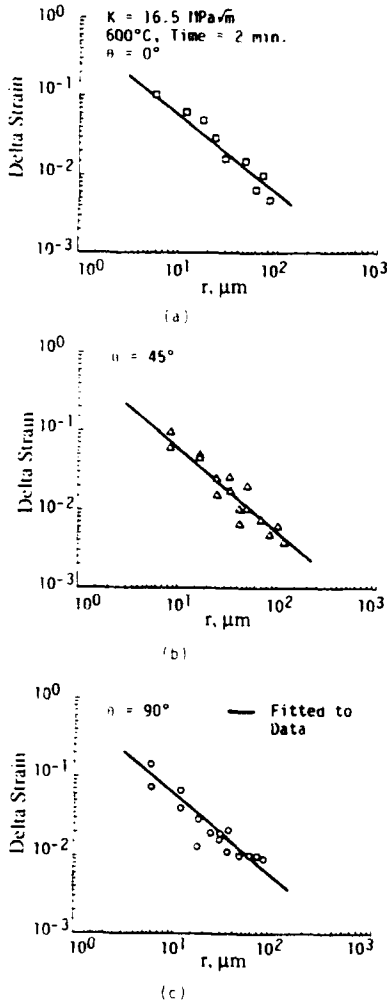

Fig. 3. Incremental creep strain as a function of distance, r, ahead of the tip of the deflected creep crack in 304 stainless steel at 600°C. The time of creep was 2 minutes and the stress intensity factor was 16.5 MPa$\sqrt{m}$.

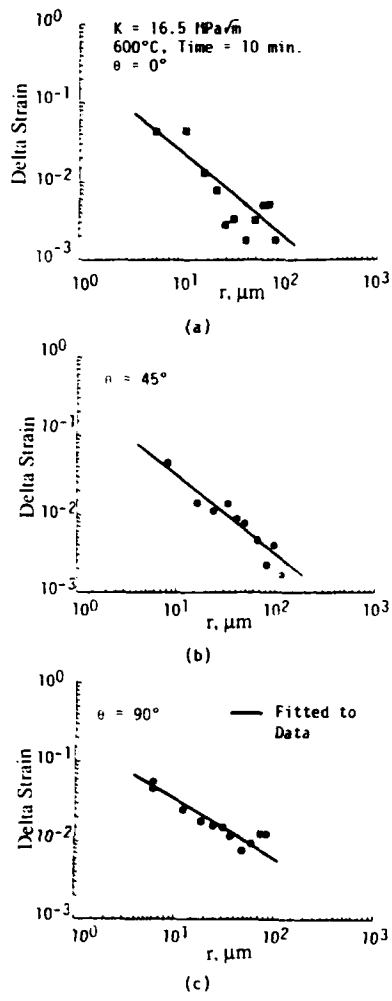

Fig. 4. Incremental creep strain as a function of distance, r, ahead of the tip of the deflected creep crack in 304 stainless steel at 600°C. The time of creep was 10 minutes and the stress intensity factor was 16.5 MPa$\sqrt{m}$.

the tables compiled by Symington, Shih, and Ortiz [9]. Plane stress calculations were not made because the relevant normalization functions were not available [14]. For the creep crack studied, the deflection angle was equal to or less than, 30°. Using a crack deflection angle of 30°, the elastic mixity and subsequently the plastic mixity factors were computed as 0.83 and 0.88, respectively. Since the normalization functions for $n = 8$ and $M^P = 0.88$ were not presented by Symington et al., values of $\tilde{\varepsilon}_{ij}$ and $\tilde{u}$ for $n = 7$ and $M^P = 0.88$ were used for the calculations shown here for $\dot{\varepsilon}_{\text{eff}}$ and later for $\dot{\delta}_{\text{eff}}$. The slight differences in n and M^P are not expected to affect the calculated values, however. In most cases the strain obtained from the RR field calculations were approximately a factor of three to ten lower than the measured values. The agreement between theory and experiment was generally better for $\theta = 45°$ than for $\theta = 0$ or 90°. Plots of normal and shear strain components for $\theta = 0°$ in Fig. 7 reveal relatively large shear strain components in front of the deflected crack, as predicted by the previous analysis of Suresh and Shih [8]. Again, the measured creep rates for individual components were higher than those calculated for a mixed mode crack under plane strain conditions.

The change in crack surface opening displacement was also measured as a function of time

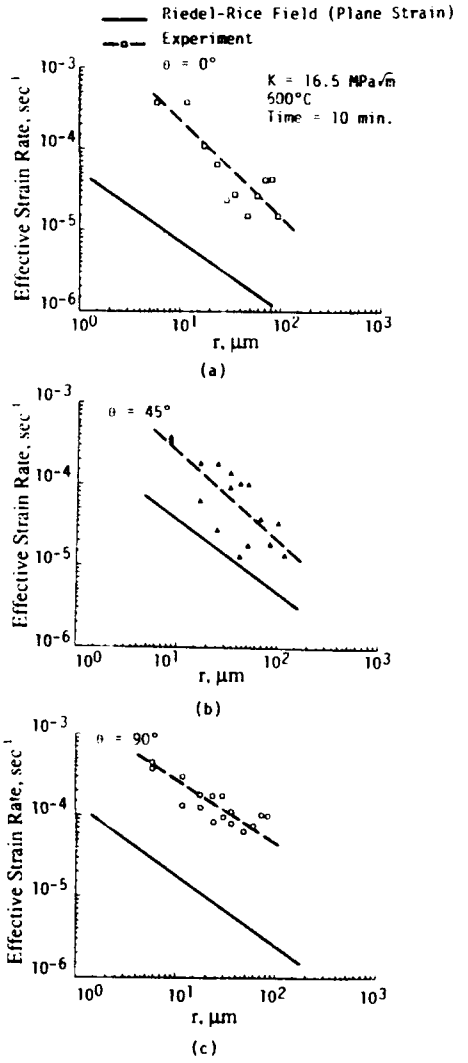

Fig. 5. Comparison of measured and RR (Riedel and Rice) near-tip effective strain rates as a function of distance, r, ahead of the tip of the deflected creep crack in 304 stainless steel after 2 minutes of creep.

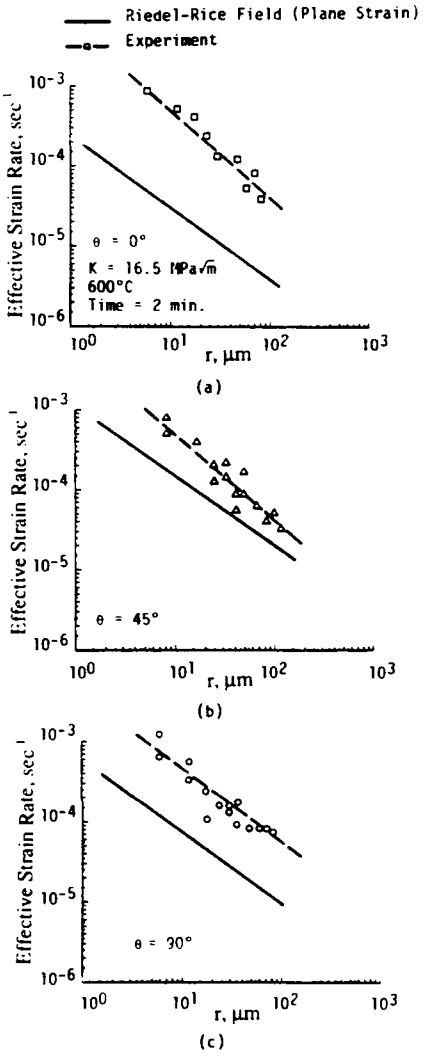

Fig. 6. Comparison of measured and RR (Riedel and Rice) near-tip effective strain rates as a function of distance, r, ahead of the tip of the deflected creep crack in 304 stainless steel after 10 minutes of creep.

of creep. Both mode I, δ_2, and mode II, δ_1, crack surface opening displacements were observed. The corresponding rates of crack surface opening displacement and their effective (root-mean-square) values, $\dot{\delta}_{\text{eff}}$, were computed by dividing the measured opening value by the two-minute time increment. Figure 8 presents $\dot{\delta}_{\text{eff}}$ as a function of time. It is evident that $\dot{\delta}_{\text{eff}} \propto t^{-n/n+1}$ with a measured slope of -0.88, while the corresponding value of the slope calculated based on (11) is -0.89. Calculated values of $\dot{\delta}_{\text{eff}}$ based on (11) are also compared with the measured values in Fig. 8. The calculated values are about a factor of four lower than the experimental values.

The mixity of cracking mode associated with the deflected crack is presented in Fig. 9 in terms of the ratio of mode II/mode I ($\dot{\delta}_1/\dot{\delta}_2$) at various creep times. As indicated in Fig. 9, the values of $\dot{\delta}_1/\dot{\delta}_2$ range from 0.03 to 0.27, reflecting the meandering nature of the crack path (see Fig. 2). The theoretical value of $\dot{\delta}_1/\dot{\delta}_2$ is

$$\frac{\dot{\delta}_1}{\dot{\delta}_2} = \frac{\tilde{u}_1(-\pi; M^P, n) - \tilde{u}_1(\pi; M^P, n)}{\tilde{u}_2(-\pi; M^P, n) - \tilde{u}_2(\pi; M^P, n)} \tag{13}$$

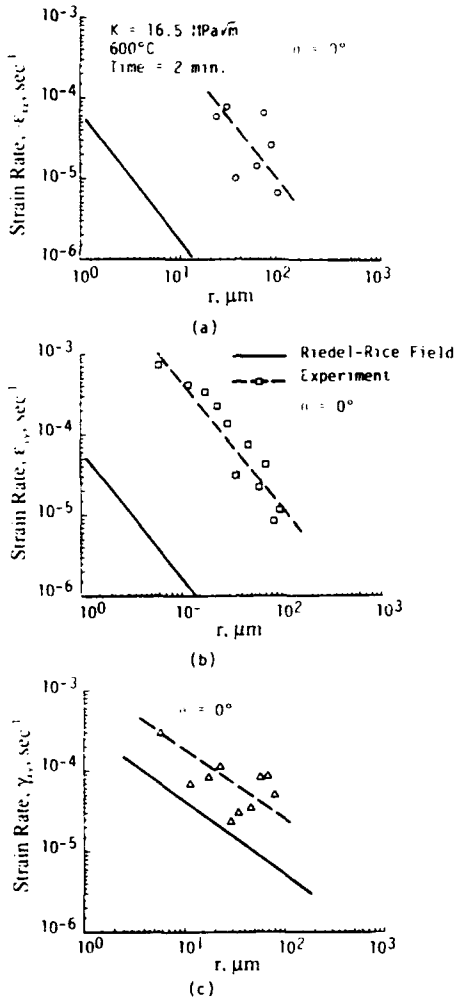

Fig. 7. Comparison of measured and RR (Riedel and Rice) near-tip strain rate components as a function of distance, r, ahead of the tip of the deflected creep crack in 304 stainless steel after 2 minutes of creep.

Using a crack deflection angle of 30° and $M^P = 0.837$, the maximum value of $\dot{\delta}_1/\dot{\delta}_2$ predicted by (13) is approximately 0.60, which is larger than the measured values. On the other hand, the measured values of the $\dot{\delta}_1/\dot{\delta}_2$ ratio lie between those predicted for $\phi = 0°$ ($M^P = 1$) and $\phi = 20°$ ($M^P = 0.92$), as shown in Fig. 9. The discrepancy between measurement and calculation may be explained on the basis of the nonlinearity of the crack path, which made the effective value of the crack angle somewhat less than the measured one.

5. Discussion

A. Riedel–Rice field for mixed mode creep cracks

The Riedel–Rice field was originally developed for a mode I crack in a power-law creeping material. One possible means of extending it to mixed mode cracks would be to utilize the results for elastic-plastic mixed mode cracks developed by Shih and co-workers [7–9]. In this approach, the RR fields for mode I cracks are related to those for mixed mode and deflected

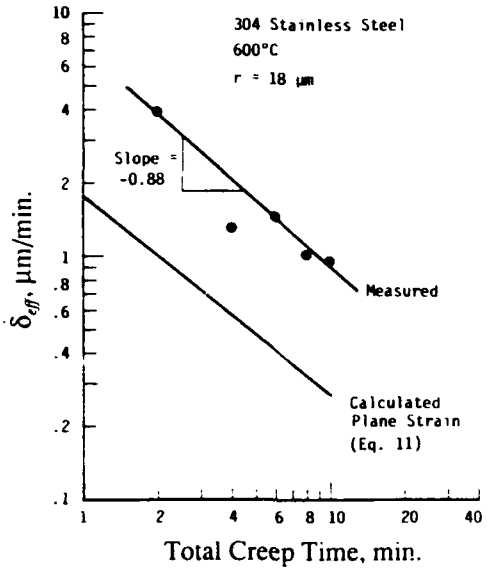

Fig. 8. Comparison of measured and calculated effective (i.e., root-mean-square) crack opening displacement rates as a function of the total creep time.

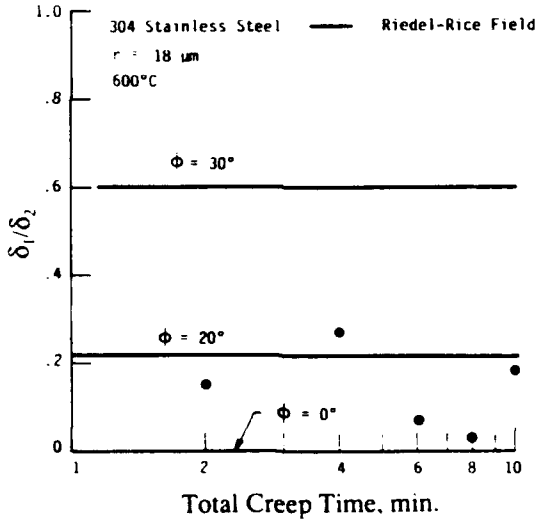

Fig. 9. Comparison of measured and calculated ratios of mode II, $\dot{\delta}_1$, to mode I $\dot{\delta}_2$, crack opening displacement rates as a function of creep time for 304 stainless steel.

cracks through the introduction of a plastic mixity factor. The type of singularity and its amplitude remain the same as those for the mode I crack; only the normalization functions of $I_n(M^P)$, $\tilde{\varepsilon}_{ij}(\theta; M^P, n)$ and $\tilde{u}_i(\theta; M^P, n)$ need to be evaluated for the mixed mode cracks. The values of these normalization functions for various values of M^P have been computed by Symington et al. [9] for the plane strain condition. The present results indicate that the near-tip strains and crack surface opening displacements for deflected creep cracks in 304 stainless steel are indeed those of the RR-type [1], indicating the Shih [7–9] approach might be used to extend the RR field [1] to mixed mode creep cracks.

The agreement observed between experiment and theory is within a factor of two in creep rates for the best case and within a factor of ten in the worst case (for $r \geqslant 10\,\mu m$). The

observation that the calculated strains and *COD*s are consistently lower than the measured values might be explained on the basis that the plane strain condition was not attained on the specimen surface because the creep zone was large compared with the specimen thickness. Since the calculated strains for the plane stress condition are expected to be higher than those for plane strain, a change of strain state from plane strain towards plane stress would reduce the discrepancies between theory and experiment. Unfortunately, the relevant normalization functions for mixed mode cracks under plane stress are not available [14]. A more direct and rigorous comparison of the measured creep rates and *COD* values with theoretical values for a plane stress mixed mode crack is, therefore, not possible. Nonetheless, the results demonstrate that a stationary deflected creep crack exhibits a RR-type near-tip field.

The observation of mode II crack opening is an indication that the deflected crack was a mixed mode crack. Even though the crack path was macroscopically normal to the loading axis the fact that the deflected crack tip, whose length was only 100 μm, was able to dominate the near-tip behavior was probably due to the fact that the creep zone was only 300 μm in length. The implication here is that local deviation of the crack path from pure mode I could change the creep rate distributions and crack opening modes when the deflected crack length is on the order of the plastic zone size. Suresh and Shih [8] previously suggested that the minimum effective deflected length might be at least half of the plastic zone, compared to the value of one-third that was observed for 304 stainless steel in this work.

B. Comparison of the near-tip behavior of creep cracks in 304 stainless steel and pyroceram

Near-tip strains and *COD*s have been determined for creep cracks in pyroceram (a glass ceramic) whose creep exponent, n, has a value of 1.5 [15]. The small value of n is the consequence of the deformation mechanism, as elevated temperature creep in this ceramic with glassy grain boundaries occurs predominantly by grain boundary sliding. It is therefore of interest to compare the results for 304 stainless steel, which has a n-value of 8, [13] with those of pyroceram. Experimental results for pyroceram are described in [5].

Creep cracks in 304 stainless steel and pyroceram both exhibited crack path deflection. The near-tip strain fields for creep cracks in 304 stainless steel and pyroceram were both of the RR type [1] when the amount of crack extension was small and the rate of crack opening displacement decreased with increasing time of creep in both materials in a manner described by (11). One of the significant differences between 304 stainless steel and pyroceram was the development of a localized shear zone ahead of the crack tip in the pyroceram. Such a clear process zone was absent in the stainless steel, as illustrated in Fig. 10 which compares the contour plots of shear strains of the two materials. Another difference is that there was relatively more mode II crack opening displacement for cracks in the pyroceram than for those in the stainless steel, even though the angles of crack path deflection were similar. The ratio of mode II mode I crack opening rate for the creep crack in pyroceram is shown in Fig. 11 as a function of time of creep. Note that the mode II opening is as large as the mode I opening, and that the ratio of $\dot{\delta}_1/\dot{\delta}_2$ is substantially larger than the maximum predicted by theory. These differences in behavior might be attributed to differences in deformation mechanism. In particular, the shear zone in pyroceram and the concurrent high degree of mode II opening might be the consequence of the ceramic's propensity for grain boundary sliding. Further work is required to confirm this hypothesis. Nonetheless, the present results suggest that the mode of deforma-

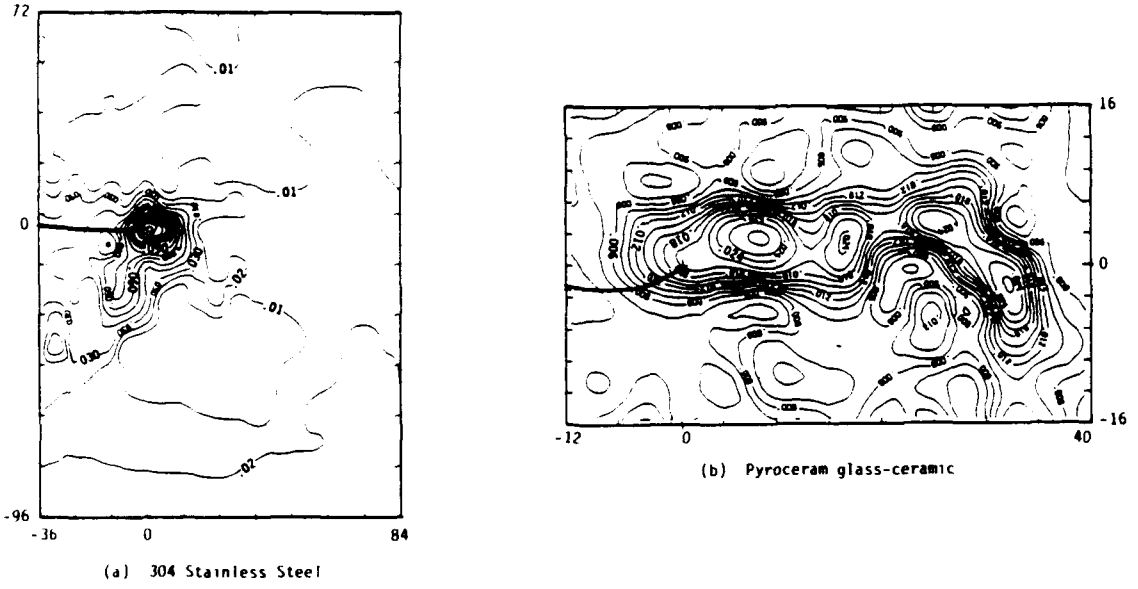

Fig. 10. Contour plot of near-tip maximum shear strains for deflected cracks in a 304 stainless steel and a pyroceram glass-ceramic: (a) 304 stainless steel after 10 minutes of creep at $K = 16.5\,\mathrm{MPa}\sqrt{m}$ and 600 C; (b) pyroceram glass-ceramic after 113 minutes of creep at $K = 0.8\,\mathrm{MPa}\sqrt{m}$ and 700 C.

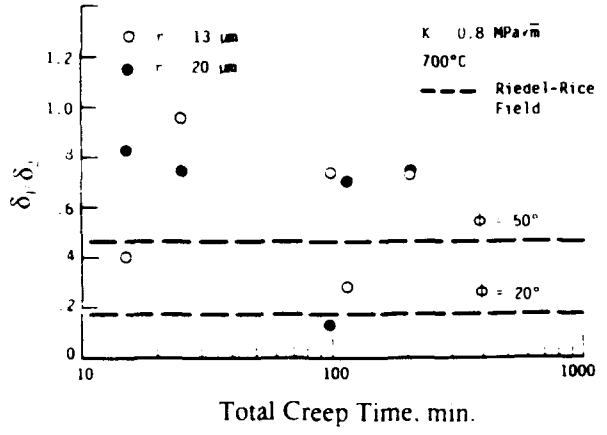

Fig. 11. Comparison of measured and calculated ratios of mode II, $\dot{\delta}_1$, to mode I, $\dot{\delta}_2$, crack opening displacement rates as a function of creep time for a pyroceram glass-ceramic.

tion affects the creep crack tip responses. Accurate crack tip analyses of creep cracks in ceramics, thus, need to consider the effects of viscous sliding of grain boundaries. Such an analysis is currently not available.

6. Conclusions:

1. The near-tip creep rates and crack surface opening displacements of a mixed mode or deflected creep crack in 304 stainless steel are those of the Riedel–Rice type.
2. The Riedel Rice field for mode I creep cracks can be extended to mixed mode or deflected cracks using Shih's solutions for mixed mode elastic-plastic cracks.

3. The near-tip creep behavior of 304 stainless steel differs from that of the pyroceram glass-ceramic by showing relatively less mode II opening displacements and the absence of a shear process zone. The mode II component in the 304 stainless steel can be explained by the deflection of the crack from mode I, while that observed in the pyroceram glass-ceramic cannot be explained by crack deflection. These differences may be due to differences in the creep deformation mechanisms.

Acknowledgement

This work was supported by the Air Force Office of Scientific Research through Contract No. F49620-88-C-0081. The encouragement by the Program Manager, Dr. L.J. Schioler, is acknowledged.

References

1. H. Riedel and J.R. Rice, in *Fracture Mechanics: Twelfth Conference, ASTM STP 700*, American Society for Testing and Materials, Philadelphia (1980) 112–130.
2. J.W. Hutchinson, *Journal of Mechanics and Physics of Solids* 16 (1968) 13–31.
3. J.R. Rice and G.F. Rosengren, *Journal of Mechanics and Physics of Solids* 16 (1968) 1–12.
4. N.L. Goldman and J.W. Hutchinson, *International Journal of Solids and Structures* 11 (1975) 575–591.
5. R.A. Page, K.S. Chan, D.L. Davidson and J. Lankford, *Journal of American Ceramic Society*, 73 (1990) 2977–2986.
6. P. Marshall, *Austenitic Stainless Steels*, Elsevier Applied Science Publishers, London, U.K. (1984) 312.
7. C.F. Shih, in *Fracture Analysis, ASTM STP 560*, American Society for Testing and Materials, Philadelphia (1974) 187–210.
8. S. Suresh and C.F. Shih, *International Journal of Fracture* 30 (1986) 237–259.
9. M. Symington, C.F. Shih and M. Ortiz, Tables of Plane Strain Mixed-Mode Plastic Crack Tip Fields, Technical Report MRG/DMR-8714665 1, Division of Engineering, Brown University (1988).
10. D.R. Williams, D.L. Davidson and J. Lankford, *Experimental Mechanics* 20 (1980) 134–139.
11. D.L. Davidson, in *Micro and Macro Mechanics of Crack Growth*, K. Sadananda, B.B. Rath and D.J. Michel (eds.) TMS, Warrendale, Pa. (1981) 161–176.
12. W.F. Simmons and H.C. Cross, *The Elevated-Temperature Properties of Stainless Steel*, ASTM, Philadelphia (1952) 60.
13. N.P. Suh and A.P.L. Turner, *Elements of the Mechanical Behavior of Solids*, McGraw-Hill, New York (1975) 376.
14. C.F. Shih, private communication, July (1989).
15. E.M. Heuse and G. Partridge *Journal of Materials Science* 9 (1974) 1255–1261.

journal

Reprinted from the Journal of the American Ceramic Society, Vol. 74, No. 7, July 1991

J. Am. Ceram. Soc., 74 [7] 1605-13 (1991)

Creep-Crack Growth by Damage Accumulation in a Glass-Ceramic

Kwai S. Chan* and Richard A. Page*

Southwest Research Institute, San Antonio, Texas 78228-0510

The growth rate, near-tip creep response, and damage processes of creep cracks in a pyroceram glass-ceramic were studied under tensile loading at elevated temperatures. The rates of crack extension were characterized as a function of the applied stress intensity factor. The damage processes which occurred near the crack tip and led to creep crack extension were identified using a replica technique and by direct observations in a scanning electron microscope equipped with a high-temperature loading stage. The accumulated creep strains near the crack tip were measured via the stereoimaging technique. The results indicate that creep-crack growth in the pyroceram glass-ceramic occurs in both continuous and discontinuous manners, with the damage processes manifested as the nucleation, growth, and coalescence of inhomogeneously distributed cavities and microcracks. Measurements of the total accumulated creep strain near the crack tip suggest that crack extension follows a critical strain criterion. Both the microcrack density and the total accumulated creep strain show similar dependence with distance from the crack tip. These observations suggest that damage accumulation and crack extension in the glass-ceramic are controlled by the near-tip creep rates. [Key words: crack growth, damage, glass-ceramics, creep, stress.]

I. Introduction

Subcritical crack growth has been observed in a number of ceramics under elevated temperature loading.[1-13] Such subcritical or creep-crack growth is generally characterized by intergranular fracture paths and occurs by the nucleation, growth, and coalescence of grain-boundary cavities and/or microcracks ahead of the crack tip.[8-13] Typically, creep-crack growth in ceramics occurs at stress intensities, K, between a threshold, K_{th}, and a critical value, K_C, which represents the onset of unstable fracture.[12,13] Below the threshold, creep cracks blunt, exhibit crack opening displacement, but no longer propagate. Furthermore, a near-tip strain distribution different from that of propagating creep cracks was observed for cracks below the threshold.[14] Above the threshold, creep-crack growth is characterized by a power-law relation between the crack velocity and the stress intensity factor.[12,13]

For ceramics with preexisting flaws, creep cavities might be localized and occur predominantly near the tip of the creep crack, forming a creep damage or fracture process zone.[8-13] This damage zone consists of individual and/or coalesced cavities. The linkage of the creep cavities with the tip of the main crack constitutes a crack extension event and occurs in an incremental and discontinuous manner. The incremental nature of the crack extension process suggests that a critical amount of creep strain and/or damage must be accumulated within the damage zone prior to crack extension. The rate of creep-crack extension thus depends on the rate, and the nature, of the damage accumulation process within the process zone, both of which are expected to be influenced by the local stresses and strain rates near the tip of the creep crack, as well as by the microstructure of the ceramics,[12] e.g., the presence of a vitreous grain-boundary phase. In particular, creep cracks in vitreous-bonded materials tend to propagate along the grain-boundary vitreous phase, occasionally leaving intact ligaments of the vitreous phase behind the crack tip.[11] Under unconstrained conditions, these amorphous ligaments can exert tractions on the crack surface, leading to a decrease in the crack growth rate by reducing the local driving force for crack extension.[12,15]

Creep-crack growth in ceramics can occur by either direct or indirect growth mechanisms.[12,16] In the latter case, crack growth proceeds by accumulation of creep damage within the crack-tip process zone. However, little work has been done to characterize the creep damage process ahead of a creep crack and its impact on, or relationship to, creep-crack growth. The incorporation of creep damage into a creep-crack growth model has been attempted by Thouless and Evans.[15] A key feature of their model is that the creep-crack growth rate depends sensitively on the ratio of cavity spacing to grain facet length, which represents the degree of local creep damage within the process zone. Characterizing the development of creep damage during creep-crack growth is therefore important for improving the current understanding of the creep-crack growth process in ceramics.

The objective of this paper is to characterize the damage process associated with creep-crack growth in a pyroceram glass-ceramic. This work is a follow-on of a previous paper[14] which examines the micromechanics of creep-crack growth in the pyroceram glass-ceramic. While the previous paper is concerned with the near-tip creep deformation, the present paper is focused on the relationship between the near-tip damage process and the resulting crack growth behavior. In particular, the creep-crack growth rate will be measured as a function of the stress intensity factor, K. A machine-vision-based stereoimaging technique will be used to measure the creep strains accumulated within the damage process zone prior to crack extension. The type and extent of creep damage in the glass-ceramic will be identified and measured as a function of distance from the crack tip. These results will be utilized with near-tip strain measurements to examine whether a critical amount of creep damage or accumulated strain within the process zone is required for creep-crack growth and to identify the relationship between creep damage and the crack growth curve.

II. Experimental Procedure

(1) Material

A magnesium aluminosilicate glass-ceramic (Corning 9606), which consisted of 0.5-μm-diameter cordierite grains

M. D. Thouless—contributing editor

Manuscript No. 197284. Received September 18, 1990; approved March 28, 1991.

Supported by the Air Force Office of Scientific Research through Contract No. F49620-88-C-0081.

*Member, American Ceramic Society

surrounded by a thin continuous amorphous phase, was utilized for this study. Previous studies have indicated that the grain-boundary vitreous phase of this glass-ceramic begins to soften at around 600°C.[17] Once the amorphous phase is softened, deformation occurs by a combination of grain-boundary sliding and cavitation. This material is thus believed to be representative of the many liquid-phase-sintered ceramics. The creep exponent, n, of the cordierite glass-ceramic was ≈2 (Ref. 18), which was somewhat higher than the n value of unity observed in the Corning 9608 lithium aluminosilicate (LAS) glass-ceramics,[19,20] but was consistent with n = 1.5 to 2.2 reported for other LAS glass-ceramics.[21]

(2) Crack Growth Rate Measurements

Creep-crack growth in the pyroceram glass-ceramic was studied in the 700° to 775°C range using single-edge-notched specimens. The dimensions of the test specimens and the experimental procedures were identical to those reported earlier.[14] In particular, the specimens were precracked by cyclic fatigue under compressive loads at room temperature. After cyclic fatigue precracking, the specimens were coated with gold to provide a conductive surface and tested under a constant tensile load in a scanning electron microscope equipped with a high-temperature loading stage.[22] The region in the vicinity of the crack tip was monitored and photographed in approximately 15- to 30-min intervals using 1000X to 2000X magnifications. The amount of crack extension within a given time interval was obtained by measuring the length of the crack from the SEM photographs taken before and after that time period. The crack velocity was computed by dividing the amount of crack extension by the time interval, and the stress intensity factor was computed using the formula due to Gray.[23]

(3) Near-Tip Cumulative Strain Measurements

The total creep strain accumulated in the region located near the tip of a crack prior to crack growth into that region was measured using a machine-vision-based stereoimaging technique.[24] The procedure for performing such strain measurements is shown schematically in Fig. 1. Prior to creep testing, the region located 100 μm directly ahead of the crack tip was photographed extensively as a reference area, using the SEM. The creep-crack growth experiment was then performed, and the referenced area was again photographed after the creep crack had extended into that region. The accumulated creep strain was then determined by analyzing photographs of the region before and after crack advance, using the machine-vision-based stereoimaging technique described in Ref. 24. This automated high-resolution displacement measurement system, known as the DISMAP system, is basically a machine-vision implementation of the human-vision-based stereoimaging technique developed earlier.[25] The machine-vision version of the stereoimaging technique is considerably more accurate (by an order of magnitude) than its counterpart based on human vision. In both cases, the stereoimaging technique measured the relative in-plane displacements of an array of material points in the region of interest. These displacements were used to obtain the displacement gradients, which were in turn used to compute the different in-plane creep strain components, ε_{ij}^c. The effective creep strains were computed from the strain components according to $\bar{\varepsilon}^c = (2/3(\varepsilon_{ij}^c \varepsilon_{ij}^c))^{1/2}$. All of the cumulative creep strains reported in this paper were effective creep strains. Since it was not known where the creep crack would advance, an extensive region ahead of the crack tip was mapped in order to obtain the accumulated strain measurements. When the region of interest contained a microcrack, the location of the microcrack was specified and taken into account in computing the displacement gradients and strain components. A more detailed description of the strain measurement technique can be found in Ref. 25. The accuracy of the DISMAP system was established by comparing the stress–strain curves of a ceramic composite obtained from clip gauge and stereoimaging strain measurements. For strain levels greater than 0.005, the maximum errors in the stereoimaging strains were less than 10%. The percentage of errors decreased to less than 1.7% with increasing strain levels above 0.006. For a total strain of 0.02, the maximum possible error in the stereoimaging strains was no more than ±0.002 in the worst case, i.e., when the maximum error of 10% was used.

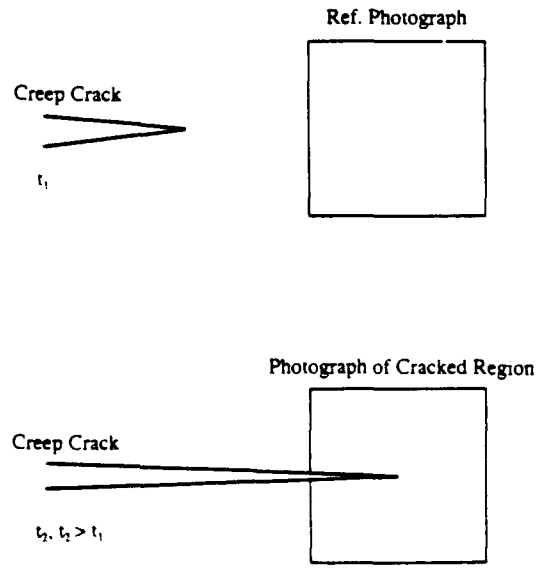

Fig. 1. Schematic showing the procedure for determining the accumulated creep strain using photographs of an area ahead of a creep crack in the uncracked and cracked conditions.

(4) Characterization of Creep Damage

After the creep-crack growth experiments, the test specimen was ion-milled for 4 h to remove the conductive coating and any other surface contaminants. The specimen surface was then replicated using acetobutyrate and cellulose acetate replicating tapes. The former was coated with aluminum and examined in the SEM, while the latter was coated with carbon, shadowed, dissolved, and examined via the TEM. The SEM and TEM micrographs were then used to characterize the distribution, size, and density of microcracks and cavities, using quantitative ceramographic techniques.

To describe the extent of microcracking, the crack density parameter proposed by Budiansky and O'Connell[26] was adopted. This particular crack density parameter, ϵ, is defined as[26]

$$\epsilon = \frac{2N}{\pi}\left\langle \frac{A^2}{P} \right\rangle \tag{1}$$

where N is the number of microcracks per unit volume, A is the area, and P is the perimeter of a microcrack. For n_i circular microcracks of length $2a_i$ in a local volume, V_i, the crack density parameter, ϵ, is

$$\epsilon = \frac{n_i \langle a_i^3 \rangle}{V_i} \tag{2}$$

which indicates that ϵ differs from the local volume fraction of microcracks in the sampling volume by a factor of $4\pi/3$. For the measurement techniques utilized in this study, it is more convenient to use a crack density parameter which is defined in terms of the area fraction of microcracks in a local sampling area. Motivated by Eq. (2), a crack density parameter, Ψ, defined as

$$\Psi = \frac{n_i \pi \langle a_i^2 \rangle}{A_i} \tag{3}$$

which is the fraction of "cracked area" in a local sampling area, A_i, is used to represent the local microcrack density. The repeated indices in Eq. (3) mean summation. A geometric representation of the crack density parameter, Ψ, is shown in Fig. 2. According to quantitative metallography,[27] the area fraction and volume fraction of a "second phase" are equal, the crack density parameters of ϵ and Ψ would be similar, but differ by a constant of $4\pi/3$. For the crack density measurements shown in this paper, a sampling square of 0.254 mm was used.

III. Results

(1) Crack Growth Behavior

The amount of crack extension in the pyroceram glass-ceramic tested at 750°C and a stress intensity factor of 0.85 MPa · $m^{1/2}$ is presented in Fig. 3 as a function of time of creep. Similar results for creep crack growth at 700° and 775°C have been shown earlier in Ref. 14. Previous results indicated that creep-crack growth in the pyroceram occurred via a saw-tooth-shaped crack path in a continuous manner at 775°C, but a discontinuous manner at 700°C.[14] These two types of growth behavior were observed in situ in the SEM and are illustrated schematically in Fig. 4. As depicted in Fig. 4(A), continuous creep-crack growth in the glass-ceramic occurred by direct extension of the main crack, without any visible microcracking directly ahead of the crack tip when viewed at 1000X to 2000X magnification. In contrast, discontinuous crack growth occurred with the formation of a microcrack ahead of the crack tip (Fig. 4(B)). Further crack extension required the linkage of the microcrack with the main crack, which was a process that could take as much as 30 min or more. In some instances, the linkage of the microcrack and main crack was not complete, leaving ligaments which bridged the crack surfaces. The crack extension curve in Fig. 3 shows periods of zero crack extension even though the crack length generally increased with time. The present results at 750°C confirmed the previous observation that creep-crack growth could occur in either a continuous or discontinuous manner.

Figure 5 summarizes the crack growth data as a function of the stress intensity factor, K, for 700°, 750°, and 775°C. The experimental curves were drawn through the data of 750° and 775°C. At both temperatures, the crack growth curve showed a threshold, K_{th}, below which no detectable crack growth occurred. The threshold was determined by unloading the propagating crack in small load increments until it was arrested. The K level was then increased until the crack resumed propagation. A duplicate specimen was used to verify the growth threshold for 775°C by testing at $K \approx K_{th}$ under increasing K levels without prior unloading. The same K_{th} values were obtained in both cases, indicating the observed growth threshold is a material property of a large crack and not a

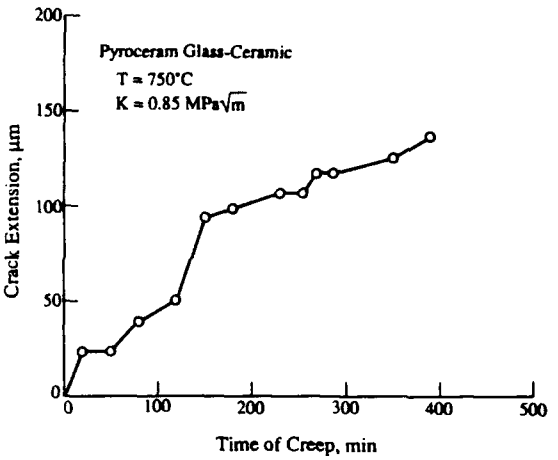

Fig. 3. Crack extension as a function of time of creep.

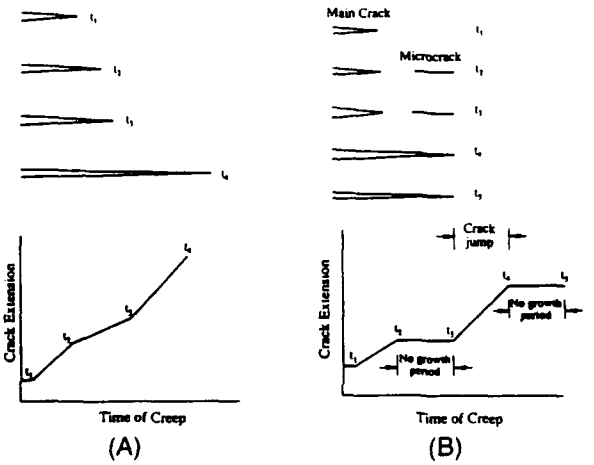

Fig. 4. Schematics showing the creep-crack growth processes observed in the pyroceram glass-ceramic: (A) continuous crack growth, and (B) discontinuous crack growth.

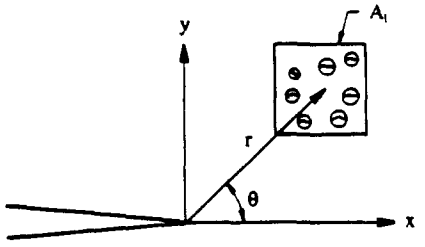

Legend:

Ψ = Crack density parameter

n_i = No. of microcracks of length a_i

a_i = Half-length of a microcrack

A_i = Area within the sampling square

$$\Psi = \frac{\pi}{A_i} n_i (a_i)^2$$

Fig. 2. Schematic showing the procedure for determining the microcrack density parameter, Ψ, in a sampling area, A_i, located at a distance, r, and angle, θ, from the crack tip.

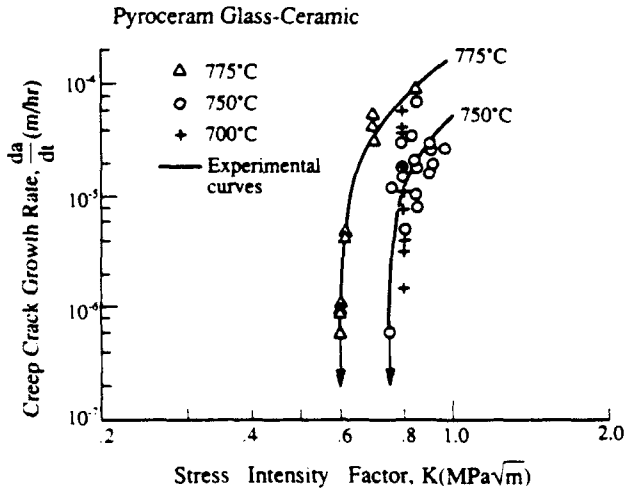

Fig. 5. Creep-crack growth curves for the pyroceram glass-ceramic, showing the existence of a growth threshold.

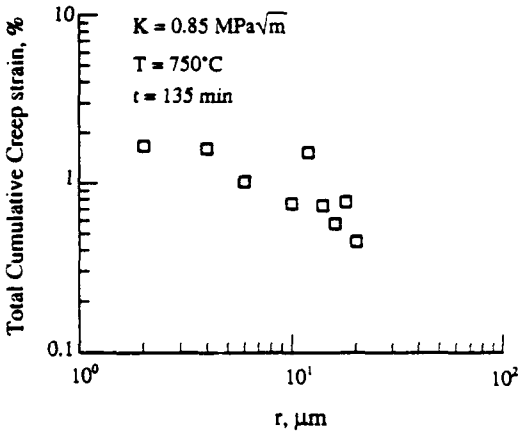

Fig. 6. Total cumulative creep strain as a function of distance, r, ahead of the crack tip, showing that the creep strain accumulated near the crack tip prior to crack growth is ≈2%. The maximum error in the stereoimaging strain measurement is less than ±0.2%.

load-history effect due to unloading. All of the test data at 700°C appeared to lie on the threshold portion of the crack growth curve. In this case, load shedding was not used. The present results are thus consistent with previous work on alumina[10] and silicon carbide,[5] which indicated the existence of a growth threshold for creep cracks that originated from preexisting flaws in the ceramics. A growth threshold, however, was not observed in creep cracks that were initiated by creep damage.[11]

(2) Accumulated Creep Strain

The total cumulative creep strains in the near-tip region of the creep crack were analyzed for various times of creep and crack propagation conditions. Figure 6 shows a typical distribution of the total cumulative creep strain as a function of distance from the crack tip for a creep crack growing in a continuous manner 135 min after the onset of creep-crack growth at K = 0.85 MPa·m$^{1/2}$. The cumulative strain distribution is similar to the incremental creep strain distributions exhibited by creep cracks after long creep times that were reported earlier in Ref. 14. In particular, the total cumulative creep strains are approximately constant near the crack tip, and they do not appear to fit the Riedel–Rice strain distribution.

The total cumulative strain distribution for a creep crack which grew in a discontinuous manner is shown in Fig. 7. At 230 min after the onset of creep-crack growth, the crack was in a stationary position, and the total cumulative creep strain ahead of the crack tip was approximately 0.8% at 4 to 20 μm

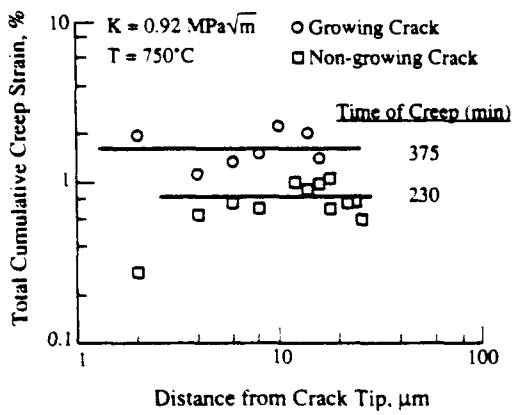

Fig. 7. Comparison of total cumulative creep strains for a creep crack in the nonpropagating and propagating conditions. The maximum error in the stereoimaging strain measurement is less than ±0.2%.

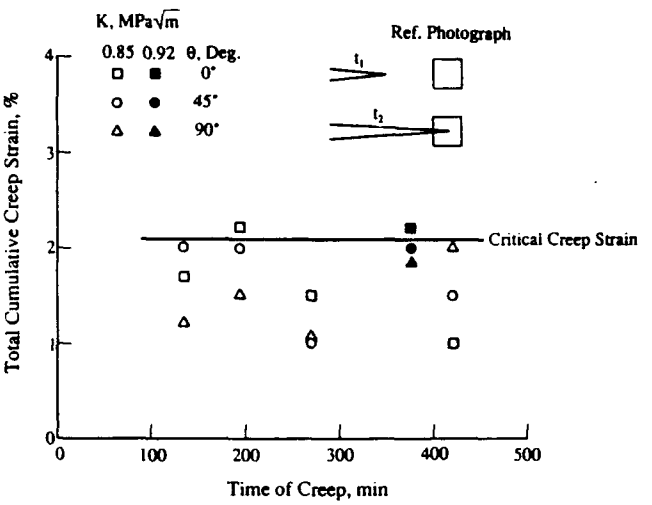

Fig. 8. Critical values of the total cumulative creep strain for various times of creep. The maximum error in the stereoimaging strain measurement is less than ±0.2%.

from the crack tip, while it was ≈0.3% at 2 μm from the crack tip. This unusual strain distribution might be related to the fact that part of the creep strain originates from cavitation of grain boundaries. As will be demonstrated later, grain-boundary cavitation in the glass-ceramic is very heterogeneous, with creep cavities nonuniformly distributed. The crack remained stationary while creep strain accumulated within the near-tip region. After an additional 145 min of creep, the crack resumed propagation when the total cumulative creep strain in the crack-tip region reached ≈2%. This result suggests that a critical value of 2% creep strain was required for fracture of the near-tip process zone. This critical value of total creep strain accumulated within the crack tip process zone prior to incremental crack extension was measured for various times of creep. These results, shown in Fig. 8, indicate that the critical value of the cumulative creep strain required for fracture of the crack-tip process zone is approximately 2%; this value does not appear to vary with the time of creep and, by implication, the amount of crack extension.

(3) Microcrack Density

The development of creep damage ahead of a creep crack in the pyroceram ceramic was studied after creep crack growth at 750°C under a K level of 0.95 MPa·m$^{1/2}$. Surface replicas revealed the presence of microcracks on the test

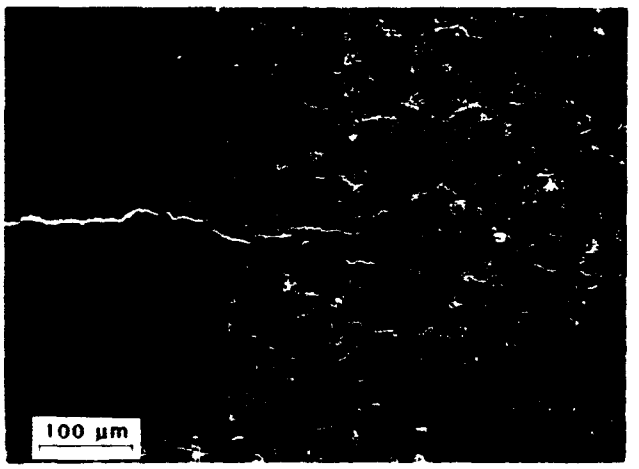

Fig. 9. Microcracks observed near the tip of the main crack in pyroceram.

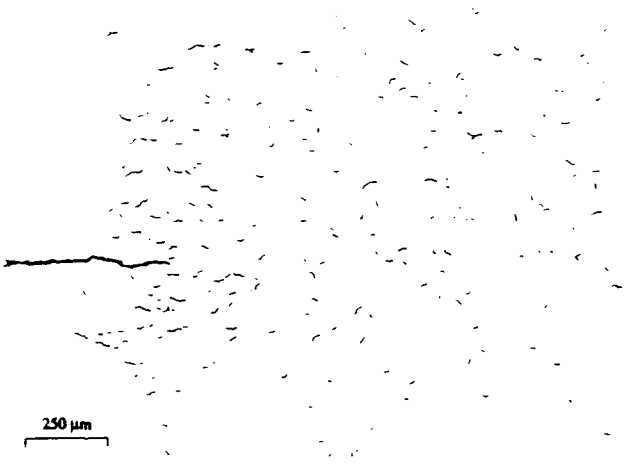

Fig. 10. Traces of microcracks showing extensive microcracking in the pyroceram.

specimen. The microcracks were concentrated near the tip of the main crack, as illustrated in Fig. 9. The microcracks, however, were not limited to the crack-tip region, but were distributed throughout the uncracked ligament. The distribution of the microcracks was studied by replicating and photographing across the width of the specimens at 200X magnification. A montage of the specimen was constructed from the SEM photographs showing the microcracks. Figure 10 shows traces of microcracks located in a region which is within 2 mm of the tip of the creep crack. As shown in Fig. 10, the microcracks are on the order of 10 to 40 μm. The smaller microcracks (<20 μm in length) show no preferred orientation with respect to the loading axis. The larger microcracks (>20 μm in length) have a tendency to align normal to the loading axis and they are generally formed by the linkage of smaller microcracks. Both of these observations are supported by TEM replica studies.

The maximum microcrack size is shown as a function of distance from the crack tip in Fig. 11, while the number of microcracks per unit area is shown in Fig. 12. In general, both the number and the size of the microcracks decrease with increasing distance from the crack tip. At distances greater than 1 mm from the crack tip, the number and the size of the microcracks appear not to vary with distance. Figure 13 shows the value of the microcrack density parameter, Ψ, as a function of distance, r, ahead of the crack tip. For distances in the range of 0.1 to 2 mm from the crack tip, the microcrack density, as measured by Ψ, decreases with increasing distance

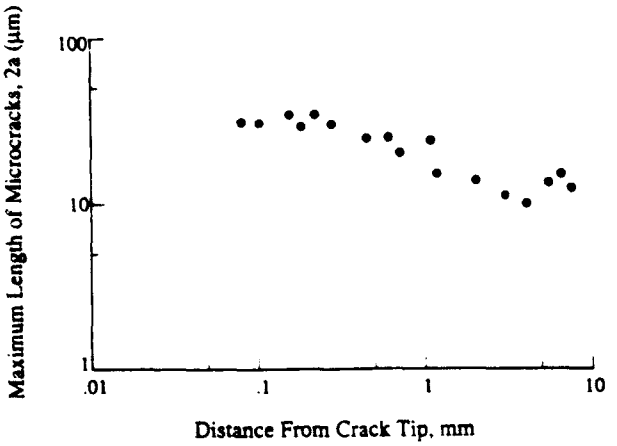

Fig. 11. Maximum length of microcracks as function of distance, r, ahead of the tip of the main crack.

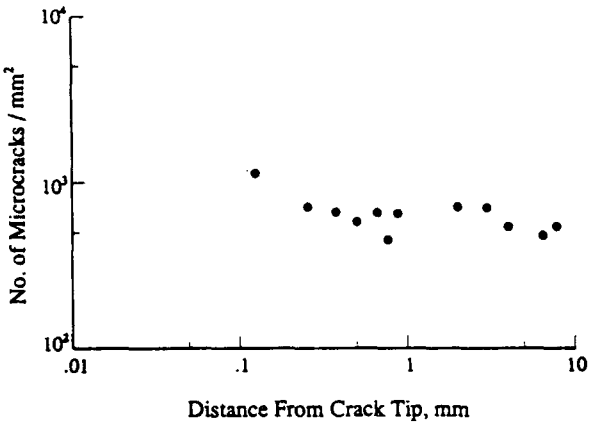

Fig. 12. Number of microcracks as function of distance, r, ahead of the tip of the main crack.

from the crack tip but remains relatively constant at $r >$ 2 mm. There is also more local variation in the microcrack density parameter at $r > 2$ mm.

(4) Grain-Boundary Cavities

TEM replicas revealed that many grain boundaries in the pyroceram test specimen were cavitated. During creep-crack growth, grain-boundary cavities were nucleated, subsequently grew, and coalesced to form microcracks, as shown in Fig. 14. Detailed examination of these microcracks at high magnification revealed that they were formed by the coalescence of rows of equally spaced and sized grain-boundary cavities; such an example is shown in Fig. 15. Microcracks, which were initiated at triple points of grain boundaries and grew into grain facet cracks, were seldom observed. The creep cavities were inhomogeneously distributed throughout the specimen. Some regions of the specimen showed a relatively large concentration of cavities, while the neighboring areas were denuded of cavities. In most instances, the heavily cavitated areas appeared as pockets of cavities surrounded by uncavitated grain boundaries, as illustrated in Fig. 16. These regions of high cavity density had an average diameter of approximately 40 μm. In addition to these volumetric pockets of high cavity density, more or less linear arrays of contiguous, highly cavitated grain boundaries were also observed. The linear arrays of cavitated boundaries appeared to be an early stage of

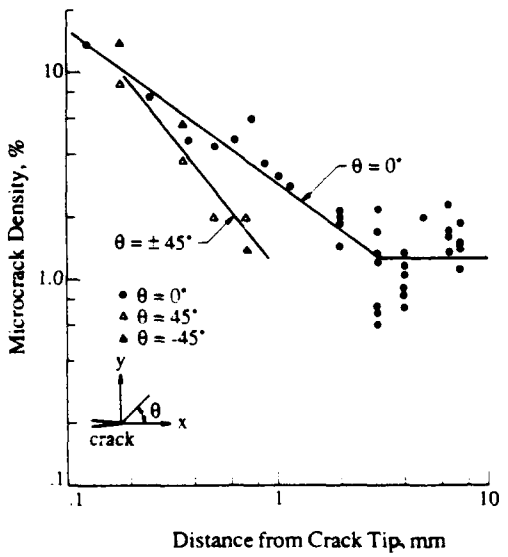

Fig. 13. Microcrack density parameter, Ψ, as function of distance from the tip of the main crack.

Fig. 14. TEM replica showing inhomogeneously distributed microcracks and grain-boundary cavities associated with creep-crack growth in pyroceram.

the microcrack formation. The three-dimensional pockets of high cavity density, on the other hand, did not generally appear to be involved in the formation of microcracks. In fact, it was not uncommon to have one or both of the tips of the microcracks end at these pockets of heavily cavitated areas, suggesting that the cavity pockets might have stopped propagation of the microcracks. Figure 17 gives an example of a microcrack terminating at two pockets of cavities.

IV. Discussion

The present results indicate that two damage processes are associated with creep-crack growth in the pyroceram glass-ceramic, they include (1) the nucleation, growth, and coalescence of grain-boundary cavities which lead to the formation of microcracks, and (2) the propagation and linkage of microcracks with the main crack. These two damage processes are interconnected, with the former preceding and leading naturally to the latter. The observation of pockets of heavily cavitated regions surrounded by uncavitated regions suggests that there are preferred grain boundaries for cavity nucleation. Microstructural reasons for the presence of soft or easily cavitated regions encompassing hundreds or thousands of grains were not readily apparent. However, one could postulate that minor changes in the composition of the grain-boundary glassy phase could affect the viscosity of the grain-boundary phase and thus its resistance to sliding and cavitation. If this is indeed the reason for the inhomogeneous damage process, similar behavior could be expected in other ceramics containing amorphous grain-boundary phases. The approximately equal size of the multiple cavities on a two-grain junction indicates that the cavities might be nucleated at the same time, possibly by the sliding of grain boundaries containing ledges. The coalescence of these cavities to form a facet sized microcrack may occur either by the growth of the nucleated cavities or through the continued nucleation of cavities at ligaments located between the cavities.

The occurrence of both continuous and discontinuous crack growth in the pyroceram glass-ceramic appeared to be the direct consequence of the nonuniform distribution of cavities and microcracks ahead of the crack tip. Crack propagation through such a nonuniform damage field would be expected to occur in a more or less continuous manner through regions of heavy damage with periodic arrest periods

Fig. 15. Rows of equally spaced and sized cavities observed during creep crack growth in pyroceram.

Fig. 16. TEM replica showing a pocket of creep cavities surrounded by relatively uncavitated regions.

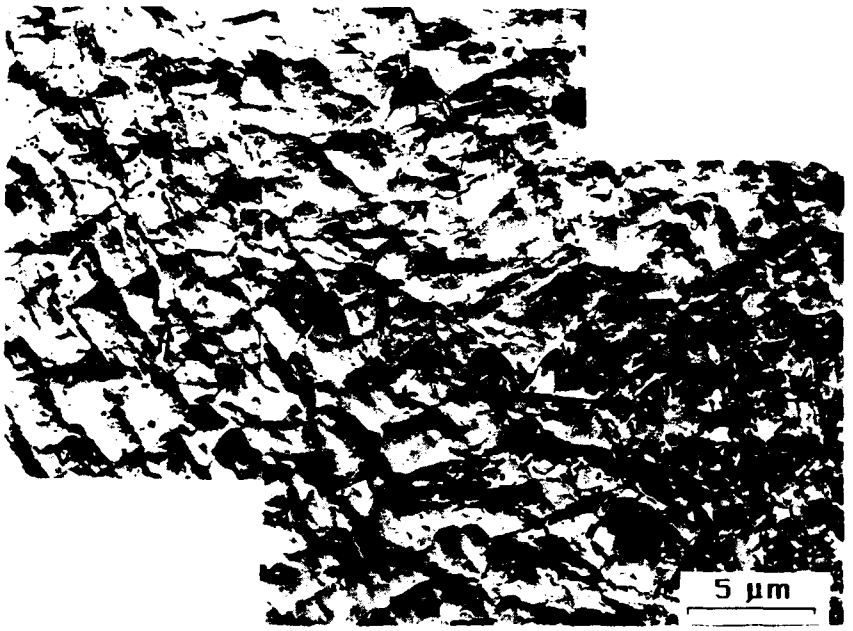

Fig. 17. Heavily cavitated regions at both ends of a microcrack.

when the crack tip encountered regions of low damage. A change of the crack growth behavior from a continuous to a discontinuous mode or vice versa is therefore expected as the creep crack propagates through a nonuniform distribution of cavitated and uncavitated regions, as was observed experimentally.

The creep-damaged area observed in the glass-ceramic was large, extending from the tip of the main crack to the opposite edge of the specimen. The large damage zone was characteristic of a crack subjected to a relatively high stress intensity factor over a relatively long period of time of creep. A previous study[14] has shown that the near-tip strain and crack opening behavior in the pyroceram glass-ceramic were those of the Riedel–Rice type[25] when the time of creep was short and the amount of crack extension was small. Furthermore, the crack opening displacement attained the steady-state condition after only 110 min of creep at a K level of 0.80 MPa·m$^{1/2}$ and at 700 C. Since the creep damage characterization presented in this paper was performed for a creep crack that had been growing at K = 0.95 MPa·m$^{1/2}$ and 750 C for more than 300 min, the large creep damage zone was probably the consequence of gross creep in the specimen. The development of creep damage over the range of small to large creep conditions can be elucidated by considering the evolution of the creep zone with time of creep. For small-scale creep, the size, r_c, of the creep zone ahead of a creep crack is described by[25]

$$r_c \propto K^2 t^{(n-1)} \tag{4}$$

and the accumulated effective creep strain, $\bar{\varepsilon}$, is

$$\bar{\varepsilon} \propto K^{2n/(n+1)} t^{(n-1)/(n+1)} \tag{5}$$

with

$$\bar{\varepsilon} = (2/3)(\varepsilon_{ij}\varepsilon_{ij})^{1/2} \tag{6}$$

where n is the creep exponent, ε_{ij} is the strain tensor, and t is the time of creep. Since the creep exponent for the pyroceram ranges from 1.5 to 2.0,[14] both the creep zone and its rate of growth increase with time at a constant K level. Figure 13 shows that the slope for the crack density parameter, Ψ, versus distance, r, plot is ≈0.75, which is approximately the same as that for the radial dependence of creep strain in the Riedel–Rice field and those observed in the pyroceram for large r.[14] The similarity in the radial dependence suggests that the crack density might be proportional to the effective creep strain accumulated within the creep zone, i.e.,

$$\Psi \propto \bar{\varepsilon} \tag{7}$$

which may be combined with Eqs. (4) and (5) to give

$$\Psi \propto K^{2n/(n+1)} t^{(n-1)/(n+1)} \tag{8}$$

$$r_d \propto K^2 t^{(n-1)} \tag{9}$$

as the extent of the damage zone, r_d. The lack of a contained near-tip damage zone in the pyroceram glass-ceramic may then be directly attributed to two factors: (1) the relatively low n value ($1 \le n \le 2$) of the pyroceram, which causes both the damage zone size and its rate of growth to increase with time, and (2) a relatively large time of creep.

The observation of a critical accumulated effective creep strain for incremental crack extension lends support to the use of such an assumption in many creep-crack growth models.[29,30] However, the relation between the crack density parameter, Ψ, and the accumulated effective creep strain (Eq. 7) implies that the observed critical creep strain criterion may in reality be a manifestation of a critical crack density or creep damage criterion; i.e., crack extension occurs when the microcrack density or creep damage in the process zone attains a critical value. In fact, a critical crack density or creep damage criterion might be more consistent with experimental observations over the whole range of the crack growth curve, including the threshold region, than does a critical accumulated effective creep strain. In particular, previous observations both for the pyroceram glass-ceramics[14] and for other ceramics[5,31] indicate that crack-tip blunting accompanied the creep crack growth threshold. Since crack-tip blunting necessarily accumulates creep strain near the crack tip, a critical accumulated creep strain criterion would lead to crack growth and is, therefore, inconsistent with the observation of a growth threshold. On the other hand, crack-tip blunting at the growth threshold is acceptable in a critical crack density or creep damage criterion if crack-tip blunting occurs without causing damage accumulation near the crack tip. Indirect evidence of a change in the damage accumulation processes at K levels below and above the growth threshold is shown in Fig. 18. At $K > K_{th}$, creep-crack growth in the pyroceram propagated along a localized shear channel of creep strain within which creep damage appeared to accumulate. As indi-

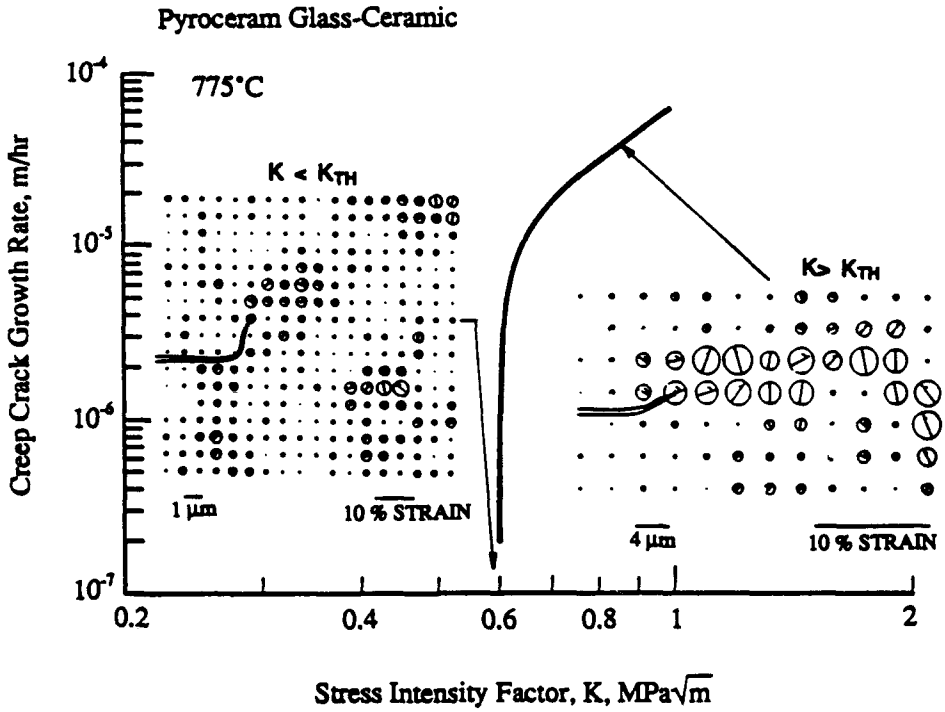

Fig. 18. Comparison of the distributions of creep strain at K levels below and above the growth threshold, K_{th}. At $K > K_{th}$, creep-crack growth occurred by propagating along a localized shear zone formed ahead of the main crack. At $K < K_{th}$, a localized crack-tip shear zone was absent and no detectable crack growth was observed.

cated in a previous paper,[14] crack-tip shear channels were frequently observed during creep-crack growth in the pyroceram glass-ceramic. Possible mechanisms attributed to the formation of these localized shear channels ahead of the crack tip are (1) a saw-tooth crack path with deflection angles ranging from 20° to 50°, and (2) anisotropic flow behavior due to stochastic sliding of grain boundaries. Such a shear channel of creep strain is absent in creep cracks below the growth threshold, as shown in Fig. 18. The implication is that the formation of a localized channel of shear strain is important in the damage accumulation process, and the lack of a shear channel leads to the growth threshold. Since the first step in the process is the nucleation of grain-boundary cavities, the growth threshold and the shear channel in the pyroceram might be related to cavity nucleation,[31] which in turn might be induced by stochastic grain-boundary sliding. Further studies of the damage accumulated around creep cracks loaded below their threshold are required to determine the origin of the shear channel and whether crack growth is indeed a critical damage-controlled process.

Another question concerning the creep-crack growth curves shown in Fig. 5 is whether the stress intensity factor, K, is the relevant correlating parameter. Based on the analysis of Riedel and Rice, one would think the stress intensity factor would be applicable only for small-creep conditions, while the C^* parameter would be pertinent for large-creep conditions.[28] Figure 5 indicates that K appears to correlate the creep-crack growth rates rather well for the pyroceram, even though gross creep and damage occurred at the higher K levels. Previously, Blumenthal and Evans[10] showed that K is the relevant parameter for correlating the creep crack growth data of alumina for which the creep exponent, n, has a value close to unity. The present results are consistent with those of Blumenthal and Evans.[10] One possible explanation of the applicability of K to the large-creep conditions might be the relatively low n values (n = 1.5 to 2) for the pyroceram, which is somewhat close to the n = 1 condition for elastic loading for which K is the relevant correlating parameter. It is possible that for materials with low n values, the differences between the stress fields under small- and large-creep conditions are not too significant such that K is adequate as the correlating parameter for crack growth rates over the whole range of small- to large-creep regimes, resulting in the good correlation as shown in Fig. 5.

IV. Conclusions

(1) Creep-crack growth in the pyroceram glass-ceramic occurs both in a continuous and discontinuous manner.

(2) The damage processes associated with creep-crack growth in the pyroceram include the nucleation, growth, and coalescence of grain-boundary cavities into microcracks, as well as the propagation and linkage of microcracks with the main crack.

(3) The microcrack density in the pyroceram glass-ceramic decreased with increasing distance from the crack tip in the same manner as the Riedel and Rice creep strain field.

(4) Creep-crack growth in the pyroceram obeys a critical accumulated effective creep strain criterion. Crack extension occurred when the accumulated effective creep strain near the crack tip reached approximately 2% at 750°C. The critical strain criterion might, however, be a manifestation of a critical microcrack density or creep damage criterion.

(5) A threshold exists in the creep-crack growth curve of the pyroceram. The threshold appears to originate from the lack of damage accumulation in the near-tip region when the K level is below a critical value.

Acknowledgment: Encouragement by the Air Force Program Manager, Dr. L. J. Schioler, is acknowledged.

References

[1]A. G. Evans and F. F. Lange, "Crack Propagation and Fracture in Silicon Carbide," *J. Mater. Sci.*, **10** [10] 1659–64 (1975).

[2]F. F. Lange, "High-Temperature Strength Behavior of Hot-Pressed Si_3N_4: Evidence for Subcritical Crack Growth," *J. Am. Ceram. Soc.*, **57** [2] 84–87 (1974).

[3]M. G. Mendiratta and J. J. Petrovic, "Slow Crack Growth from Controlled Surface Flaws in Hot-Pressed Si_3N_4," *J. Am. Ceram. Soc.*, **61** [5–6]

226–30 (1978).
[4]K. D. McHenry and R. E. Tressler, "Fracture Toughness and High-Temperature Slow Crack Growth in SiC," *J. Am. Ceram. Soc.*, **63** [3–4] 152–56 (1980).
[5]E. J. Minford and R. E. Tressler, "Determination of Threshold Stress Intensity for Crack Growth at High Temperature in Silicon Carbide Ceramics," *J. Am. Ceram. Soc.*, **66** [5] 338–40 (1983).
[6]H. G. Schmid, T. Haug, A. Bornhauser, V. Gerold, and R. F. Pabst, "Crack Growth in Al_2O_3 with 3 wt% Glassy Phase"; pp. 631–41 in *Deformation of Ceramics II*. Edited by R. E. Tressler and R. C. Bradt. Plenum Press, New York, 1984.
[7]N. J. Tighe, S. M. Wiederhorn, T. J. Chuang, and C. L. McDaniel, "Creep Cavitation and Crack Growth in Silicon Nitride"; pp. 587–604 in Materials Science Research, Vol. 18, *Deformation of Ceramics II*. Edited by R. E. Tressler and R. C. Brandt. Plenum Press, New York, 1984.
[8]R. L. Tsai and R. Taj, "Creep Fracture in Ceramics Containing Small Amounts of a Liquid Phase," *Acta Metall.*, **30**, 1043–58 (1982).
[9]A. G. Evans and W. Blumenthal, "High-Temperature Failure in Ceramics"; pp. 423–48 in Fracture Mechanics of Ceramics, Vol. 6, *Measurements, Transformations and High-Temperature Fracture*. Edited by R. C. Bradt, A. G. Evans, D. P. H. Hasselman, and F. F. Lange. Plenum Press, New York, 1985.
[10]W. Blumenthal and A. G. Evans, "High-Temperature Failure of Polycrystalline Alumina: II. Creep Crack Growth and Blunting," *J. Am. Ceram. Soc.*, **67** [11] 751–59 (1984).
[11]K. Jakus, S. M. Wiederhorn, and B. J. Hockey, "Nucleation and Growth of Cracks in Vitreous-Bonded Aluminum Oxide at Elevated Temperatures," *J. Am. Ceram. Soc.*, **69** [10] 725–31 (1986).
[12]A. G. Evans and B. J. Dalgleish, "Some Aspects of the High Temperature Performance of Ceramics and Ceramic Composites," *Ceram. Eng. Sci. Proc.*, **7** [9–10] 1073–1094 (1986).
[13]B. J. Dalgleish, E. Slamovich, and A. G. Evans, "High Temperature Failure of Ceramics," *J. Mater. Energy Syst.*, **8** [2] 211–25 (1986).
[14]R. A. Page, K. S. Chan, D. L. Davidson, and J. Lankford, "Micromechanics of Creep-Crack Growth in a Glass Ceramic," *J. Am. Ceram. Soc.*, **73** [10] 2977–86 (1990).
[15]M. D. Thouless and A. G. Evans, "On Creep Rupture in Materials Containing an Amorphous Phase," *Acta Metall.*, **34** [1] 23–31 (1986).
[16]T.-J. Chuang, "A Diffusive Crack Growth Model for Creep Fracture," *J. Am. Ceram. Soc.*, **65** [2] 93–103 (1982).
[17]J. Lankford, "Strength of Monolithic and Fiber-Reinforced Glass Ceramics at High Rates of Loading and Elevated Temperature," *Ceram. Eng. Sci. Proc.*, **9** [7–8] 843–52 (1988).
[18]T. I. Barry, L. A. Lay, and R. Morrell, "High Temperature Mechanical Properties of Cordierite Refractory Glass Ceramics," *Proc. Br. Ceram. Soc.*, **24**, 67–84 (1975).
[19]R. Raj and C. K. Chyung, "Solution-Precipitation Creep in Glass Ceramics," *Acta Metall.*, **29** [1] 159–66 (1981).
[20]R. F. Cooper, D. L. Kohlstedt, and K. Chyung, "Solution-Precipitation Enhanced Creep in Solid Liquid Aggregates Which Display a Non-Zero Dihedral Angle," *Acta Metall.*, **37** [7] 1759–71 (1989).
[21]E. M. Heuse and G. Partridge, "Creep Testing of Glass-Ceramics," *J. Mater. Sci.*, **9** [8] 1255–61 (1974).
[22]A. Nagy, J. B. Campbell, and D. L. Davidson, "A High Temperature Cyclic Loading Stage for the SEM," *Rev. Sci. Instrum.*, **55** [5] 778–82 (1984).
[23]T. G. F. Gray, "Convenient Closed Form Stress Intensity Factors for Common Crack Configurations," *Int. J. Fract.*, **13** [1] 65–75 (1977).
[24]E. A. Franke, D. J. Wenzel, and D. L. Davidson, "Measurement of Micro-Displacements by Machine Vision Photogrammetry (DISMAP)," *Rev. Sci. Instrum.*, **62** [5] 1270–79 (1990).
[25]D. R. Williams, D. L. Davidson, and J. Lankford, "Fatigue-Crack-Tip Plastic Strains by the Stereoimaging Technique," *Exp. Mech.*, **20** [4] 134–39 (1980).
[26]B. Budiansky and R. J. O'Connell, "Elastic Moduli of a Cracked Solid," *Int. J. Solids Struct.*, **12** [2] 81–97 (1976).
[27]E. E. Underwood, "The Mathematical Foundations of Quantitative Stereology"; pp. 3–38 in *Stereology and Quantitative Metallography*, ASTM STP 504. American Society for Testing and Materials, Philadelphia, PA, 1972.
[28]H. Riedel and J. R. Rice, "Tensile Cracks in Creeping Solids"; pp. 112–30 in *Fracture Mechanics: Twelfth Conference*, ASTM STP 700. American Society for Testing and Materials, Philadelphia, PA, 1980.
[29]H. Riedel and W. Wagner, "The Growth of Macroscopic Cracks in Creeping Materials"; pp. 683–90 in Proceedings of the Fifth International Conferences on Fracture, Vol. 2, *Advances in Fracture Research*. Edited by D. Francois. Pergamon Press, New York, 1981.
[30]H. Riedel, *Fracture at High Temperatures*; pp. 319–23. Springer-Verlag, Berlin, FRG, 1986.
[31]M. D. Thouless and A. G. Evans, "Some Considerations Regarding the Creep Crack Growth Threshold," *Scr. Metall.*, **18** [10] 1175–80 (1984). □

ORIGIN OF THE CREEP CRACK GROWTH THRESHOLD IN A GLASS-CERAMIC

by

K. S. Chan and R. A. Page
Department of Materials and Mechanics
Southwest Research Institute
San Antonio, Texas 78228-0510

ABSTRACT

The growth threshold, K_{th}, of large creep cracks in a glass-ceramic has been investigated to determine the causes of the arrest and nonpropagating behaviors below the characteristic stress intensity, K, value. Using replication techniques, the dominant, or the lack of, creep damage mechanisms, including grain boundary cavity and microcrack formation, during creep crack growth were identified as a function of K levels and crack extension rates. Quantitative measurements of cavity density, $D_c(r)$, and microcrack density, $\Psi(r)$, revealed that the values of $D_c(r)$ and $\Psi(r)$ both decrease with the K level and with increasing distance, r, from the crack tip at a given K level. At K values below K_{th}, the cavity density became zero as preexisting grain boundary cavities were sintered, suggesting that the growth threshold originated from sintering of creep cavities. At K levels above K_{th}, microcracks located in the wake of the main crack were observed to be sintered also. Possible mechanisms responsible for the apparent self-healing of microcracks and creep cavities in the glass-ceramic are provided, together with theoretical and experimental support.

INTRODUCTION

Creep or subcritical crack growth in a number of ceramics, either with or without an amorphous phase along grain boundaries, has been studied at elevated temperatures, by many investigators [1-15]. The results of these studies have demonstrated that the crack growth rate, $V = da/dt$, where a is crack length and t is time of creep, can generally be correlated in terms of the stress intensity factor, K, in a manner as shown in Figure 1 [4]. A special feature of the crack velocity curve, shown in Figure 1, is the existence of a threshold stress intensity, K_{th}, below which creep crack growth does not occur [8,10,15]. The existence of this growth threshold, which is typical for large flaws, has been predicted by previous analyses [8,16,17] that related K_{th} to the threshold stress, σ_{th}, for nucleating cavities near the tip of a creep crack [8,16,17]. At $K > K_{th}$, the crack growth rate increases with K, usually according to a power-law relation (i.e., $V = CK^n$) until fast fracture intervenes when K approaches K_{IC}. For naturally initiated creep cracks, a growth threshold is generally not observed [11], and the crack velocity is described by another power-law relationship that remains valid in the regime where stress intensity levels are well below the large crack threshold, K_{th}.

In a recent study [15], a growth threshold was also observed for creep cracks in a glass-ceramic. At $K \leq K_{th}$, the crack was found to exhibit crack-tip blunting without causing crack extension. The crack arrest or nonpropagation behavior was accompanied by a change in the near-tip creep strain field when compared to the behavior observed at higher K levels [14,15]. At $K > K_{th}$, the near-tip creep strains were characterized by the presence of a localized shear zone located ahead of the tip of the creep crack, which usually assumed a deflected path by propagating along the shear zone. In contrast, the near-tip shear strains were lower, but without the formation of the localized shear zone or detectable crack extension at $K < K_{th}$. Those observations suggest that the localized shear zone, whose mechanism of formation has not been determined, is an important feature of the creep crack growth process in the glass-ceramic. In particular, the shear zone might be a manifestation

of the creep damage process that occurs near the crack tip. If proven to be true, then the growth threshold can be interpreted as the stress intensity level above which creep damage accumulates ahead of the crack tip and below which creep damage does not occur.

The objective of this paper is to present results of a study that examines the origin of the growth threshold in the Corning 9606 MAS glass-ceramic. Specifically, the damage processes associated with creep crack growth in the glass-ceramic have been measured quantitatively for various K levels at different regions of the crack growth curve, including that below the growth threshold, K_{th}. These quantitative results are then related to the crack growth responses in order to assess the origin of the growth threshold for creep cracks in ceramics. Furthermore, previous results have indicated creep crack growth in the MAS glass-ceramic obeys a critical effective creep strain criterion [15]. As indicted earlier [15], the critical strain criterion is inconsistent with the observed K_{th}, and it is expected not to hold at K levels below K_{th} due to crack-tip blunting and continuing creep strain accumulation. It has been suggested that the critical creep strain criterion is probably a manifestation of a critical cavity or microcrack density criterion. As a continuation of the previous work [14,15], the present paper will also assess the validity of using either the cavity density or microcrack density parameter as a measure of damage during creep crack growth in the glass-ceramic.

EXPERIMENTAL PROCEDURES

A magnesium-aluminosilicate glass-ceramic (Corning 9606) was used as a model material for liquid-phase-sintered ceramics. The microstructure consisted of approximately 0.5 μm cordierite grains surrounded by a thin continuous grain-boundary amorphous phase whose softening point is about 600°C [18]. Above the softening point, deformation of the glass-ceramic occurs by a combination of grain boundary sliding and cavitation.

Both round-bar and single-edge-notched (SEN) specimens were used for the study; geometries and dimensions of these two types of specimen are presented in Figure 2. The round-bar specimens were utilized for characterizing creep rate and bulk damage, while the single-edge-notched specimens were used for creep crack growth studies. For comparison with tensile creep data, compression creep specimens in the form of 6.35 mm diameter cylinders 12.7 mm in height were also used. The SEN specimens were precracked by cyclic fatigue under compressive loads at room temperature. After precracking, the specimens were coated with gold to provide a conductive surface and tested under a constant tensile load using a high-temperature loading stage located inside a scanning electron microscope [19]. Both the tensile and compressive creep tests were conducted in a MTS servo-hydraulic testing machine equipped with an Instron Pancake furnace and Instron grips for ceramics. All the tests were performed at 775°C in air. Displacements were measured using a high-temperature capacitance extensometer made by Instron. The resolution of the extensometer was better than 8 microstrain.

During creep crack growth tests, the near-tip region of the creep crack was photographed at various times of creep. Two micrographs of the same region at two different times of creep constituted a stereo-pair that was analyzed by the machine-vision-based stereoimaging technique [20], DISMAP, to obtain both crack opening displacements and near-tip creep strain distributions. The procedures for performing these local strain and displacement measurements were reported earlier [14,15,21].

After the creep crack growth experiments, the SEN specimens were ion-milled for four hours to remove the conductive coating and other surface contaminants. The specimen surface was then replicated using acetobutyrate and cellulose acetate tapes. The former was coated with aluminum and examined in the SEM, while the latter was coated with carbon, shadowed, dissolved, and

examined via the TEM. Both the SEM and TEM micrographs were then used to characterize the distribution, size, and density of microcracks and cavities, using quantitative ceramographic techniques.

The local density of microcracks, Ψ, in a local sampling area, A_l, was measured as [15]

$$\Psi(r) = \frac{n_i \pi a_i^2}{A_l} \tag{1}$$

where n_i is the number of microcracks of half-length, a_i. The values of both n_i and a_i depend on the distance, r, from the crack tip, with the repeated indices indicating summation. Defined in this manner, Ψ represents the fraction of cracked area in the local sampling area, A_l, located at the distance r from the crack tip. The value of $\Psi(r)$ is related to the volumetric microcrack density parameter of Budiansky and O'Connell [22] by a constant of $4\pi/3$ [15]. A sampling square of 0.254 mm was generally used in the present study. For microcrack density near the crack tip, the sampling area was halved. The local cavity density was determined according to the expression

$$D(r) = A_{C.R.}(r)\, D_{C.R.}(r) \tag{2}$$

where $A_{C.R.}(r)$ is the area fraction of cavitation pockets (i.e., cavitated area) in a sampling area situated at a distance, r, from the crack tip, and $D_{C.R.}(r)$ is the average cavity density within individual cavitation pockets. To determine $A_{C.R.}(r)$, cavitation pockets were traced from TEM micrographs taken at 1300X magnification; their area fraction was then measured using the Tracor Image Analyzer. The cavity density parameter, $D_{C.R.}(r)$, was measured as the area fraction of cavities within the sampling area using high-magnification (>3600X) TEM micrographs. As in the case of cavitation pockets, the cavities were traced and analyzed using the Tracor Image Analyzer.

RESULTS

The steady-state creep rates of the glass-ceramic (Corning 9606 MAS) obtained under tension and compression are compared in Figure 3. Power-law creep was observed in both cases, with an identical creep exponent, n, of approximately 1.36. This particular value of n is slightly higher than the value of unity ($n = 1$) observed in Corning 9608 LAS [23,24], but it is somewhat lower than the values of 1.5 to 2.2 reported for similar pyroceram glass-ceramics [25,26]. The tension creep data were obtained at stresses whose magnitudes were lower than those for compression. Extrapolation of the compression creep data to the same stress range used in the tension creep experiment revealed that the steady-state creep rates were about five times higher in tension than in compression at the same stress level. Similar discrepancies between tension and compression creep data were previously reported for glass-ceramics [27,28], vitreous bonded aluminum oxide [29], silicon nitride and composites [29-32], and for siliconized silicon carbides [33-36]. The higher steady-state creep rates under tensile loading in those ceramics were shown to arise from the contribution of grain boundary cavitation to the overall macroscopic creep strain and strain rate [33,34,37]. The higher tensile rate of creep in the pyroceram is believed to originate also from a higher rate of cavitation along grain boundaries during tensile creep.

Mode I and II crack opening displacements were measured as a function of distance, r, behind the crack tip for various K levels and times of creep. The rates of Mode I and II crack opening displacement (COD) were obtained by dividing the incremental COD values by the time increments. The rate of effective COD at the distance r was then computed as the root-mean-square of the individual COD rate components. The rates of effective crack opening displacement, $\dot{\delta}_{eff}$, for creep cracks in the pyroceram tested at 775°C are shown in Figure 4 for K levels of 0.6, 0.59, and 0.5 $MPa\sqrt{m}$. The former two K levels were slightly above the growth threshold, K_{th}, while the latter was below K_{th}. Figure 4 shows that the creep crack continued to blunt, thereby resulting in crack opening displacements, at K levels below the growth threshold. At the near threshold regime, the

crack opening displacement rate increased rapidly with increasing K levels. This behavior is consistent with the crack growth rate, which also showed a strong dependence on the K level near the threshold. The near-tip creep strain measurements, which are presented in Figure 5 in terms of Mohr's circles for strains, show accumulation of creep strains near the crack tip for $K \approx K_{th}$ (Figure 5a), as well as for $K = 0.5\ MPa\sqrt{m}$, which was below the threshold (Figure 5b). This set of results clearly indicates that accumulation of creep strain near the tip of a crack is not a sufficient condition for creep crack growth. In other words, the critical effective creep strain criterion observed earlier for the pyroceram is probably an indirect manifestation of the actual failure criterion.

The more appropriate failure criterion for creep crack growth in the glass-ceramic is believed to be one that is based on a critical value of cavity or microcrack density. To assess this possibility, quantitative measurements of cavity density, $D(r)$, and microcrack density, $\Psi(r)$, were obtained as a function of distance, r, from the crack tip for several K levels at different crack growth regimes. Figure 6 shows traces of microcracks ahead of the crack tip for K levels of 0.95 and 0.7 $MPa\sqrt{m}$, respectively. For both cases, microcracks tended to concentrate near the tip of the creep crack. Note that the orientations of the microcracks are not exclusively normal to the external stress axis. At short crack lengths, the microcracks tended to orient in a random orientation. As the length of microcracks was increased by linkage of several microcracks, the resulting microcracks generally exhibited a tendency to align more or less normal to the applied stress.

In Figure 7, the microcrack density ahead of creep crack at $K = 0.7\ MPa\sqrt{m}$ is compared before and after an increment of crack extension. In both cases, the microcrack density decreased with increasing distance from the crack tip according to a power-law, with an exponent of ≈ 1.0, which is somewhat larger than the value of $\approx .75$ observed earlier for $K = .95$ MPa$\sqrt{m}$ [15]. Prior to crack extension, the near-tip microcrack density was as high as 30%; its value was reduced to 7% after crack extension by linkage of microcracks with the main crack tip. The amplitude or value of the near-tip microcrack density thus depends on the time of creep and on the crack extension

process. The spatial distributions of microcrack density as a function of distance from crack tip are shown in Figure 8 for K levels of 0.95, 0.7, and 0.59 $MPa\sqrt{m}$. At the two higher K levels, there were high concentrations of microcracks ahead of the crack tips, and the creep crack growth rates were relatively high. At $K = 0.59\ MPa\sqrt{m}$, the creep crack was found to propagate at finite growth rates, even though no well-defined microcracks were observed anywhere on the specimen surface. The implication of these results is that creep crack growth in the pyroceram is probably not controlled by attaining a critical microcrack density near the crack tip, as creep crack extension can occur without the presence of microcracks near the dominant crack tip.

Quantitative measurements of cavity density characteristics of the glass-ceramic are presented in Figure 9 for $K = 0.95\ MPa\sqrt{m}$ at 750°C and in Figure 10 for $K = 0.59\ MPa\sqrt{m}$ at 775°C. Results presented in these two figures include the area fraction of cavitation pockets, $A_{C.R.}(r)$, cavity density within individual cavitation pockets, $D_{C.R.}(r)$, and the average cavity density, $D(r)$. One of the significant findings in Figures 9 and 10 is that cavitation during creep crack growth in the pyroceram was not limited to the near-tip region, but extended over the entire ligament of the cracked specimen. Both the area fraction of cavitation pockets, $A_{C.R.}(r)$ and the cavity density, $D(r)$, decrease with increasing distance from the crack tip. On the other hand, the dependence of the cavity density within individual cavitation pockets, $D_{C.R.}(r)$, on the distance, r, was less defined. For $K = 0.95\ MPa\sqrt{m}$, $D_{C.R.}(r)$ was relatively independent of r, while it was mildly dependent on r for $K = 0.59\ MPa\sqrt{m}$. The relatively large scatter for the latter case made it difficult to establish the proper relationship in a definitive manner.

Figure 11 compares results of cavity density, $D(r)$, for three different K levels in the 750-775°C range. For both 0.95 $MPa\sqrt{m}$ and 0.59 $MPa\sqrt{m}$, the cavity density decreased with increasing distance from the crack tip. The results for $K = 0.5\ MPa\sqrt{m}$, which were obtained by testing a pre-cavitated specimen ($K = 0.59\ MPa\sqrt{m}$), indicated that all of the preexisting creep cavities were sintered away, suggesting that the growth threshold in this material arises from the removal of creep

damage by sintering of creep cavities. Comparison of the near-tip regions of the creep cracks at $K = 0.59\ MPa\sqrt{m}$ and $K = 0.5\ MPa\sqrt{m}$ is shown in Figure 12, with Figure 12(a) showing the presence of near-tip creep cavities at $K = 0.59\ MPa\sqrt{m}$ and Figure 12(b) showing the removal of those cavities by sintering at $K = 0.5\ MPa\sqrt{m}$. The near-tip region where creep cavities were observed were traced and superimposed on the near-tip creep strain field in Figure 5(a). The comparison revealed that there was almost a one-to-one correlation between regions of high creep strains and creep cavities. This finding indicates that creep cavitation had contributed to the near-tip creep strains. Figure 5(a) also demonstrates that the localized shear zone ahead of the creep crack tip is a region that is heavily cavitated. Thus, the notion that the localized shear zone is a "process" zone within which creep damage accumulates and crack extension occurs is valid. Detailed examination of the TEM replicas obtained for $K = 0.59\ MPa\sqrt{m}$ revealed creep damage in the form of creep cavities only; no well-defined microcracks were observed anywhere on the surface of the specimen. However, incipient microcracks in the form of grain boundary cavities aligned in linear arrays were observed, as shown in Figure 13. Since creep crack growth occurred at $K = 0.59\ MPa\sqrt{m}$, these observations suggested that creep crack growth might be controlled by a critical cavity density criterion.

IMPLICATIONS

Sintering of Crack-Wake Microcracks

The observation of sintering of cavities at positive K levels below the growth threshold, K_{th}, raised several interesting questions, including one about the possibility that microcracks located in the wake of the creep crack could be sintered. This possibility arises because the local stress intensity of the microcracks decreases with increasing distance from the dominant crack tip [38]. As the creep crack propagates, microcracks located behind the tip of the main crack should experience a reduction in the local stress intensity. When the local K values for the crack-wake microcracks

drop below K_{th}, creep cavities and microcracks that were formed by coalescence of creep cavities should sinter at least partially, if not completely. To investigate the possibility of microcrack sintering in the crack wake, individual microcracks located behind the tip of the main crack in the pyroceram specimen that was previously crept at 0.7 $MPa\sqrt{m}$ and at 775°C were characterized by the replication technique. The cracked specimen was then crept at 0.85 $MPa\sqrt{m}$ and at 775°C in the SEM. The higher K value was used so that any residual stresses introduced during unloading of the test specimen for replication purposes would be relieved. During the experiment, the creep crack, shown in Figure 14, was found to exhibit both active and inactive branches. The active branches of the main crack continued to blunt, exhibit crack opening displacements, and propagate, while the inactive one manifested tightly closed crack surfaces, giving the appearance of being sintered. Micrographs of the inactive branch of the creep crack were taken at two different times of creep. When this stereo-pair of micrographs was analyzed by the stereoimaging technique, both the crack opening displacements and the near-tip creep strains were found to be negative during the period of interest, as shown in Figure 15. The results indicated that the inactive microcrack was indeed being sintered. Replicating the wake region of the creep crack after the crack growth experiment revealed that several microcracks located behind the tip of the dominant creep crack had been sintered, either partially or completely, as shown in Figure 16. Remnants of the inactive branch of the creep crack, whose sintering process is shown in Figure 14 and 15, are indicated by an arrow. Quantitative measurements of microcrack density in the crack wake region also revealed lower values for Ψ, indicating the removal of microcracks in the crack wake by sintering. This point can best be illustrated by the contour plots of microcrack density in Figures 17(a)and (b) for K of 0.95 and 0.7 $MPa\sqrt{m}$, respectively. The contours in these plots represent lines of equal values of the microcrack density parameter, Ψ, in percent area fraction. In both cases, the value of Ψ decreases rapidly with increasing distance behind the crack tip, rather than remaining at a constant

value representative of the near-tip value. This particular profile of microcrack density in the crack wake is consistent with the notion that sintering occurred as the result of a decrease in the local K levels of the microcrack to values below K as the main crack propagated away from the microcracks.

Sintering Characteristics of Creep Cavities

The strong tendency of the glass-ceramic to exhibit sintering of microcracks and cavities at $K < K_{th}$ implies that cavity sintering in this material can take place under small tensile loads, probably due to high sintering stresses. To verify this hypothesis, a smooth round-bar specimen of the glass-ceramic was crept under a uniform tensile stress of 42 MPa at 775°C, yielding the creep curve shown in Figure 18(a). After 16 hours of creep, the applied tensile stress was lowered to 1.4 MPa, resulting in contraction of the specimen, as shown in Figure 18(b). Subsequent increases in tensile loads led to temporary extension, followed by contraction of the creep specimen, as the time of creep was increased. As shown in Figure 18(b), contraction of the creep specimen was observed at tensile stresses of 1.4, 4.1, and 6.1 MPa. At 6.9 MPa, the specimen was found to neither extend nor contract, but maintained a constant length. A possible explanation for the observed behavior is that creep cavities were nucleated during tensile creep at 42 MPa. Experimental support of this thinking is shown in Figure 19, which shows the local density values along the gauge length and at the grip sections of the crept specimen. Determined by precision density measurement techniques, these local density values are accurate up to three digits behind the decimal point. The lower density values along the gauge section of the crept specimen compared to those at the grip sections strongly suggest the generation of creep cavities and/or microcracks in the gauge section as the result of tensile creep. As the applied stress was lowered, it was likely that sintering of some of the previously nucleated cavities would take place, leading to the observed contraction of the test specimen. Raising the applied tensile stress caused an increase in the cavity density, which accounted for the increase in creep strain and extension of the specimen. Subsequent sintering of the creep cavities, both newly and previously formed, led to further contraction of the test specimen with increasing time of creep.

Extension of the test specimen occurred without subsequent contraction, which happened at 14MPa (not shown in Figure 18), only when generation of creep cavities overwhelmed their removal by sintering. Comparison of the creep rate at 42 MPa and the contraction rate at 1.4MPa in Figure 20 indicates that the sintering rate, taken to be the contraction rate, is on the order of the creep rate, despite the much lower stress value used for sintering. The creep rate for 1.4 MPa could be obtained by extrapolation of the data in Figure 3. In doing so, a creep rate of 2×10^{-10}sec^{-1} was obtained for 1.4 MPa, compared to a sintering rate of 2×10^{-8}sec^{-1} or higher at the same stress level. The self-healing process exhibited in the crack wake of the glass-ceramics is therefore the consequence of two factors: (1) unloading of the local stress intensity of microcracks below the K_{th} value due to diminishing influence of the dominant crack, and (2) the dominance of sintering kinetics over cavitation kinetics at K levels below K_{th}.

DISCUSSIONS

The combination of creep damage characterization and crack-tip opening measurements suggests that at least two different mechanisms contribute to the creep strains measured for the glass-ceramic. One of these two mechanisms is creep cavitation [33,34,37] in the form of either cavities or microcracks, while the other is probably grain boundary sliding [8,14]. Other deformation mechanisms such as solution and re-precipitation [23,24], percolation [11], and diffusional flow [11] are possible, but their contributions, if indeed present, might be quite limited. At K levels above K_{th}, the measured creep strain includes contributions from cavitation grain boundary sliding and other deformation mechanisms (diffusional flow, and solution and re-precipitation) that do not lead to cavity or microcrack formation. At K levels below K_{th}, the contribution by cavitation is nil, leading to much lower near-tip strains and crack opening displacements, as shown in Figures 4 and 5. Judging from the relatively large variations in crack opening displacement with K in the near threshold regime, the cavitational strains appear to be large compared to those by other deformation mechanisms. This assessment is confirmed by the results shown in Figure 21, which

compares the measured near-tip effective creep strain rate computed for the Riedel-Rice (RR) field [39] based on steady-state creep tensile data shown in Figure 3. The measured creep rates are about 28X higher than the calculated results. This discrepancy can be attributed to the presence of microcracks and/or cavities in the cracked specimen during creep crack growth. Previous analysis by Hutchinson [40] has shown that the presence of microcracks ahead of the tip of a creep crack under the plane strain condition would lead to enhancement in the near-tip creep rates, in qualitative agreement with the present observation. A direct comparison of Hutchinson's plane strain results with our experimental measurements has not been made because the surface strain measurements might pertain to the plane stress condition.

The damage mechanisms observed at the various regimes of the crack growth curve are consistent with those predicted based on micromechanical models (e.g., see Figure 20 in [8] and Figure 7 in [16]). In particular, the growth threshold, K_{th}, is the K level above which cavities grow and below which cavities sinter. The model by Tsai and Raj [8] predicts a threshold stress, σ_{th}, given by

$$\sigma_{th} = \frac{4.2\gamma_g}{d\sqrt{V_g}} \tag{3}$$

where γ_g and V_g are the surface energy and volume fraction of the grain boundary amorphous phase, respectively, and d is the grain size. Tsai and Raj estimated that σ_{th} ranges from 5-15 MPa for liquid-phase-sintered ceramics. In comparison, the threshold stress for the glass-ceramic, estimated based on the stress level at which the contraction rate was nil, was approximately 7 MPa, in agreement with the theory of Tsai and Raj. Furthermore, the model of Thouless and Evans [16] predicts a growth threshold given by

$$K_{th} = 2\gamma_g\sqrt{\pi l}/h_o \tag{4}$$

where h_o is the thickness of the glassy phase, and l is the facet length. Eq (4) yields $K_{th} = 0.38 - 0.75\ MPa\sqrt{m}$ for the glass-ceramic when substituting $d = l = 0.5\ \mu m$, $\gamma_g = 0.3\ J/m^2$, and h_o = 1-2 nm. The estimated range of K_{th} values is in agreement with the observed value.

The good agreement between experimental observations and micromechanical models, however, needs to be put into proper perspective by noting that there are two important features of the micromechanical models that differ from the experimental observations. The first difference is that creep cavitation in the pyroceram occurs throughout the entire ligament of the cracked specimen, rather than being limited to the near-tip region as assumed in the models [8,16]. The second difference is that the creep damage process in the pyroceram does not occur by the nucleation of cavities at triple-points nor by the growth of triple-point cavities across two-grain facets [8]. At K levels above the near-threshold regime, the creep crack growth mechanisms in the pyroceram include both the growth and coalescence of cavities along two-grain facets [15], and the nucleation, growth, and coalescence of microcracks due to the formation of well-aligned, equally-spaced, and equally-sized creep cavities [15].

The cavitation and sintering behaviors associated with creep crack growth in the glass-ceramic can be understood on the basis of the recent transient cavity growth model of Chan and Page [41]. Originally proposed for ceramics under compressive creep, the model is equally applicable to cavitation under tensile creep. The salient feature of the transient cavity growth model is that nucleation of cavities requires relatively high local tensile stresses that can be attained only at local stress concentrations generated by transient grain boundary sliding. Cavities that are generated during transient grain boundary sliding may grow or be sintered, depending upon whether or not a critical steady-state creep or grain boundary sliding rate is exceeded. The critical steady-state creep rate, whose value depends on the viscosity of the grain boundary amorphous phase, is required so that the local tensile stress, induced by grain boundary sliding, exceeds the sintering stress at all times. Above the critical steady-state creep rate, cavities nucleated by the transient local tensile

stress can continue to grow until coalescing with contiguous cavities. At the critical steady-state creep rate, cavities that are nucleated will not grow beyond a certain size. In contrast, cavities will be sintered when the steady-state creep rate drops below the critical value. Since the measured near-tip creep rates for the glass-ceramic were indeed transient, the above-mentioned cavity growth and sintering process is entirely consistent with the experimental observations. Thus, the present results suggest that transient grain boundary sliding and creep play an important role in the creep crack growth process in the MAS glass-ceramics, and possibly in liquid-phase-sintered ceramics in general.

CONCLUSIONS

1. Cavitational strains resulting from cavity and microcrack formation contribute to the overall near-tip creep strains for creep cracks in a MAS glass ceramic.

2. The growth threshold, K_{th}, represents the K level above which creep cavities grow and below which creep cavities sinter.

3. Creep crack growth in the glass ceramic appears to obey a critical cavity density criterion.

4. Microcracks located in the crack wake are sintered as the dominant crack propagates away from the microcracks.

5. Cavities generated during tensile creep can be removed by sintering under small tensile loads.

6. Transient grain boundary sliding may be responsible for the cavitation and sintering characteristics exhibited by the glass-ceramic.

ACKNOWLEDGEMENTS

The authors are grateful for the support provided by the Air Force Office of Scientific Research through Contract No. F49620-88-C-0081. The encouragement by the Program Manager, Dr. L. J. Schioler, is acknowledged. Technical assistance by Messrs. J. B. Campbell, H. G. Saldana, J. F. Spencer, and R. J. Railsback, and by Ms. J. McCombs are acknowledged.

REFERENCES

1. A. G. Evans and F. F. Lange, "Crack Propagation and Fracture in Silicon Carbide," *J. Mate. Sci.*, 10 [10] 1659-64 (1975).

2. F. F. Lange, "High-Temperature Strength Behavior of Hot-Pressed Si_3N_4: Evidence for Subcritical Crack Growth," *J. Am. Ceram. Soc.*, 57 [2] 84-87 (1974).

3. M. G. Mendiratta and J. J. Petrovic, "Slow Crack Growth from Controlled Surface Flaws in Hot-Pressed Si_3N_4," *J. Am. Ceram. Soc.*, 61 [5-6] 226-30 (1978).

4. K. D. McHenry and R. E. Tressler, "Fracture Toughness and High-Temperature Slow Crack Growth in SiC," *J. Am. Ceram. Soc.*, 63 [3-4] (1980).

5. E. J. Minford and R. E. Tressler, "Determination of Threshold Stress Intensity for Crack Growth at High Temperature in Silicon Carbide Ceramics," *J. Am. Ceram. Soc.*, 66 [5] 338-40 (1983).

6. H. G. Schmid, T. Haug, A. Bornhauser, V. Gerold, and R. F. Pabst, "Crack Growth in Al_2O_3 with 3 wt% Glassy Phase," pp. 631-41 in *Deformation of Ceramics II*, R. E. Tressler and R. C. Bradt, eds., Plenum Publishing Corporation, New York (1984).

7. N. J. Tighe, S. M. Wiederhorn, T. J. Chuang, and C. L. McDaniel, "Creep Cavitation and Crack Growth in Silicon Nitride," pp. 587-604 in *Deformation of Ceramics II*, Materials Science Research, Vol. 18, R. E. Tressler and R. C. Brandt, eds., Plenum Press New York (1984)

8. R. L. Tsai and R. Taj, "Creep Fracture in Ceramics Containing Small Amounts of a Liquid Phase," *Acta Metal.*, 30 1043-58 (1982)

9. A. G. Evans and W. Blumenthal, "High-Temperature Failure in Ceramics," pp. 423-48 in *Fracture Mechanics of Ceramics*, Vol. 6, Measurements, Transformations and High-Temperature Fracture, R. C. Bradt, A. G. Evans, D. P. H. Hasselman, and F. F. Lange, eds., Plenum Press, New York (1985).

10. W. Blumenthal and A. G. Evans, "High-Temperature Failure of Polycrystalline Aluminia: II. Creep Crack Growth and Blunting," *J. Am. Ceram. Soc.*, 67 [11] 751-59 (1984)

11. K. Jakus, S. M. Wiederhorn, and B. J. Hockey, "Nucleation and Growth of Cracks in Vitreous-Bonded Aluminum Oxide at Elevated Temperatures," *J. Am. Ceram. Soc.*, 69 [10] 725-31 (1986)

12. A. G. Evans and B. J. Dalgleish, "Some Aspects of the High Temperature Performance of Ceramics and Ceramic Composites," *Ceramic Engineering and Science Proceedings*, 7 [9-10] 1073-1094 (1986).

13. B. J. Dalgleish, E. Slamovich, and A. G. Evans, "High Temperature Failure of Ceramics," *J. Materials for Energy Systems*, 8 [2] 211-225 (1986).

14. R. A. Page, K. S. Chan, D. L. Davidson, and J. Lankford, "Micromechanics of Creep-Crack Growth in a Glass Ceramic," *J. Am. Ceram. Soc.* 73 [10] 2977-86 (1990).

15. K. S. Chan and R. A. Page, "Creep Crack Growth by Damage Accumulation in a Glass-Ceramic," *J. Am. Ceram. Soc.*, in press (1991).

16. M. D. Thouless and A. G. Evans, "On Creep Rupture in Materials Containing an Amorphous Phase," *Acta Met.*, 34 [1] 23-31 (1986).

17. M. D. Thouless, "A Review of Creep Rupture in Materials Containing an Amorphous Phase," *Res Mechanica*, 22 [2] 213-242 (1987).

18. J. Lankford, "Strength of Monolithic and Fiber-Reinforced Glass Ceramics at High Rates of Loading and Elevated Temperature," *Ceram. Eng. Sci. Proc.*, 9 [7-8] 843-52 (1988).

19. A. Nagy, J. B. Campbell, and D. L. Davidson, "A High Temperature Cyclic Loading Stage for the SEM," *Review of Sci. Instruments*, 55 [5] 778-782 (1984).

20. E. A. Franke, D. J. Wenzel, and D. L. Davidson, "Measurement of Micro-Displacements by Machine Vision Photogrammetry (DISMAP)," *Rev. Sci. Inst.* (in press).

21. D. R. Williams, D. L. Davidson, and J. Lankford, "Fatigue-Crack-Tip Plastic Strains by the Stereoimaging Technique," *Experimental Mech.*, 20 [4] 134-39 (1980).

22. B. Budiansky and R. J. O'Connell, "Elastic Moduli of a Cracked Solid," *Int. J. Solids Structures*, 12 [2] 81-97 (1976).

23. R. Raj and C. K. Chyung, "Solution-Precipitation Creep in Glass Ceramics," *Acta Met.*, 29 [1] 159-166 (1981).

24. R. F. Cooper, D. L. Kohlstedt, and K. Chyung, "Solution-Precipitation Enhanced Creep in Solid Liquid Aggregates Which Display a Non-Zero Dihedral Angle," *Acta Met.*, 37 [7] 1759-1771 (1989).

25. T. I. Barry, L. A. Lay, and R. Morrell, "High Temperature Mechanical Properties of Cordierite Refractory Glass Ceramics," *Proc. British Ceramic Soc.*, 24 67-84 (1975).

26. E. M. Heuse and G. Partidge, "Creep Testing of Glass-Ceramics," *J. Mat. Sci.*, 9 [8] 1255-1261 (1974).

27. R. Morrell and K. H. G. Ashbee, "High-Temperature Creep of Lithium Zinc Silicate Glass-Ceramics," *J. Mater. Sci.*, 8 1253-70 (1973).

28. J.-G. Wang and R. Raj, "Mechanics of Superplastic Flow in a Fine-Grained Ceramic Containing Some Liquid Phase," *J. Am. Ceram. Soc.*, 67 [6] 399-409 (1984).

29. M. K. Ferber, M. G. Jenkins, and V. J. Tennery, "Comparison of Tension, Compression, and Flexure Creep for Alumina and Silicon Nitride Ceramics," *Ceramic Engineering and Science Proceedings*, in press (1990).

30. B. J. Hockey, S. M. Widerhorn, W. Liu, J. G. Baldoni, and S.-T. Buljan, "Tensile Creep of SiC Whisker Reinforced Silicon Nitride," Proceedings of the Twenty-Seventh Automotive Technology Development Contractors' Coordination Meeting, P-230, Dearborn, MI, October 23-26, 1989, Society of Automotive Engineers, Inc., 4007 Commonwealth Drive, Warrendale, PA 15096-0001, pp. 251-264.

31. D. A. Koester, R. D. Nixon, S. Chevacharoenkul, and R. F. Davis, "High Temperature Creep of SiC Whisker-Reinforced Ceramics," in Whisker- and Fiber-Toughened Ceramics, R. A. Bradley, D. E. Clark, D. D. Larsen, and J. O. Stiegler, eds., (ASM International, 1988) pp. 139-145.

32. R. D. Nixon, D. A. Koester, S. Chevacharoenkul, and R. F. Davis, "Steady-State Creep of Hot-Pressed SiC Whisker-Reinforced Silicon Nitride," *Comp. Sci. and Techn.*, 37 [1-3] 313-28 (1990).

33. D. F. Carroll and R. E. Tressler, "Accumulation of Creep Damage in a Siliconized Silicon Carbide," *J. Am. Ceram. Soc.*, 71 [6] 472-77 (1988).

34. S. M. Wiederhorn, D. E. Robers, T.-J. Chuang, and L. Chuck, "Damage-Enhanced Creep in a Siliconized Silicon Carbide: Phenomenology," *J. Am. Ceram. Soc.*, 71 [7] 602-608 (1988).

35. D. F. Carroll and R. E. Tressler, "Effect of Creep Damage on the Tensile Creep Behavior of a Siliconized Silicon Carbide," *J. Am. Seram. Soc.*, 72 [6] 49-53 (1989).

36. S. M. Wiederhorn, W. Liu, D. F. Carroll, and T.-J. Chuang, "Creep Rupture of Two Phase Ceramics," Presented at the 91st Annual Meeting and Exposition of the American Ceramic Society, April 23-27, 1989, Paper 7-JIII-89.

37. S. M. Wiederhorn and B. J. Hockey, "High Temperature Degradation of Structural Composites," Proceedings of the 7th Cimtec World Ceramics Congress, Montecatini Terme, Italy, Ceramics International, in press (1990).

38. L. R. F. Rose, "Microcrack Interaction with a Main Crack," *Int. J. Fracture*, 31 [3] 233-42 (1986).

39. H. Riedel and J. R. Rice, "Tensile Cracks in Creeping Solids," pp. 112-130 in Fracture Mechanics: Twelfth Conference, ASTM STP 700, American Society for Testing and Materials, Philadelphia, PA (1980).

40. J. W. Hutchinson, "Constitutive Behavior and Crack Tip Fields for Materials Undergoing Creep-Constrained Grain Boundary Cavitation," *Acta Met.*, 31 [7] 1078-1088 (1983).

41. K. S. Chan and R. A. Page, "Transient Cavity Growth in Ceramics Under Compression," *J. of Mat. Sci.*, in press (1991).

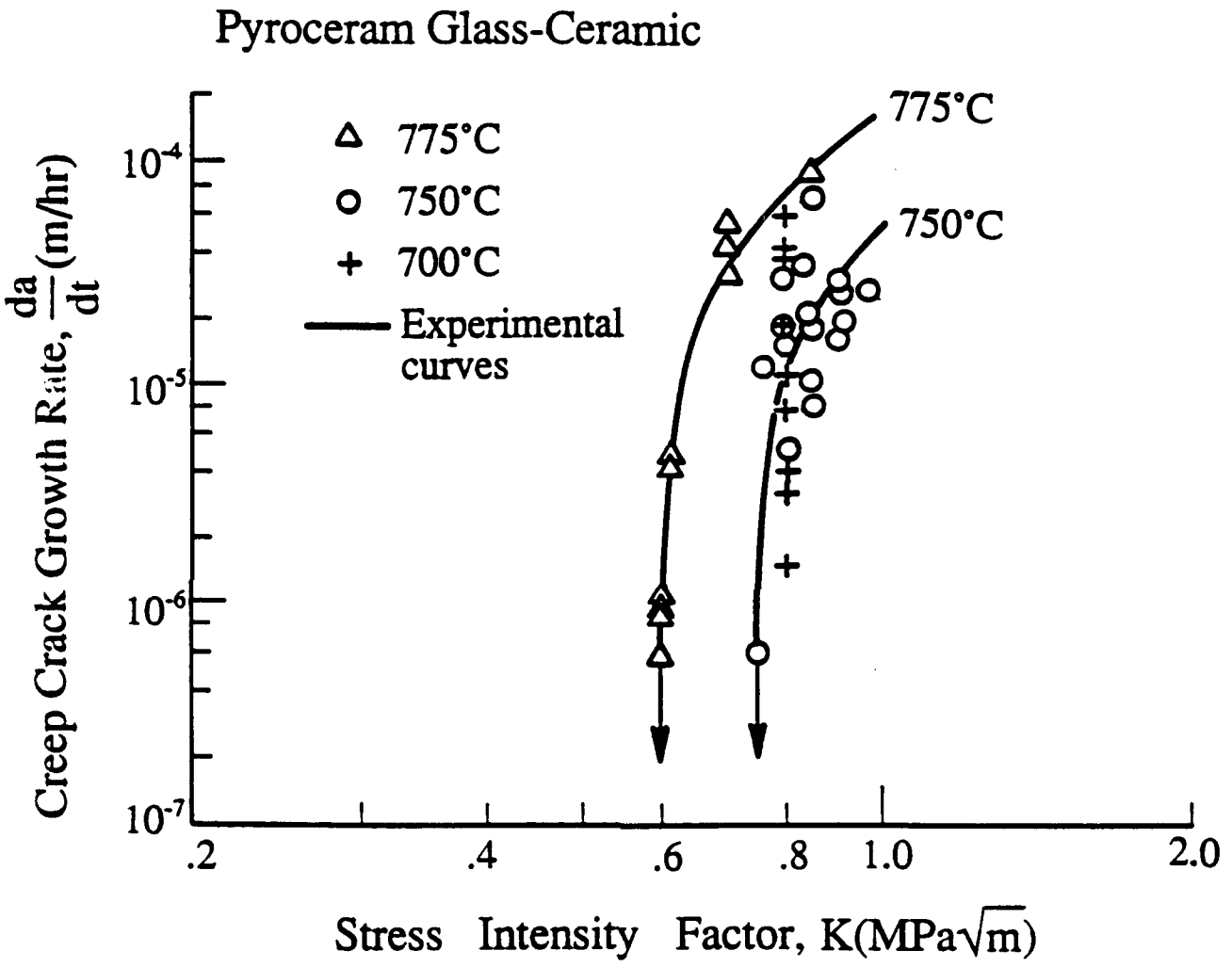

Figure 1. Creep-crack growth curves for the pyroceram glass-ceramic showing the existence of a growth threshold. Data are from Chan and Page [15].

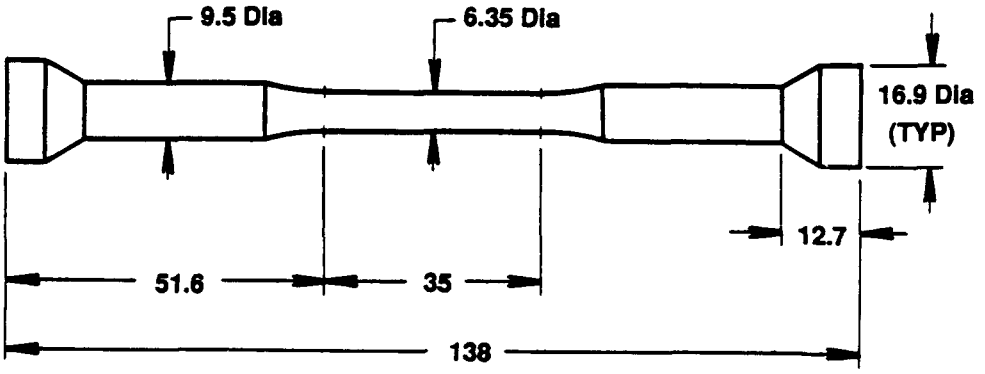

(a)

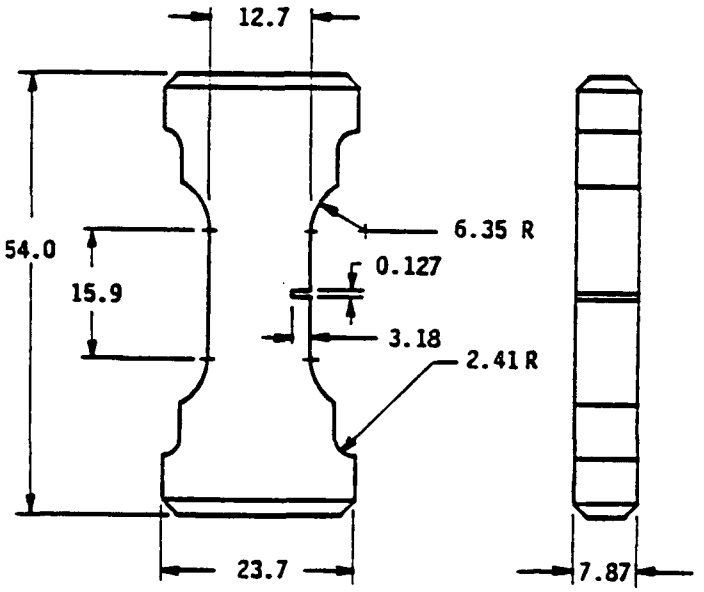

(b)

Figure 2. Schematic of the tensile creep (a) and single-edge-notched (b) specimens used for the creep deformation and crack growth experiments. All dimensions are listed in millimeters.

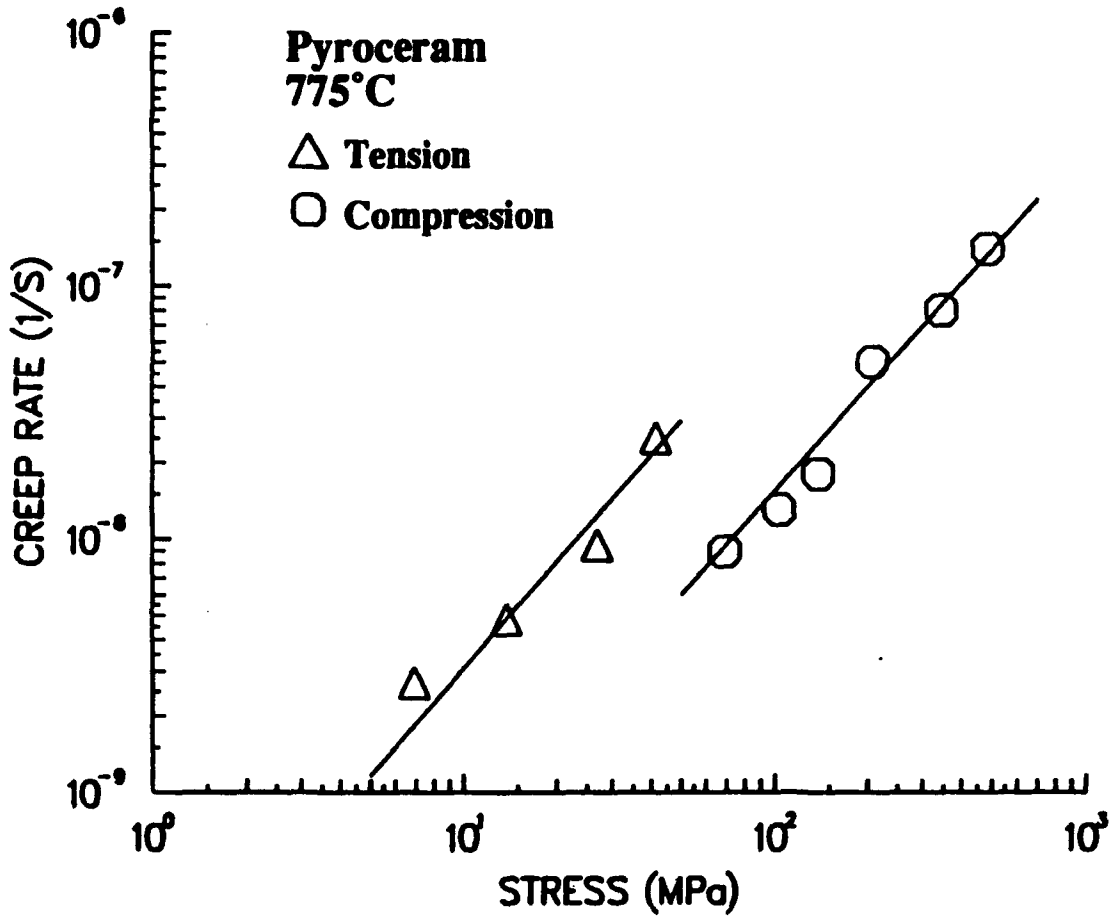

Figure 3. Comparison of steady-state creep rates of pyroceram in tension and in compression.

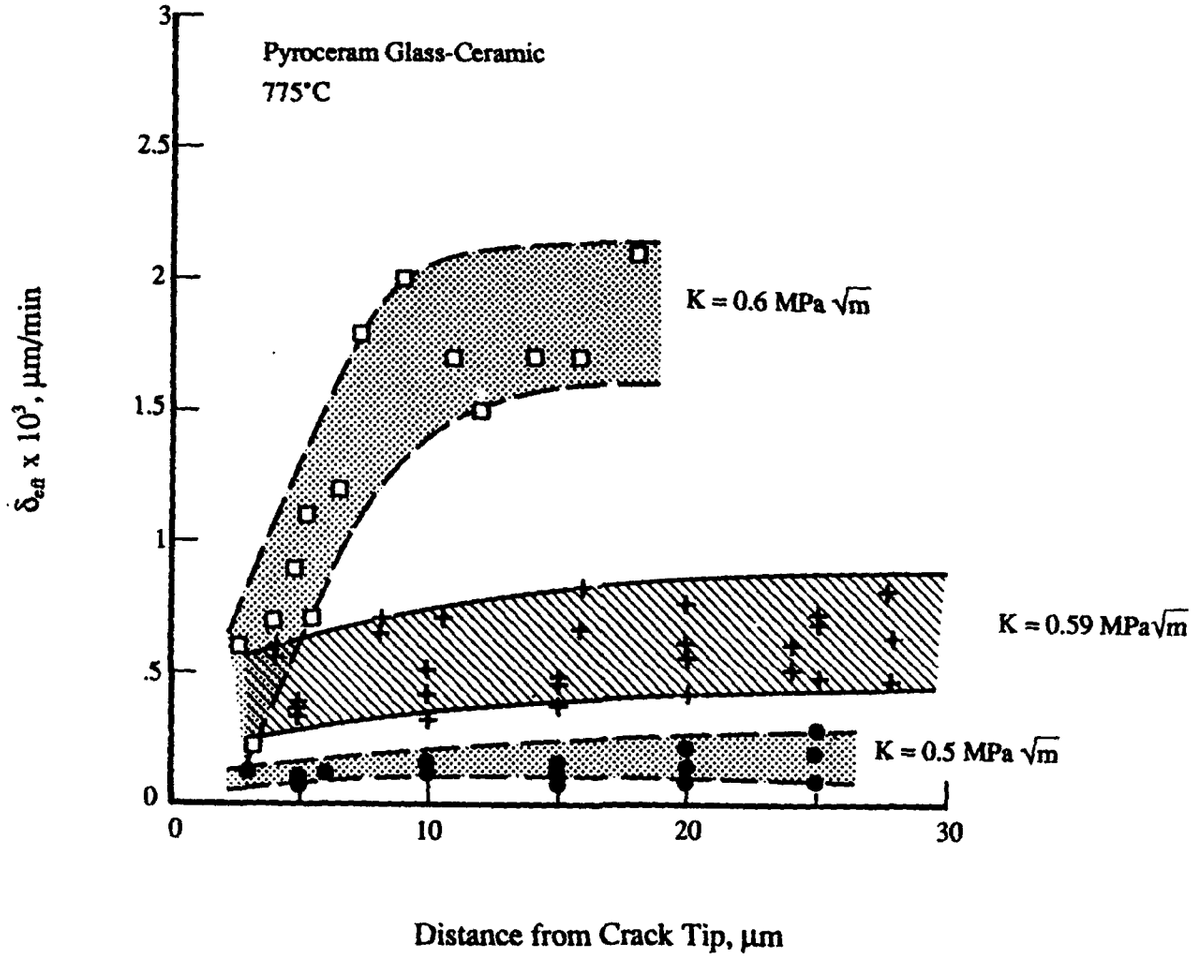

Figure 4. Rates of the effective crack opening displacement for creep cracks loaded at K levels above the threshold (K_{th} = 0.59 and 0.6 MPa$\sqrt{m}$) and below the threshold (K = 0.5$\sqrt{m}$).

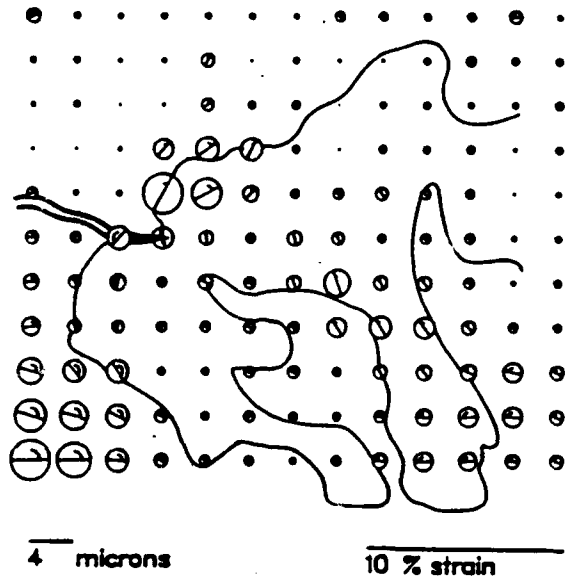

(a)

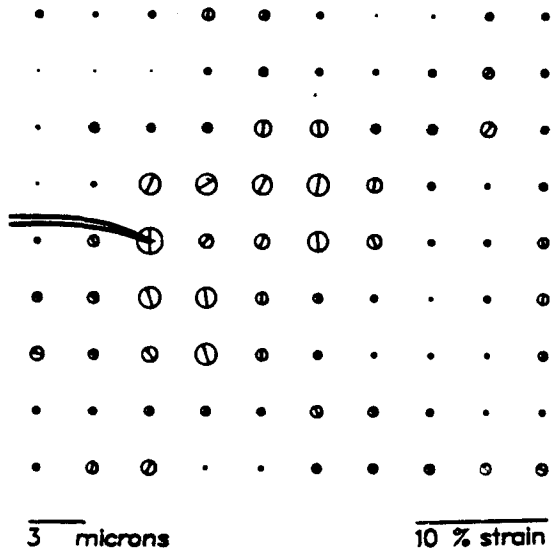

(b)

Figure 5. Comparison of the near-tip creep strain distributions at two K levels: (a) $K \geq K_{th}$; and (b) $K < K_{th}$. The line contour in (a) represents the region within which creep cavities are located.

(a)

(b)

Figure 6. Traces of microcracks located near the tip of dominant creep crack: (a) $K = 0.95\sqrt{m}$ at 750°C, and (b) $K = 0.7\sqrt{m}$ at 775°C.

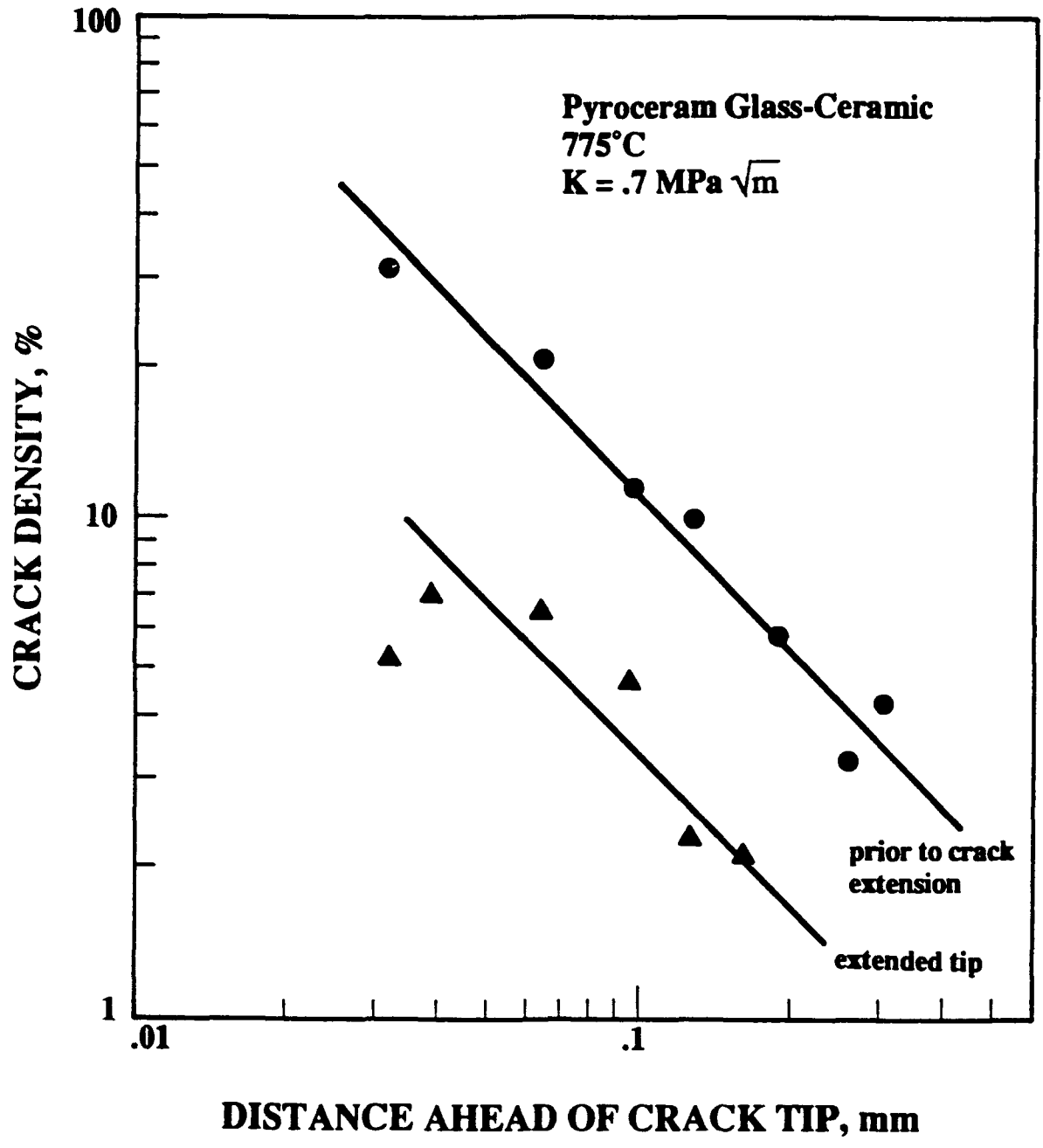

Figure 7. Microcrack density as a function of distance ahead of the main crack tip before and after an incremental extension of the main crack.

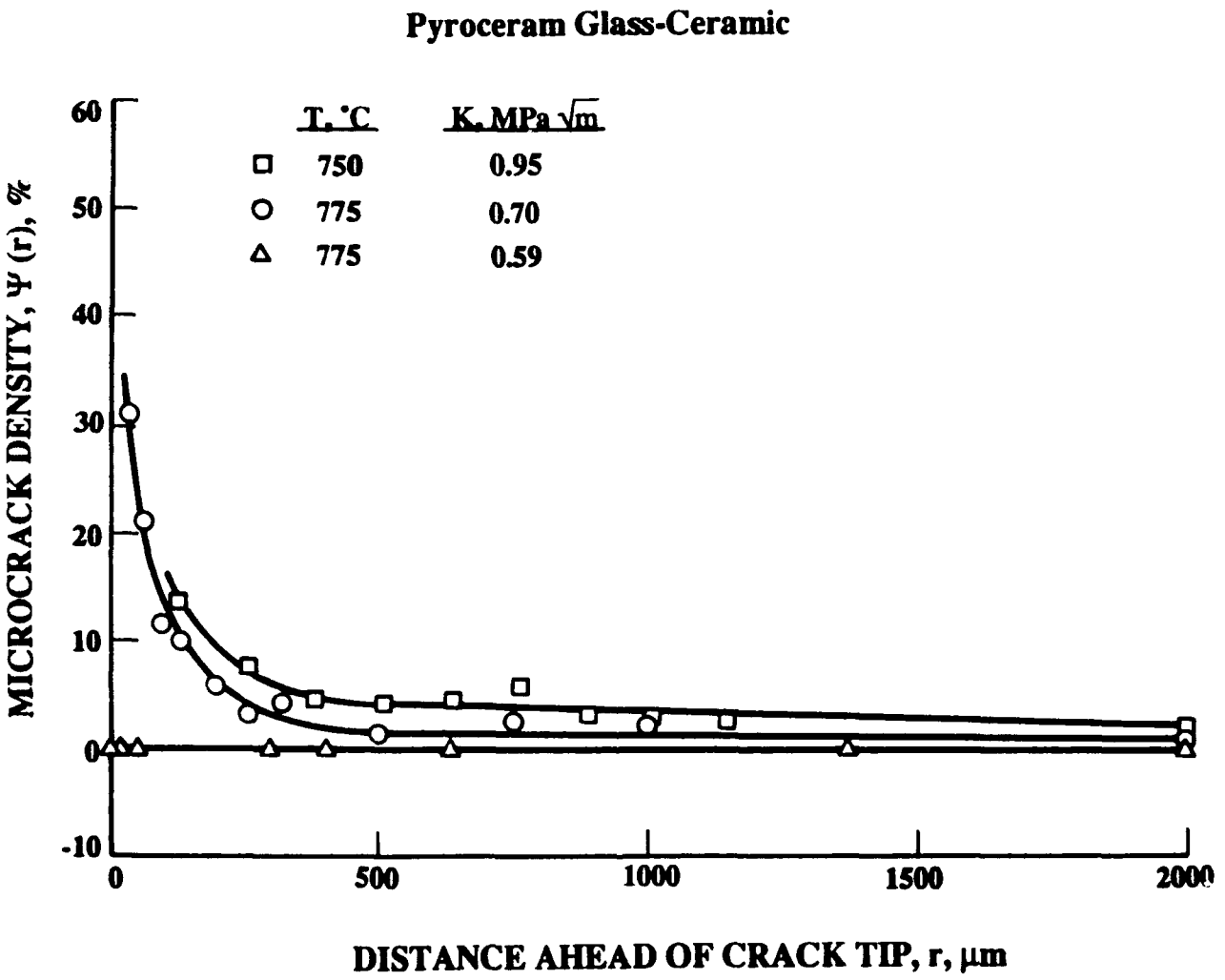

Figure 8. Microcrack density as a function of distance, r, ahead of the crack tip for various K levels.

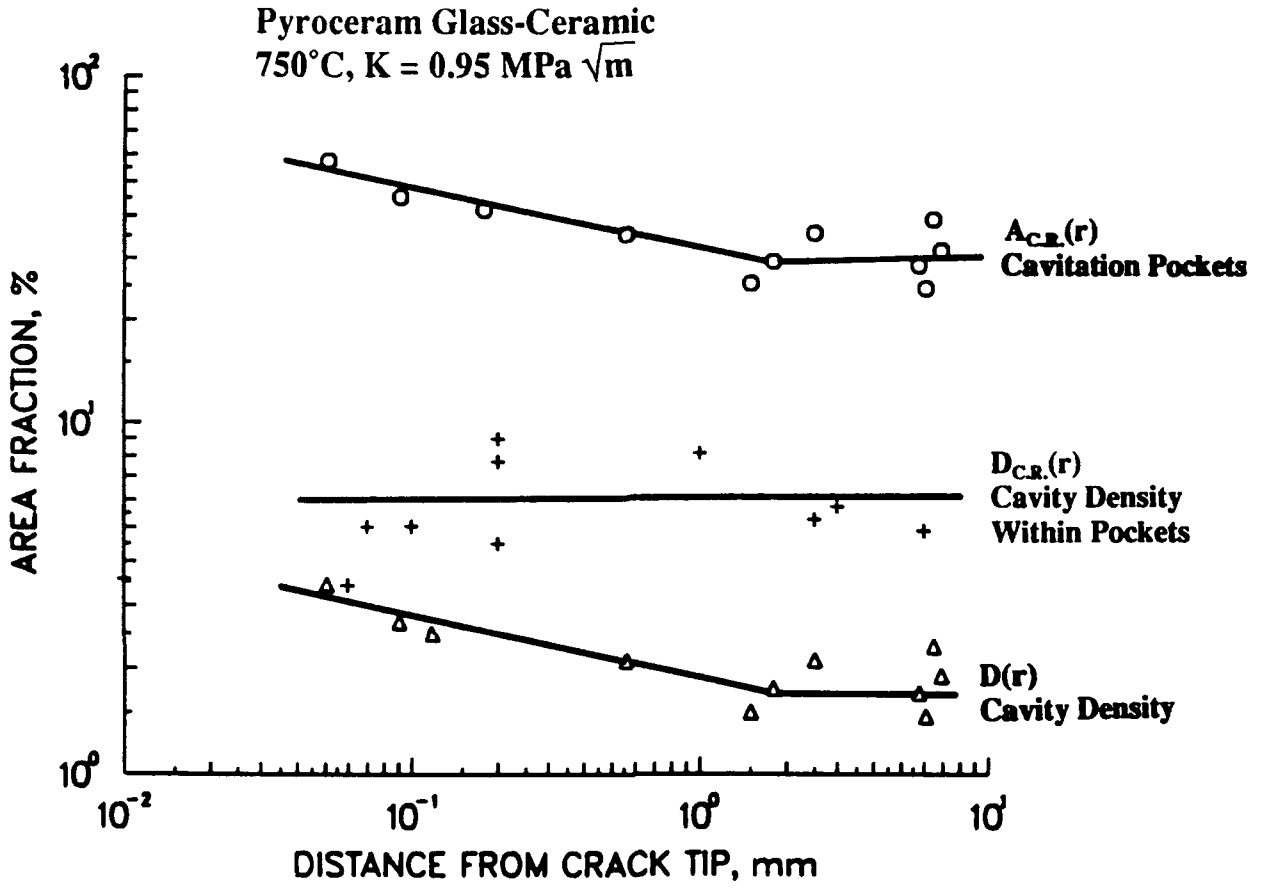

Figure 9. Distributions of cavitation pockets, $A_{CR}(r)$, cavity density within pockets, $D_{C.R.}(r)$, and cavity density, D(r), for creep cracks in pyroceram for $K = 0.95\sqrt{m}$ at 750°C.

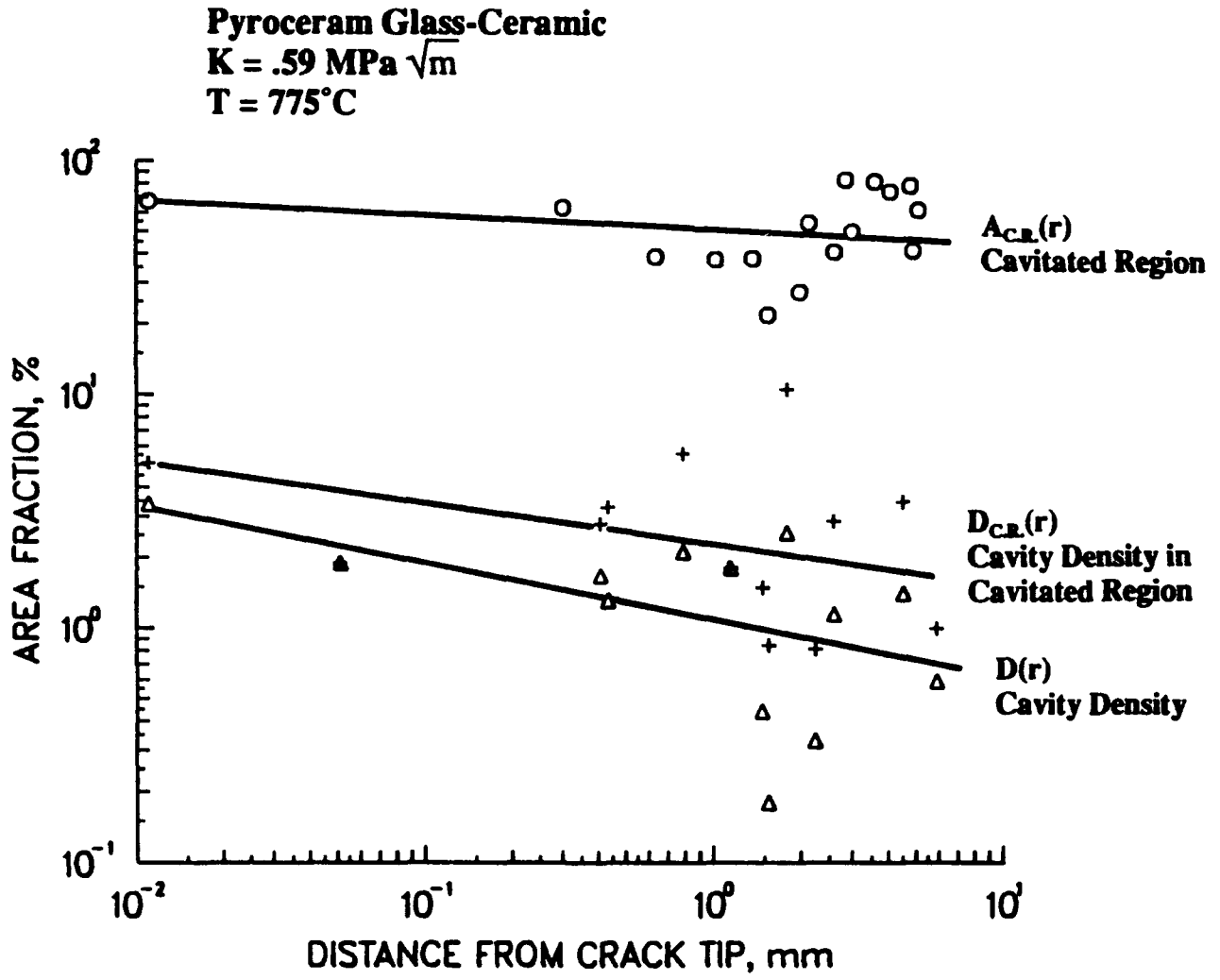

Figure 10. Distributions of cavitation pockets, $A_{CR}(r)$, cavity density within pockets, $D_{C.R.}(r)$, and cavity density, D(r), for creep cracks in pyroceram for $K = 0.59\sqrt{m}$ at 775°C.

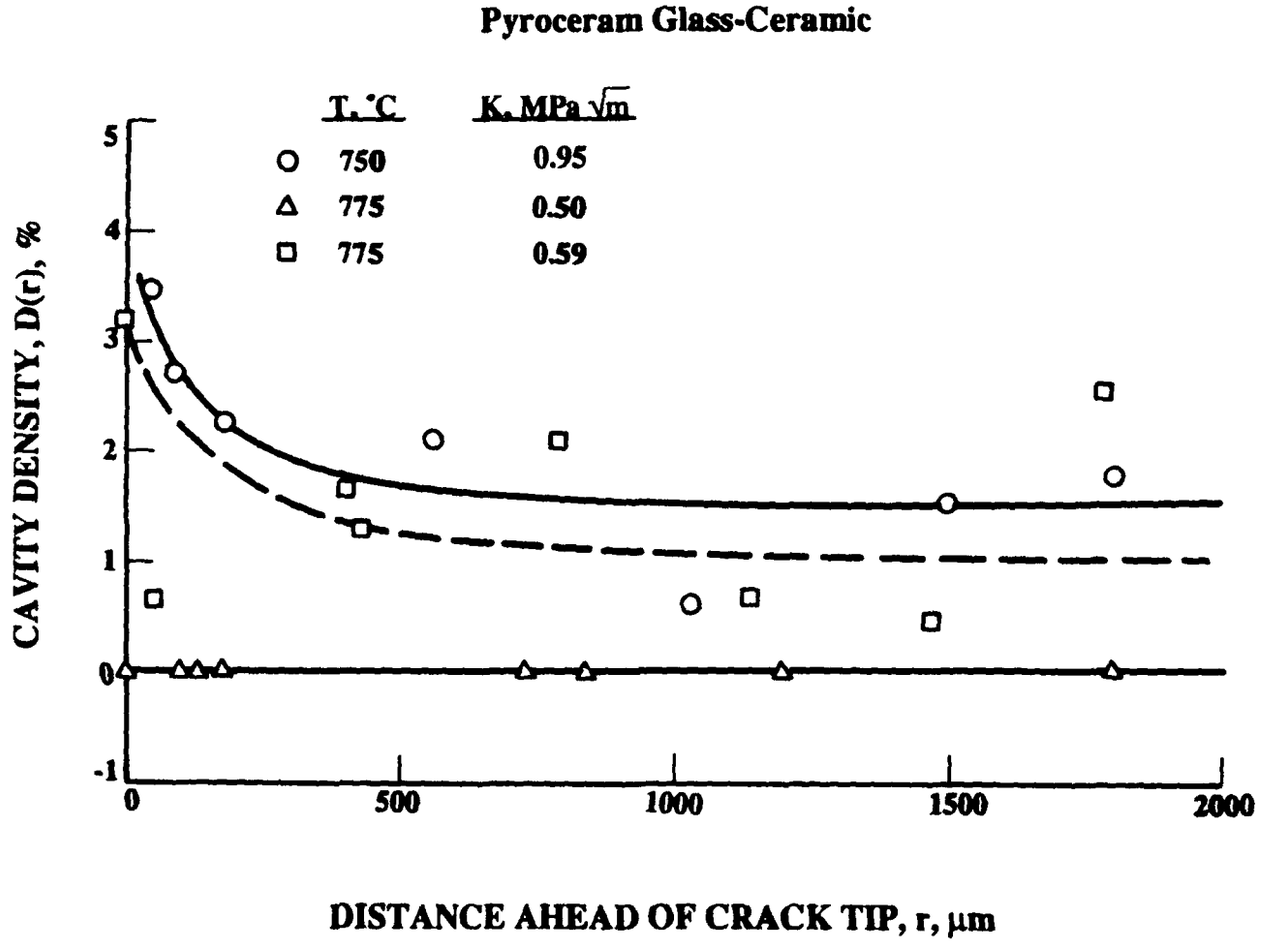

Figure 11. Comparison of cavity density distribution for K levels (K = 0.59 and $0.6\sqrt{m}$) above the growth threshold, K_{th}, and for K = $0.5\sqrt{m}$ which is below the threshold.

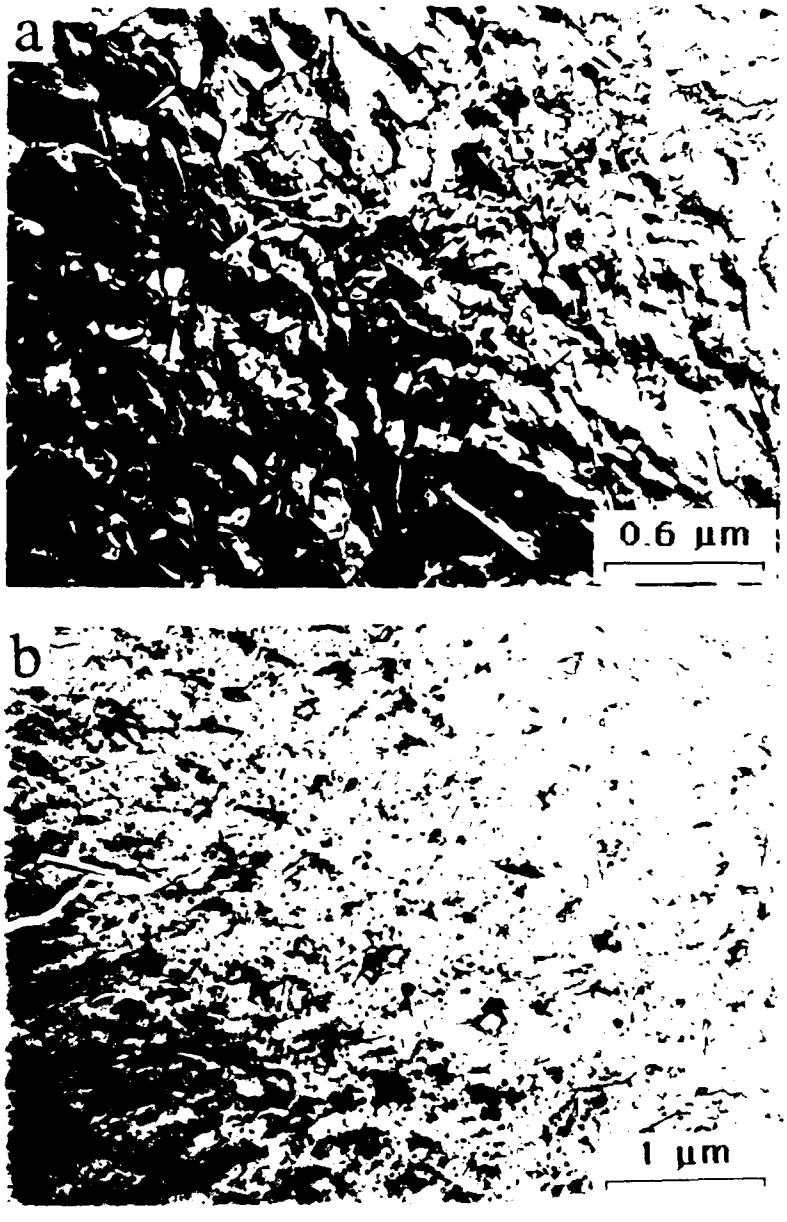

Figure 12. Comparison of the near-tip cavitation processes in the pyroceram glass-ceramic at K levels at and below the growth threshold: (a) formation of creep cavities at $K \geq K_{th}$; (b) removal of creep cavities by sintering at $K < K_{th}$.

Figure 13. An incipient microcrack formed by a linear array of equally sized and spaced creep cavities.

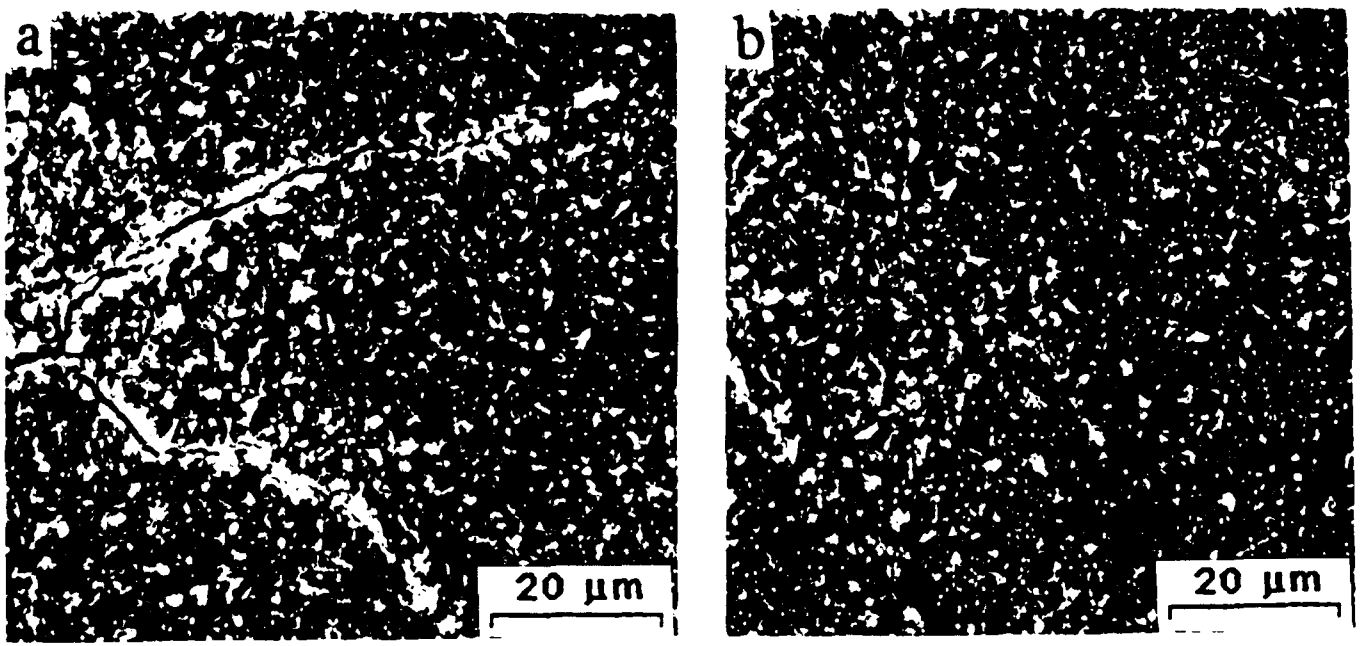

Figure 14. Active (A) and inactive (I) cracks located near the tip of the dominant crack: (a) near-tip region, and (b) high-magnification view of the inactive microcrack.

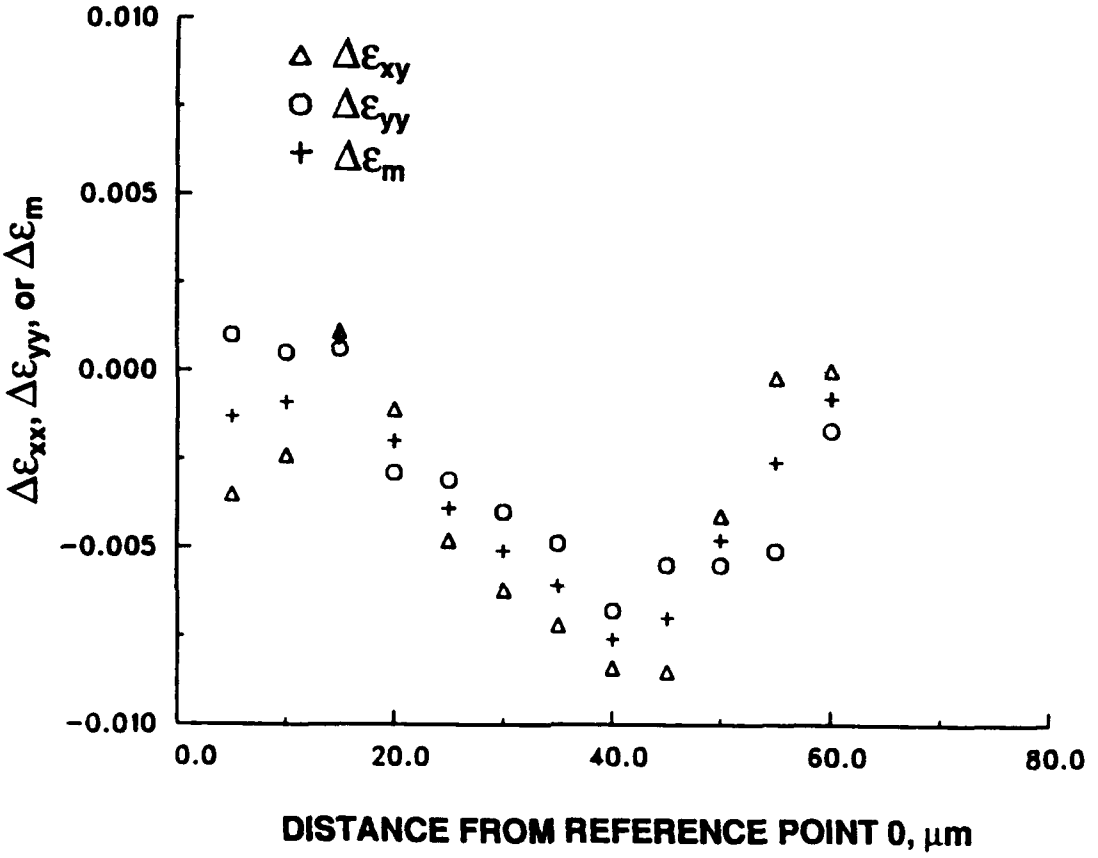

Figure 15. Negative values of incremental strain components ($\Delta\varepsilon_{xy}$) and the mean strain ($\Delta\varepsilon_m = 1/2\ [\Delta\varepsilon_{xx} + \Delta\varepsilon_{yy}]$) across the surfaces of the inactive microcrack indicating sintering of the microcrack.

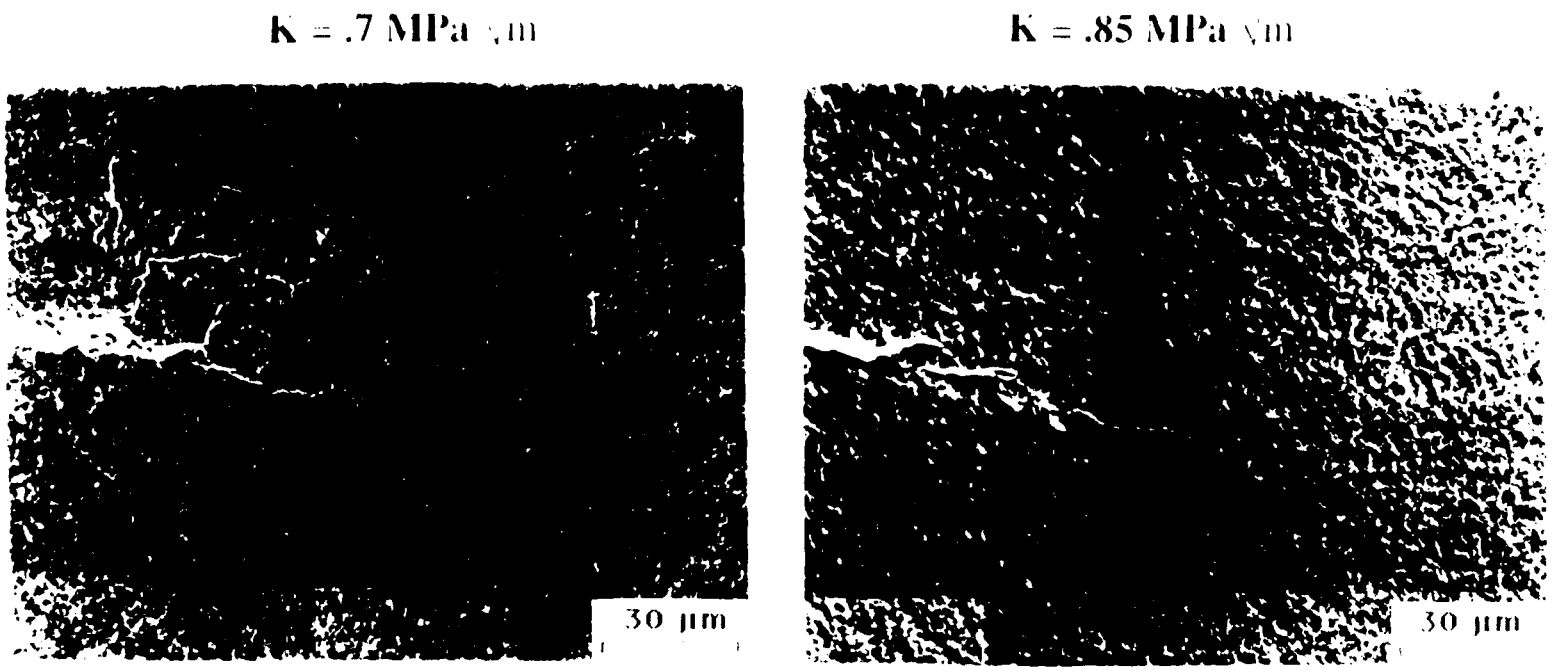

Figure 16. Micrographs of the near-tip regions at K = 0.7 and K = 0.85$\sqrt{m}$ showing sintering of microcracks located behind the dominant crack tip. Remnants of the microcrack whose sintering is shown in Figures 14 and 15 is indicated by an arrow.

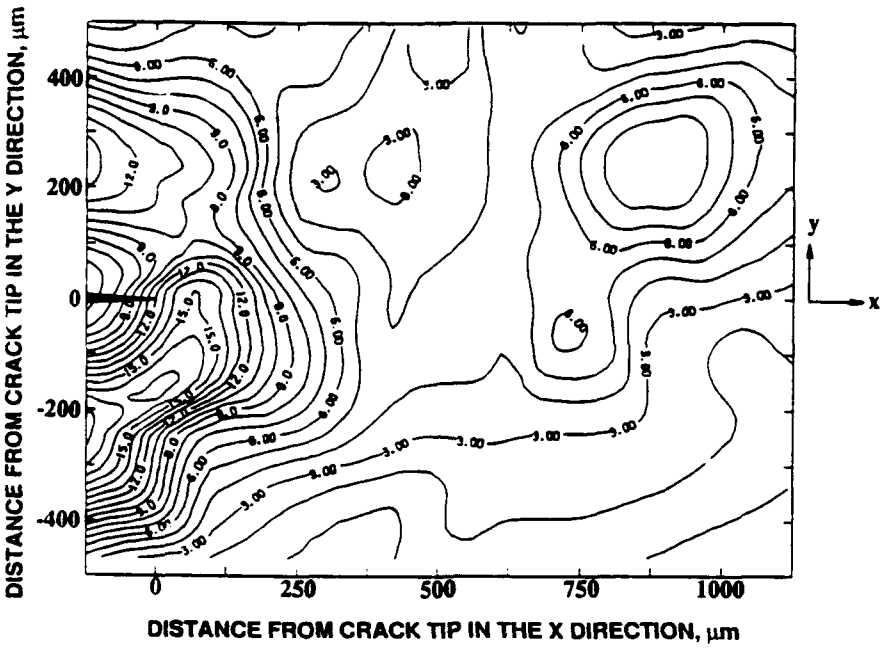

(a)

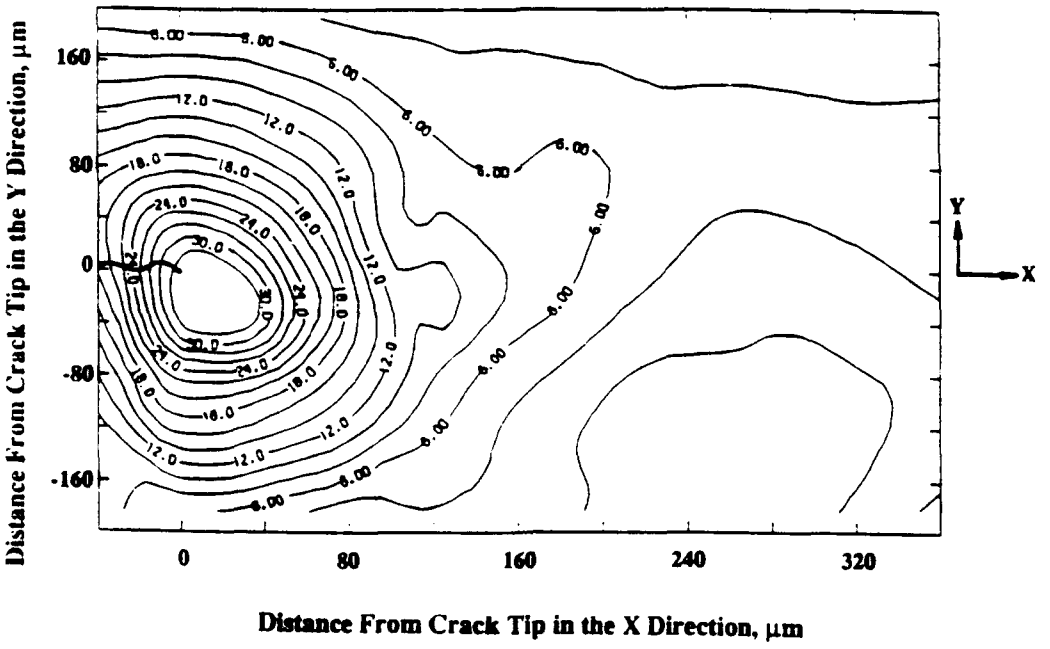

(b)

Figure 17. Contour plots of equal microcrack density in percent for creep cracks in pyroceram: (a) $K = 0.95\sqrt{m}$ at 750°C, and (b) $K = 0.7\sqrt{m}$ at 775°C. The lower values of microcrack density in the crack wake suggest healing of creep damage at locations behind the crack tip.

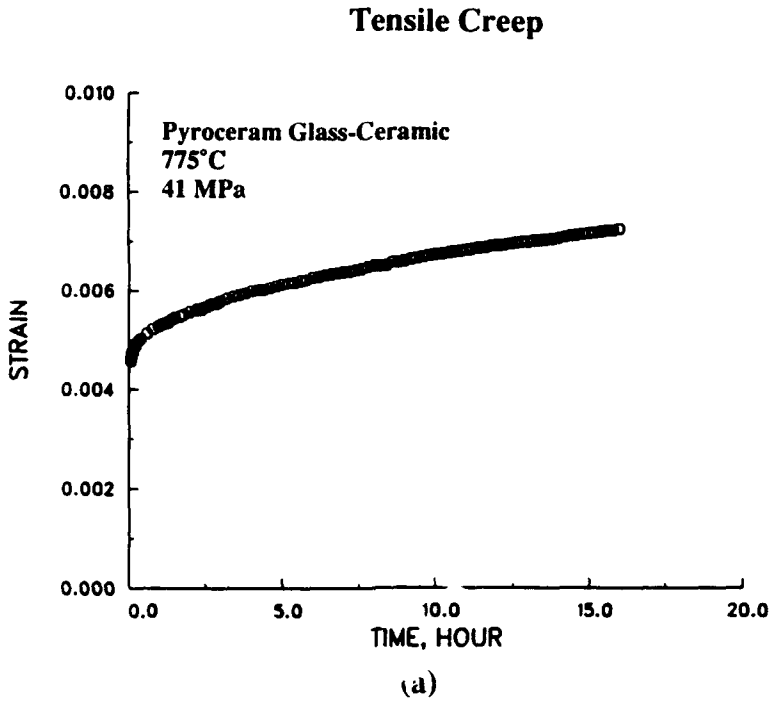

(a)

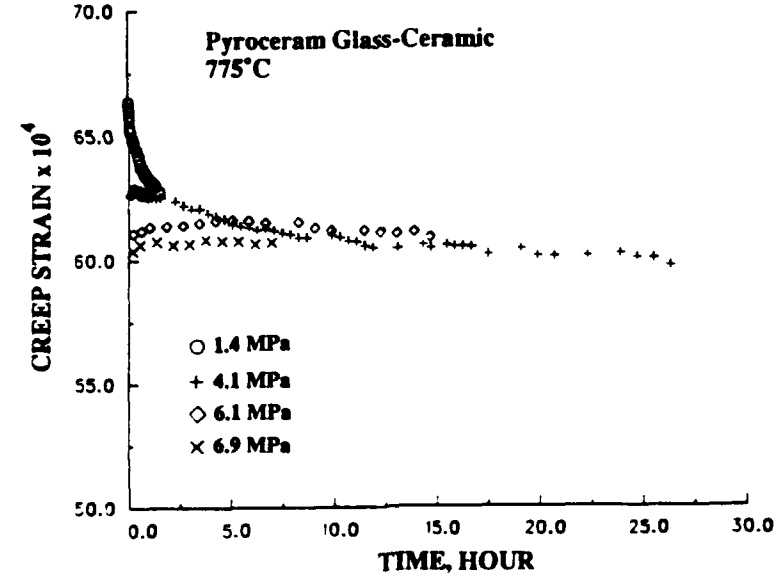

(b)

Figure 18. Creep and sintering responses of pyroceram at 775°C: (a) creep curve for 41 MPa, and (b) contractions of pre-crept specimen (41 MPa for 16 hours) observed at various applied sintering stresses. The applied tensile stress was lowered from 41 MPa to 1.4 MPa and subsequently increased to 4.1, 6.1, and 6.9 MPa.

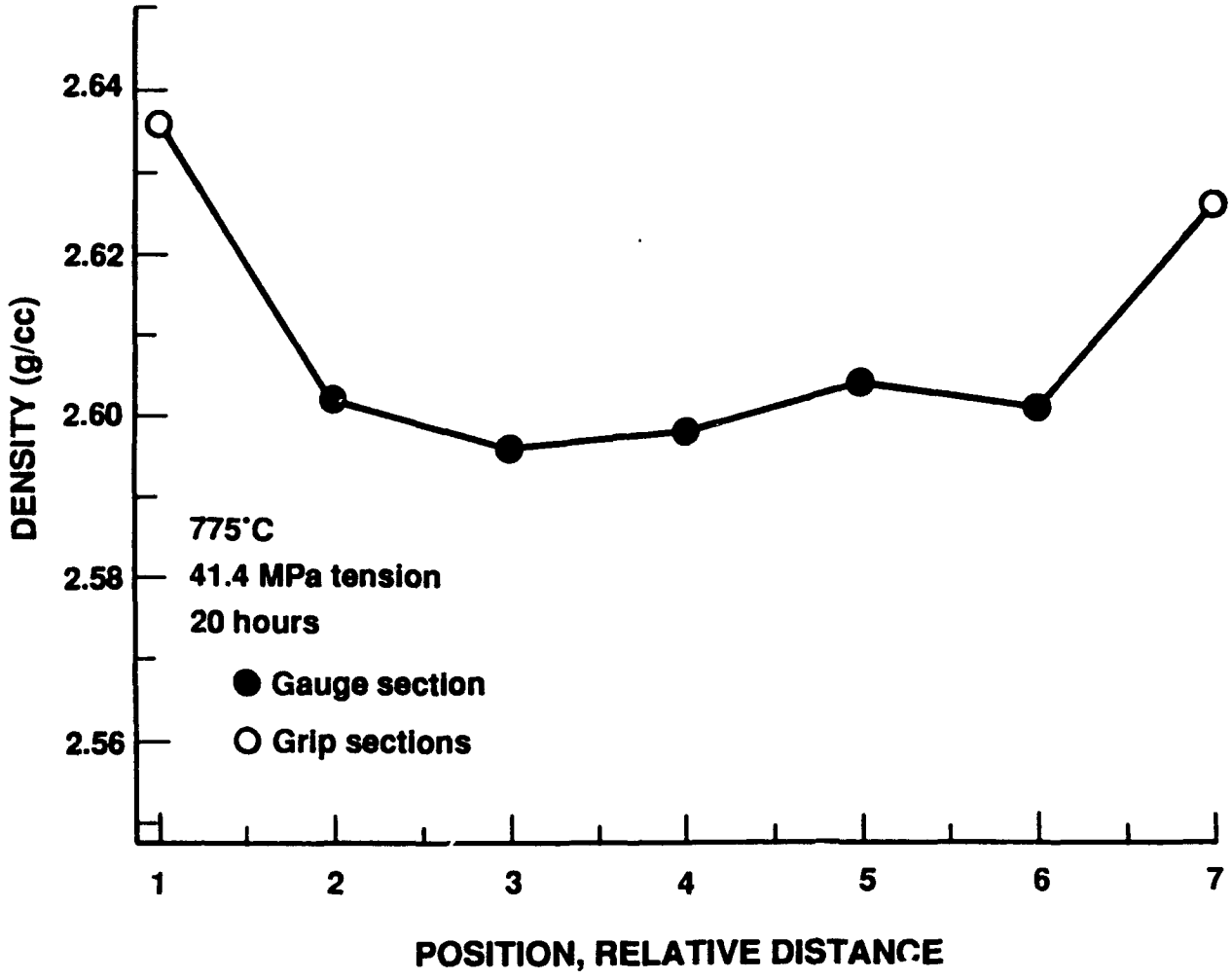

Figure 19. Local density of pyroceram at various locations of the tensile creep specimen. The lower density values in the gauge section indicate the presence of creep cavities and/or microcracks.

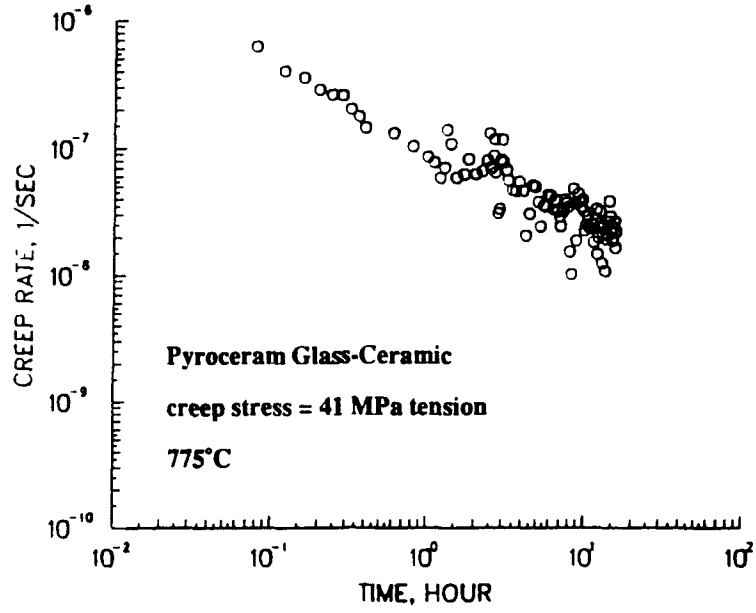

(a)

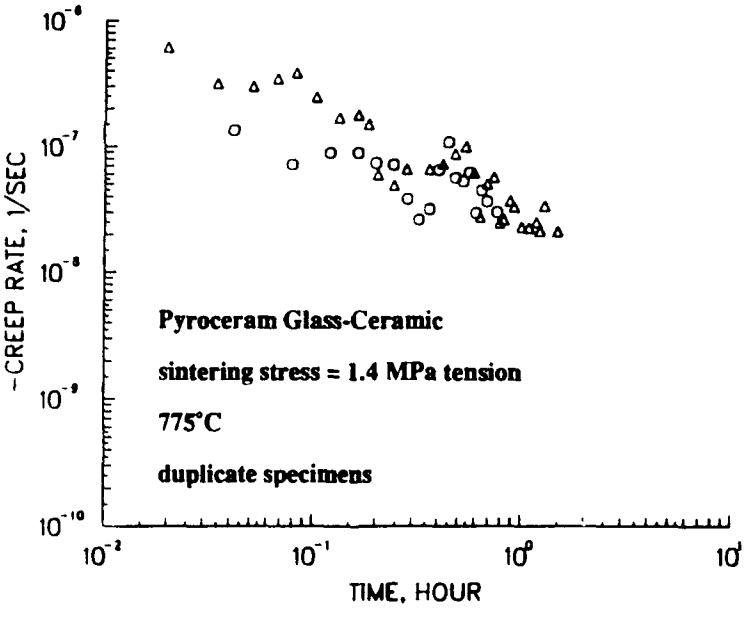

(b)

Figure 20. Creep and sintering rates as a function of time: (a) creep rates for MAS glass-ceramic tested at 41 MPa at 775°C, and (b) negative creep rate (contraction rate) as a function of time of sintering at a tensile stress of 1.4 MPa. The pyroceram glass-ceramic specimens were pre-crept at 41 MPa for ≈ 16 hours at 775°C.

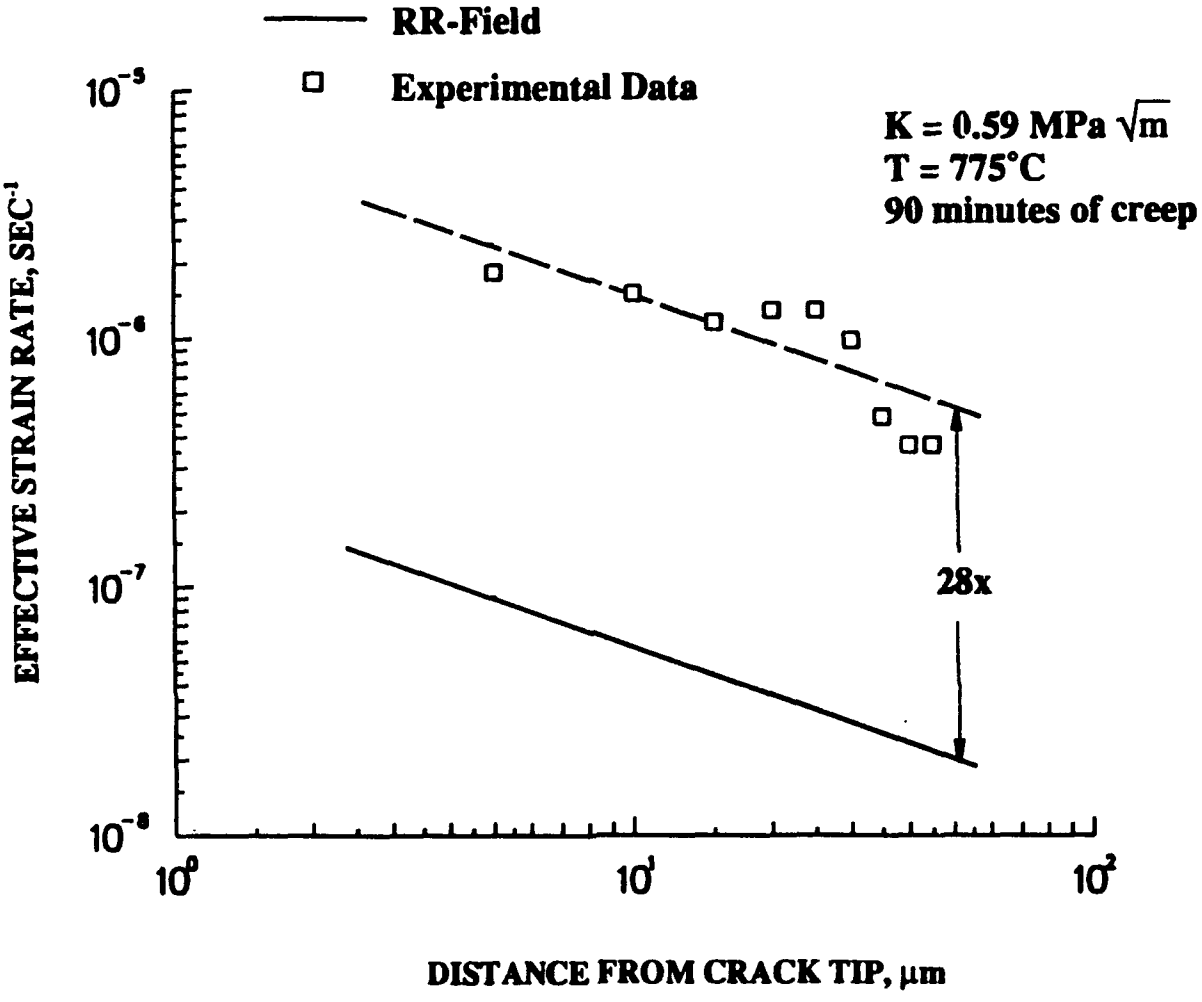

Figure 21. Comparison of the observed and calculated (Riedel-Rice Field) near-tip effective strain rates indicate a factor of 28X difference between theory and experiment. The discrepancy is attributed to the presence of microcracks ahead of the creep crack.